NASA TM X-676

(NASA-TM-X-676) STATIC STABILITY AND CONTROL CHARACTERISTICS OF A PROPOSED WINGED REENTRY VEHICLE AT MACH NUMBERS OF 1.50, 2.96, AND 4.63 J.D. Reed, et al (NASA) Apr. 1962 71 p

N72-71635

Unclas
00/99 24754

TECHNICAL MEMORANDUM

X-676

STATIC STABILITY AND CONTROL CHARACTERISTICS OF A PROPOSED WINGED REENTRY VEHICLE AT MACH NUMBERS OF 1.50, 2.96, AND 4.63

By James D. Reed and David S. Shaw

Langley Research Center
Langley Station, Hampton, Va.

NATIONAL AERONAUTICS AND SPACE ADMINISTRATION

WASHINGTON

April 1962

REPRODUCED BY
NATIONAL TECHNICAL
INFORMATION SERVICE
U.S. DEPARTMENT OF COMMERCE
SPRINGFIELD, VA 22161

NATIONAL AERONAUTICS AND SPACE ADMINISTRATION

TECHNICAL MEMORANDUM X-676

STATIC STABILITY AND CONTROL CHARACTERISTICS OF A PROPOSED WINGED REENTRY VEHICLE AT MACH NUMBERS OF 1.50, 2.96, AND 4.63*

By James D. Reed and David S. Shaw

SUMMARY

An investigation has been conducted in the Langley Unitary Plan wind tunnel to determine the static longitudinal and lateral stability and control characteristics of a proposed winged reentry vehicle at supersonic speeds. Effects of nose cant, elevon size, elevon deflection, and deflection of a single rudder were observed. Tests were conducted at angles of attack from approximately -5° to 25° for a Mach number of 1.50 and at -5° to $>50^{\circ}$ for Mach numbers of 2.96 and 4.63. Angle of sideslip was varied from approximately -4° to 10° at Mach numbers of 2.96 and 4.63, and Reynolds number per foot varied from 1.78×10^{6} to 3.09×10^{6}.

The results indicate that, for the selected center-of-gravity location of 70 percent theoretical root chord, there is a longitudinal trim problem in the desired angle-of-attack range between that for maximum lift-drag ratio and maximum lift. Also, there are large Mach number effects on the pitching-moment characteristics of the vehicle; thus, the shape of the pitching-moment curves changes markedly between Mach numbers of 1.50 and 2.96. Elevon effectiveness and longitudinal stability both decrease with upward elevon deflection at the two higher Mach numbers.

Lateral stability appears to be satisfactory at all angles of attack above about 10°. Deflection of the right rudder gives adequate control at lower angles of attack, but effectiveness falls off rapidly with increase in angle of attack up to that corresponding to maximum lift (angle of attack $\approx 50^{\circ}$). Differential elevon roll control introduces yawing moments which may be difficult to trim out at higher angles of attack because of the fall off in rudder effectiveness.

---

*[redacted]

INTRODUCTION

At the present time there is intense interest in placing man into space and assuring his safe return. The two main categories of vehicles under consideration for such a task are the ballistic (lift-drag ratio of 0) and the lifting type (lift-drag ratio greater than 0). The major development effort up to this time has been directed toward use of the ballistic-type vehicle. While this type of configuration is well suited for reentry, one of its disadvantages is the restriction of landing-site selection to points along or near its trajectory. The winged vehicles, on the other hand, allow reduction of the gravity forces associated with reentry and afford a much wider choice of landing sites, their range being dependent to a large degree on the lift-drag ratio of the configuration.

The National Aeronautics and Space Administration has made a number of exploratory studies on winged reentry aircraft, both theoretical and experimental. (See refs. 1 to 15.) The vehicle for which results are presented herein is one such configuration, which was designed to have a trimmed lift-drag ratio of between 2.0 and 3.0 at supersonic and hypersonic speeds. The design geometry of this aircraft was based primarily on reentry heating considerations.

One of the major problems involved in a configuration of this type is the need for satisfactory stability and control over a wide velocity spectrum from hypersonic to subsonic speeds. The purpose of this paper is to determine the stability and control characteristics of the configuration in the supersonic speed range, Mach numbers of 1.50, 2.96, and 4.63.

The tests were performed in the Langley Unitary Plan wind tunnel at angles of attack from approximately -5° to 25° at a Mach number of 1.50, and at -5° to $>50^\circ$ at Mach numbers of 2.96 and 4.63. Tests were also performed through an angle-of-sideslip range from approximately -4° to 10° at Mach numbers of 2.96 and 4.63, and Reynolds number per foot varied from 1.78×10^6 to 3.09×10^6.

SYMBOLS

The aerodynamic force and moment data are referred to the axes system shown in figure 1, with the center of gravity located at 70 percent of the theoretical root chord, measured from the theoretical apex to the body base. (See fig. 2.) The coefficients are based on the wing area (including elevons) of the particular configuration being tested. (See table I.) The symbols are defined as follows:

b wing span, in.

C_A axial-force coefficient, $\frac{\text{Axial force}}{qS}$

$C_{A,c}$ chamber axial-force coefficient, $\frac{\text{Chamber axial force}}{qS}$

C_D drag coefficient, $\frac{\text{Drag}}{qS}$

C_l rolling-moment coefficient, $\frac{\text{Rolling moment}}{qSb}$

C_{l_β} rolling moment due to sideslip (positive dihedral effect if sign is negative)

C_L lift coefficient, $\frac{\text{Lift}}{qS}$

C_m pitching-moment coefficient, $\frac{\text{Pitching moment}}{qSc_r}$

$C_{m,o}$ pitching-moment coefficient at zero normal force

$\Delta C_m/\delta_e$ elevon effectiveness parameter

C_n yawing-moment coefficient, $\frac{\text{Yawing moment}}{qSb}$

C_{n_β} yawing moment due to sideslip

C_N normal-force coefficient, $\frac{\text{Normal force}}{qS}$

c_r wing root chord (from theoretical apex to base of body)

C_Y side-force coefficient, $\frac{\text{Side force}}{qS}$

C_{Y_β} side force due to sideslip

p_t	stagnation pressure, lb/sq ft
L/D	lift-drag ratio, C_L/C_D
M	Mach number
q	free-stream dynamic pressure, lb/sq ft
R	Reynolds number per foot
S	wing area (including area of elevons), sq ft
T_t	stagnation temperature, $^{\circ}F$
α	angle of attack, deg
β	angle of sideslip, deg
δ_e	elevon deflection angle (positive for trailing edge down), deg
δ_n	nose deflection angle (positive for nose up), deg
δ_r	right rudder deflection angle (positive for trailing edge left), deg

Subscript:

max	maximum

Model Component Designations:

B	body
W	wing
E_1	large elevons
E_4	small elevons
F	fins

APPARATUS AND TESTS

Tunnel

Tests were conducted in both the low and high Mach number test sections of the Langley Unitary Plan wind tunnel, which is a variable-pressure continuous flow tunnel. The nozzle leading to each test section is of the asymmetric sliding-block type, which permits a continuous variation in test-section Mach number from about 1.5 to 2.9 in the low Mach number test section, and from about 2.3 to 4.7 in the high Mach number test section.

Model

A three-view drawing of the model is shown in figure 2, and certain dimensional details are given in table I. Model photographs are presented in figure 3. The model wing was of clipped-delta planform, with 75° of leading-edge sweep. The bottom surface of the wing was essentially a flat plate except when the nose was canted. Interchangeable noses were constructed for the model to give nose cant angles of 0°, 5°, and 10°.

Two sizes of elevons were tested (shown in fig. 2) and, for each set, elevon angle was varied remotely by means of a motor-driven gearing system housed within the model. Each elevon was capable of independent movement. A calibrated slide wire system was used to obtain the desired elevon-angle settings. Vertical fins were mounted at the wing tips and toed in 5°. Rudder deflection angles of -5°, -15°, and -25° were obtained by means of wedge blocks fitted to the outboard surface of the right vertical fin. (See fig. 2.)

Reference will be made throughout the report to a "basic configuration." This consists of the 5° nose, body and wing, vertical fins, and either designated set of elevons.

Test Conditions

The following table presents the conditions under which the tests were performed:

M	p_t, lb/sq ft	R	T_t, °F	q, lb/sq ft
1.50	932	1.78×10^6	125	400
2.96	2,030	1.88	150	360
4.63	8,163	3.09	175	360

Transition strips of sparsely seeded No. 60 carborundum grit were placed at approximately the 5-percent-chord line of all airfoil sections and around the nose 1 inch behind the tip. Dewpoint was maintained below -30° F to minimize condensation effects.

Measurements and Methods

Aerodynamic forces and moments on the model were measured by means of an internal, six-component, electrical strain-gage balance. The balance was attached to a sting which, in turn, was rigidly fastened to the sting support system. Two sting arrangements were used in order to obtain the desired elevon-angle range (20° to -50°) and model angle-of-attack range. (See fig. 4.) In addition, a 0° straight sting was used to obtain comparison data for the undeflected and downward deflected elevons. By use of the 15° offset sting, elevon deflection angles to -15° were obtained at model angles of attack to about 25°. The top-mounted sting was necessary in order to extend the angle-of-attack and elevon-angle ranges to the maximum values for this test program. A portion of the upper surface of the elevons was removed to allow clearance for the rear-mounted stings. (See figs. 2 and 4.)

L 1905

Balance chamber pressure was measured by means of a single static orifice located in the model. This pressure was only measured for the rear-mounted sting conditions, and figure 5 illustrates representative values of $C_{A,c}$. Schlieren photographs of the model were taken and selected views are presented in figure 6.

Corrections

Corrections to the indicated model angle of attack have been made for both tunnel airflow misalinement and deflection of model and sting support due to aerodynamic load. The data are uncorrected for $C_{A,c}$.

RESULTS AND DISCUSSION

Sting Interference

A comparison of the longitudinal data for the three different sting mounting systems is presented in figure 7 for Mach numbers of 2.96 and 4.63. (At a Mach number of 1.50, only the 15° offset sting was used.) The data for the two rear-mounted stings are generally the same at both Mach numbers tested. Although there is no overlap in angle of attack of the top-mounted-sting data with that of the rear-mounted stings, it is noted that there is a slight offset in the curves.

This is probably due to a change in the flow field on the top of the model as a result of the position of the top-mounted sting. The slopes of the curves appear to be the same on both sides of the discontinuity, however, and it is believed that any incremental or slope information derived from these curves is valid.

Longitudinal Stability and Control Characteristics

The longitudinal aerodynamic characteristics of the basic configuration with both large and small elevons are presented in figures 8 and 9, respectively. The reference center-of-gravity location of $0.70c_r$ was dictated by hypersonic considerations and is not necessarily the optimum location for the entire velocity spectrum.

A change in Mach number from 1.50 to 2.96 or 4.63 results in marked changes in the shape of the pitching-moment curves. At $M = 1.50$ the vehicle is stable in the lower range of C_N, but exhibits pitch-up at higher values of C_N. Conversely, at $M = 2.96$ and 4.63 ($\delta_e = 0^\circ$) the trend is from low stability or unstable conditions in the lower range of C_N to higher stability at increased C_N.

At $M = 1.50$, elevon deflection appears to have very little effect on vehicle stability over the limited angle-of-attack and elevon-deflection ranges of the tests. However, at $M = 2.96$ and 4.63, upward elevon deflection results in marked decreases in vehicle stability over the test angle-of-attack range, because of the decreased wing loading behind the center of gravity. As would be expected, the configuration with small elevons is more unstable than that with the large elevons.

Elevon control effectiveness decreases rather rapidly with upward elevon deflection. (See fig. 10.) In general, for any given elevon deflection angle, elevon effectiveness increases with angle of attack at the two higher test Mach numbers.

One of the prime prerequisites for a vehicle of this type is that it be capable of stable trim over its entire velocity spectrum at angles of attack from those corresponding to $(L/D)_{max}$ up to those for maximum lift. In order to show more clearly the trim characteristics of the aircraft, figure 11 presents C_m plotted against C_N for the BWE_1F configuration. Data from the results obtained at each of the test Mach numbers are plotted for several elevon deflections. In addition, limited data from unpublished test results in the Langley 11-inch hypersonic tunnel at Mach numbers of 6.8 and 9.6 are included. Lines connecting the values of C_N at which $(L/D)_{max}$ and $C_{L,max}$ occur are superimposed on the figure.

Hypersonically, it appears that the vehicle can trim with positive stability over the range from $(L/D)_{max}$ to $C_{L,max}$ ($\alpha \approx 50^{\circ}$). Stable trim at Mach numbers 6.8 and 9.6 with $\delta_e = 0^{\circ}$ is near $(L/D)_{max}$, showing ability to trim at or slightly below this value. Data at $M = 9.6$ for $\delta_e = -10^{\circ}$ are limited to a range below $C_N \approx 0.4$; however, extrapolation over the higher range of C_N, similar in shape to the supersonic curves presented, indicates that the vehicle can possibly accomplish stable trim to $C_{L,max}$ at this Mach number.

The supersonic data, on the other hand, leave much to be desired from a trim standpoint. The trend of the data indicates that the vehicle can accomplish stable trim at $M = 1.50$ only below $C_N \approx 0.40$. This should allow trim to $(L/D)_{max}$ but not far above that point. Conversely, at Mach numbers of 2.96 and 4.63, the configuration may attain stable trim at moderate values of C_N and values of C_N near maximum lift (see $\delta_e = -10^{\circ}$) but not in the region near $(L/D)_{max}$ or below, because of a combination of negative $C_{m,o}$ and the nonlinearity of the pitching-moment curves. For example, at $M = 4.63$, it appears that stable trim conditions cannot be obtained below $C_N \approx 0.25$ ($\delta_e = -5^{\circ}$) and, at $M = 2.96$, stable trim cannot be obtained below $C_N \approx 0.60$ ($\delta_e = -10^{\circ}$).

Thus, it appears that there is a trim problem in the supersonic speed regime that does not exist hypersonically. The solution to this problem lies in a corrective device, for supersonic use, that would both increase $C_{m,o}$ and increase the stability and linearity of the pitching-moment curves.

The effects of nose cant on the longitudinal stability and trim characteristics of the vehicle are presented in figure 12. As would be expected, increased nose cant angle produces a positive shift in $C_{m,o}$ with only minor changes in vehicle stability. While increased nose cant angle will help the problem of negative $C_{m,o}$, it will not give needed increase in vehicle stability. There is the further drawback of increased heating during the reentry portion of flight, which would discourage use of higher nose cant angles.

Performance Characteristics

The maximum lift-drag ratio for the basic configuration with either the large or the small elevons appears to be only slightly affected by variation in Mach number over the test range. (See fig. 13.) The vehicle with large elevons at 0° has slightly higher values of $(L/D)_{max}$ than does the one with the small elevons. Negative deflection of the

elevons to -15° has little or no effect on $(L/D)_{max}$ of the vehicle; however, positive elevon deflections lead to significant losses in $(L/D)_{max}$ (about 0.7 for a 20° positive deflection of the large elevons). There was little effect of nose cant up to 10° on the maximum lift-drag ratio of the vehicle at any of the test Mach numbers as shown in figure 14.

Lateral Stability and Control Characteristics

The lateral stability and control characteristics of the BWE_1F configuration are presented in figures 15 and 16 and summarized in figures 17 and 18 for Mach numbers of 2.96 and 4.63. At a Mach number of 2.96, the model exhibited positive dihedral effect at all test angles of attack above about 10° (fig. 17). The angle of attack for positive dihedral effect was lowered slightly with increase in Mach number to 4.63. There was a small effect of single rudder deflection to -25° on C_{l_β} of the model. Removal of both vertical fins reduced positive dihedral effect somewhat.

The configuration with undeflected rudder exhibits positive directional stability over all but the lower angle-of-attack range ($\alpha < 10°$). Increased deflection of the right rudder increased the directional stability. Removal of the vertical fins leads to directional instability at all test angles of attack.

The control effectiveness of deflecting a single rudder (right) is summarized in figure 18 for Mach numbers of 2.96 and 4.63. There is a rapid fall off in rudder effectiveness with increasing angle of attack, suggesting a control problem at the higher angles of attack near maximum lift ($\alpha \approx 50°$). There appears to be no significant Mach number effect on rudder control in this speed regime.

The ability of the elevons to produce roll control is presented in figure 19(a) for both sizes of elevons. The effectiveness appears to be directly proportional to the size of the elevons and the deflection angle, up to differential elevon deflections of ±10°. The interaction of roll control on vehicle yawing moment can be seen in figure 19(b). There is an adverse yawing moment introduced which will be difficult to trim out at the higher angles of attack, because of the reduced rudder effectiveness previously mentioned.

The effect of nose cant on the lateral stability characteristics of the configuration is presented in figures 20 and 21 and summarized in figure 22. Other than an increase in positive dihedral effect with increased nose cant, there is little effect of nose cant on the vehicle lateral characteristics.

CONCLUDING REMARKS

An investigation has been conducted in the Langley Unitary Plan wind tunnel to determine the static longitudinal and lateral stability and control characteristics of a proposed winged reentry vehicle at supersonic speeds. The results indicate that, for the selected center-of-gravity location of 70 percent theoretical root chord, there is a longitudinal trim problem in the desired angle-of-attack range between that for maximum lift-drag ratio and maximum lift. Also, there are large Mach number effects on the pitching-moment characteristics of the vehicle; thus, the shape of the pitching-moment curves changes markedly between Mach numbers of 1.50 and 2.96. Elevon effectiveness and longitudinal stability both decrease with upward elevon deflection at the two higher Mach numbers.

L
1
9
0
5

Lateral stability appears to be satisfactory at all angles of attack above about 10°. Deflection of the right rudder gives adequate control at lower angles of attack, but effectiveness falls off rapidly with increase in angle of attack up to that corresponding to maximum lift (angle of attack $\approx 50^{\circ}$). Differential elevon roll control introduces yawing moments which may be difficult to trim out at higher angles of attack because of the fall off in rudder effectiveness.

Langley Research Center,
National Aeronautics and Space Administration,
Langley Air Force Base, Va., February 2, 1962.

REFERENCES

1. Grimaud, John E.: Wind-Tunnel Investigation at a Mach Number of 2.91 of Stability and Control Characteristics of Three Lifting Reentry Configurations at Angles of Attack up to 90°. NASA TM X-455, 1961.

2. Rainey, Robert W., and Close, William H.: Studies of Stability and Control of Winged Reentry Configurations. NASA TM X-327, 1960.

3. Close, William H.: Hypersonic Longitudinal Trim, Stability, and Control Characteristics of a Delta-Wing Configuration at High Angles of Attack. NASA TM X-240, 1960.

4. Foster, Gerald V.: Static Stability Characteristics of a Series of Hypersonic Boost-Glide Configurations at Mach Numbers of 1.41 and 2.01. NASA TM X-167, 1959.

5. Ladson, Charles L., Johnston, Patrick J., and Trescot, Charles D., Jr.: Effects of Wing Plan-Form Geometry on the Aerodynamic Characteristics of a Hypersonic Glider at Mach Numbers up to 9.6. NASA TM X-286, 1960.

6. Clark, Frank L., and Evans, Joanna M.: Some Aerodynamic and Control Studies of Lifting Reentry Configurations at Angles of Attack up to 90° at a Mach Number of 2.91. NASA TM X-338, 1960.

7. Penland, Jim A., and Armstrong, William O.: Static Longitudinal Aerodynamic Characteristics of Several Wing and Blunt-Body Shapes Applicable for Use as Reentry Configurations at a Mach Number of 6.8 and Angles of Attack up to 90°. NASA TM X-65, 1959.

8. Rainey, Robert W., Fetterman, David E., Jr., and Smith, Robert: Summary of the Static Stability and Control Results of a Hypersonic Glider Investigation. NASA TM X-277, 1960.

9. Rainey, Robert W.: Static Stability and Control of Hypersonic Gliders. NACA RM L58E12a, 1958.

10. Armstrong, William O., and Ladson, Charles L. (With Appendix A by Donald L. Baradell and Thomas A. Blackstock): Effects of Variation in Body Orientation and Wing and Body Geometry on Lift-Drag Characteristics of a Series of Wing-Body Combinations at Mach Numbers From 3 to 18. NASA TM X-73, 1959.

11. Penland, Jim A., and Armstrong, William O.: Preliminary Aerodynamic Data Pertinent to Manned Satellite Reentry Configurations. NACA RM L58E13a, 1958.

12. McLellan, Charles H., and Ladson, Charles L.: A Summary of the Aerodynamic Performance of Hypersonic Gliders. NASA TM X-237, 1960.

13. Shanks, Robert E.: Investigation of the Low Subsonic Stability and Control Characteristics of a Hypersonic Boost-Glide Type Airplane With Wing, Fuselage, and Vertical-Tail Modifications. NASA TM X-450, 1961.

14. West, F. E., Jr., Trescot, Charles D., Jr., and Wiley, Alfred N., Jr.: Aerodynamic Characteristics for Two Hypersonic Glider Models With and Without Wing and Vertical-Tail Trailing-Edge Chord-Extensions at a Mach Number of 0.94. NASA TM X-66, 1960.

15. Allen, Clyde Q.: Low-Speed Aerodynamic Characteristics of a Model of the DS-1 Glider. NASA TM X-573, 1961.

TABLE I.- MODEL DIMENSIONAL CHARACTERISTICS

	BWE_1	BWE_1F	BWE_4F
Wing area, sq ft	0.90618	0.90618	0.82715
Nose area, sq ft	0.14555	0.14555	0.14555
Elevon area (plan, both), sq ft . .	0.15792	0.15792	0.07896
Vertical fin area (plan, both), sq ft . .	-------	0.23561	0.23561
Rudder area (plan, one), sq ft . .	-------	0.04708	0.04708
c_r, in.	20.246	20.246	20.246

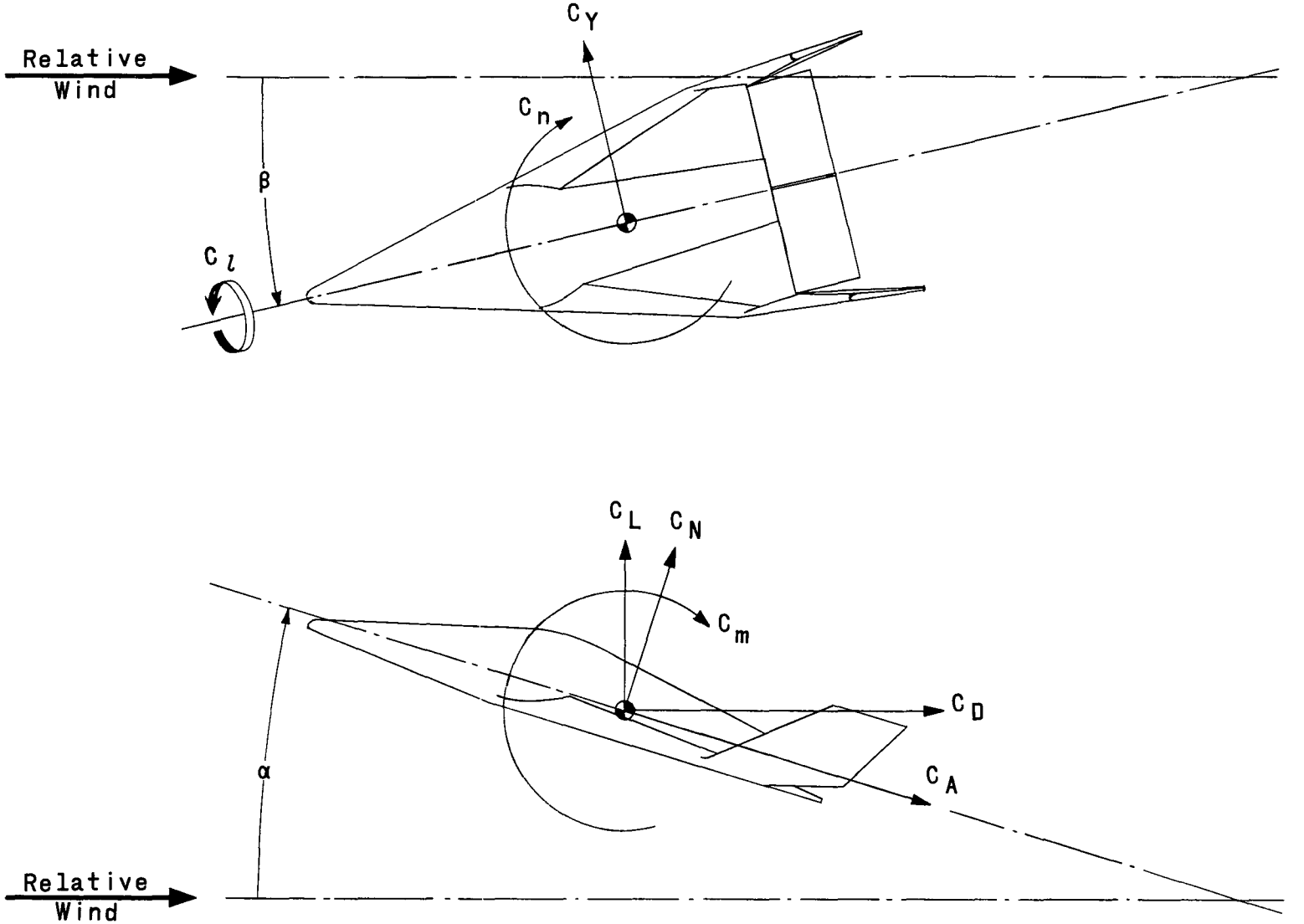

Figure 1.- Axes system. Arrows indicate positive directions.

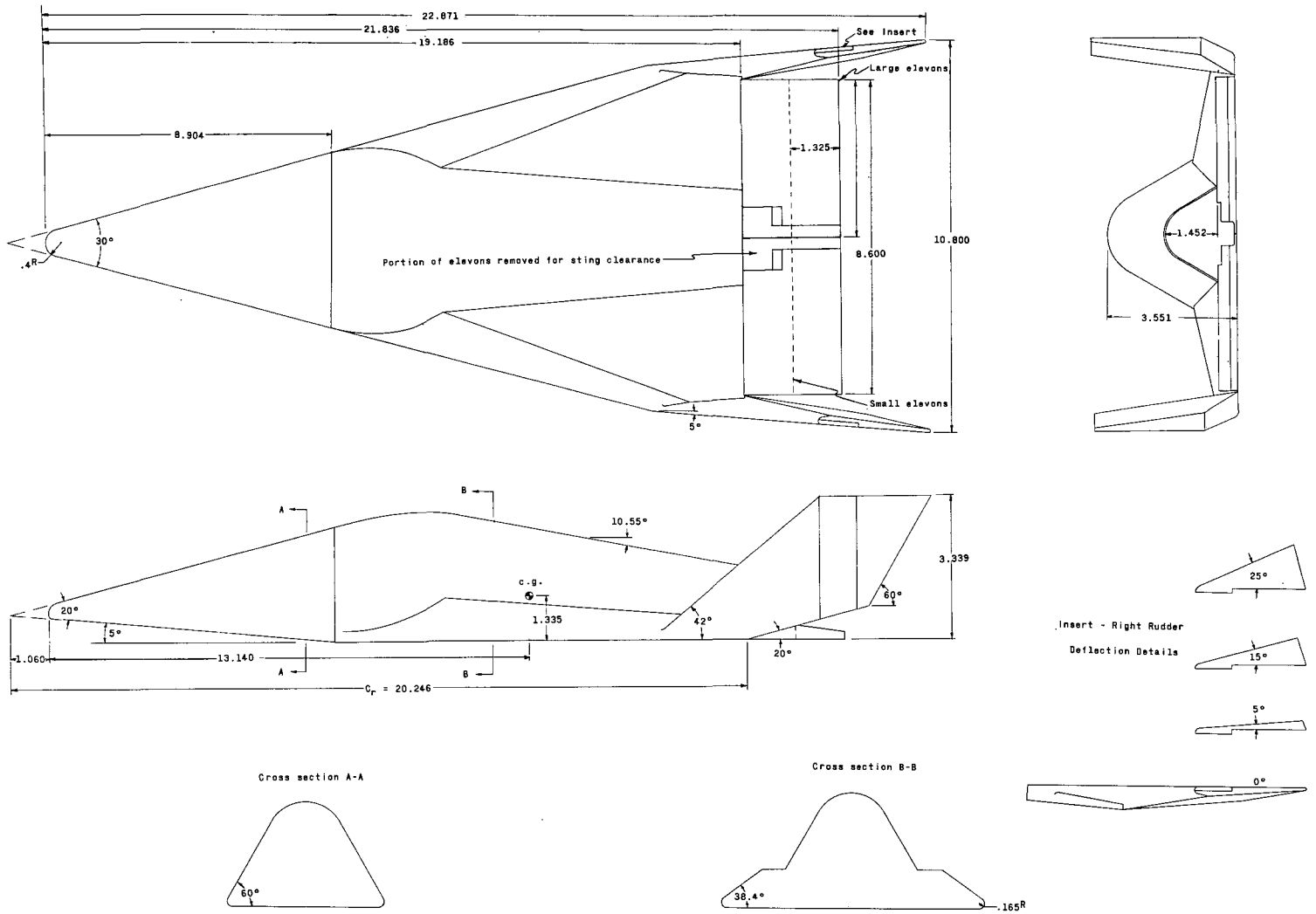

Figure 2.- Three-view drawing of model. All dimensions are in inches unless otherwise noted.

CONFIDENTIAL

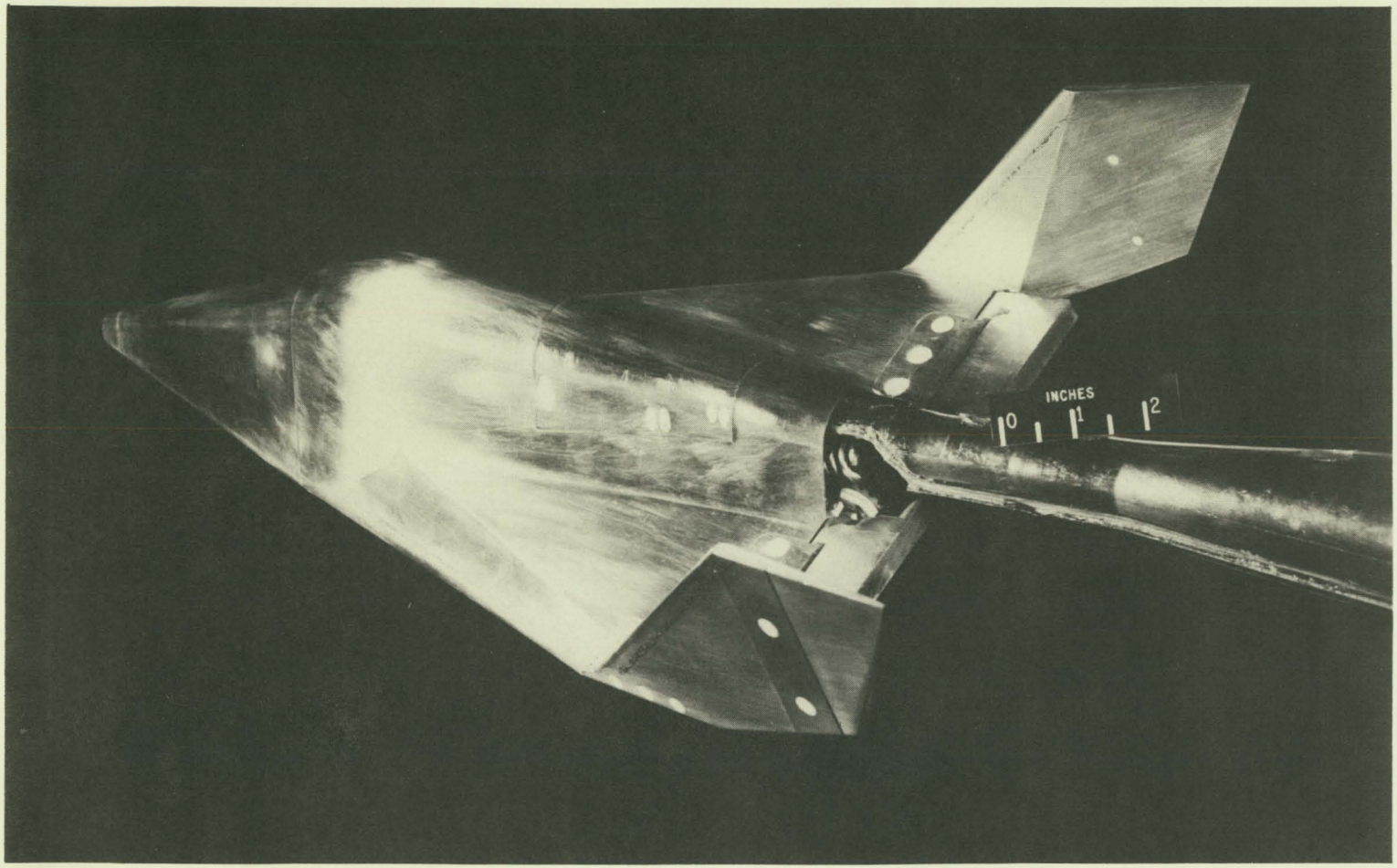

CONFIDENTIAL

L-61-6325

(a) Three-quarter rear top view of basic BWE_4F configuration on 0° straight sting. $\delta_e = 0^\circ$.

Figure 3.- Model used in investigation.

CONFIDENTIAL

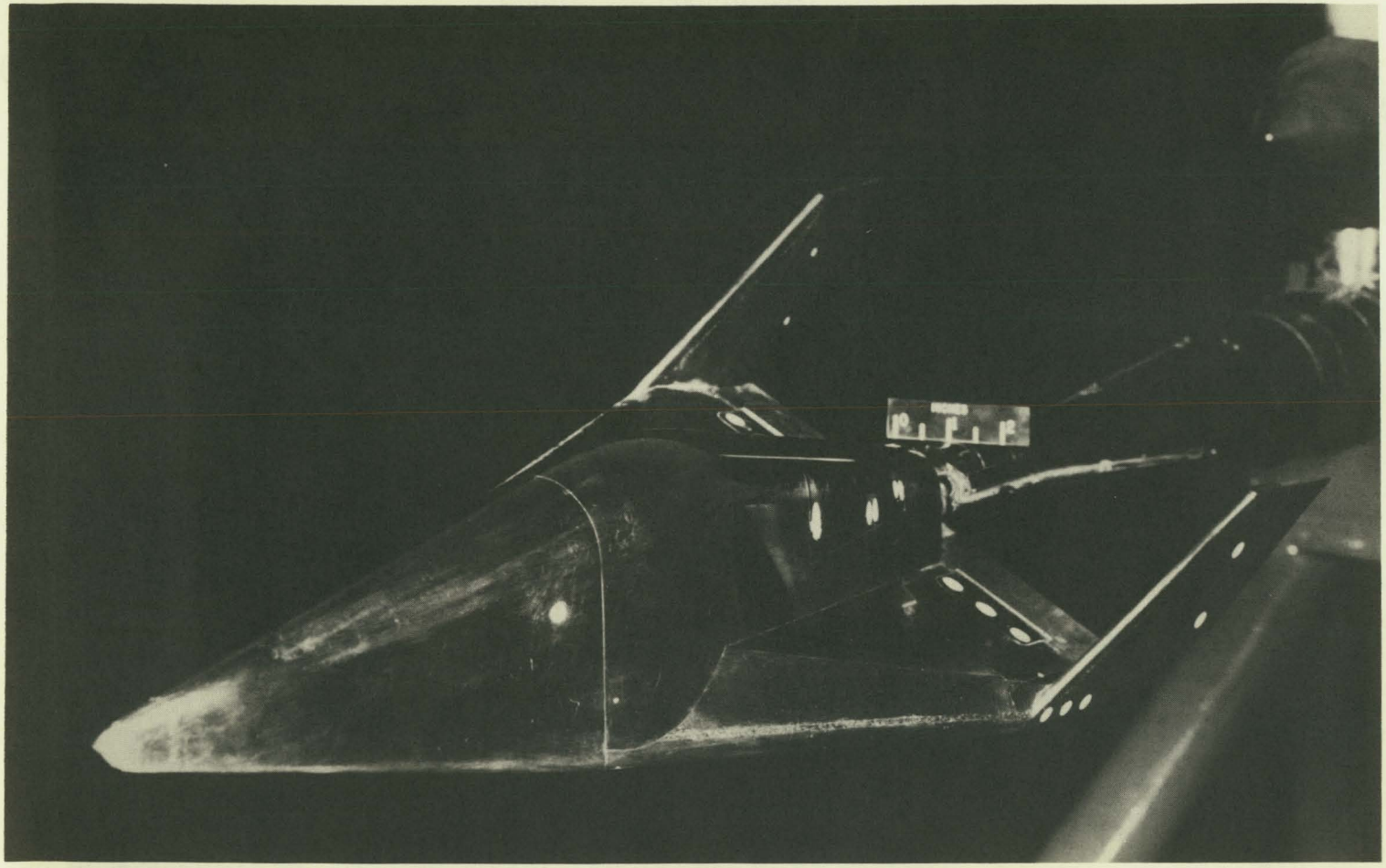

L-61-6324

(b) Three-quarter front top view of basic BWE_4F configuration on 0° straight sting. $\delta_e = 0°$.

Figure 3.- Continued.

CONFIDENTIAL

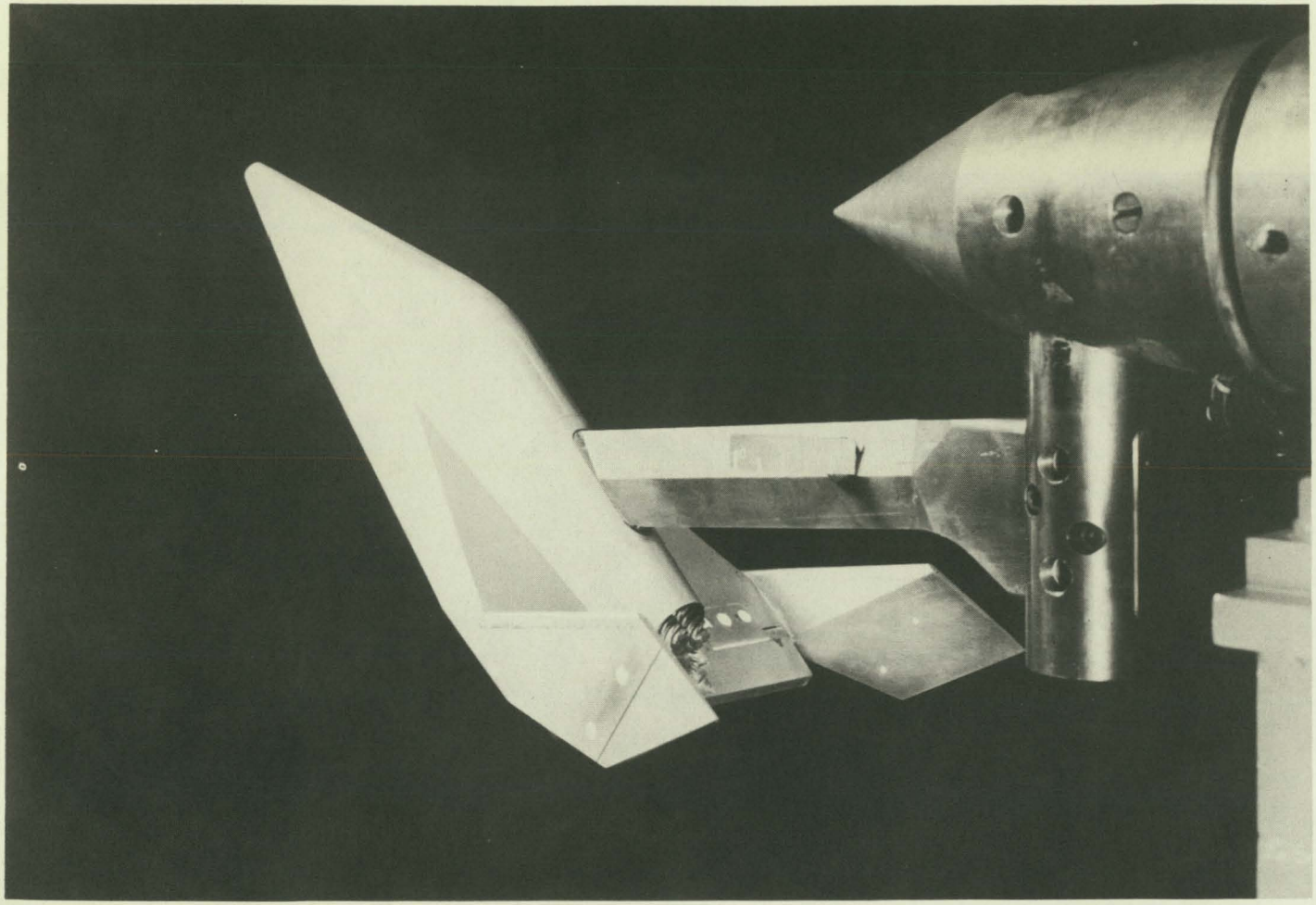

L-61-6317

(c) Three-quarter rear view of basic BWE_4F configuration on high angle sting. $\delta_e = 0^\circ$.

Figure 3.- Continued.

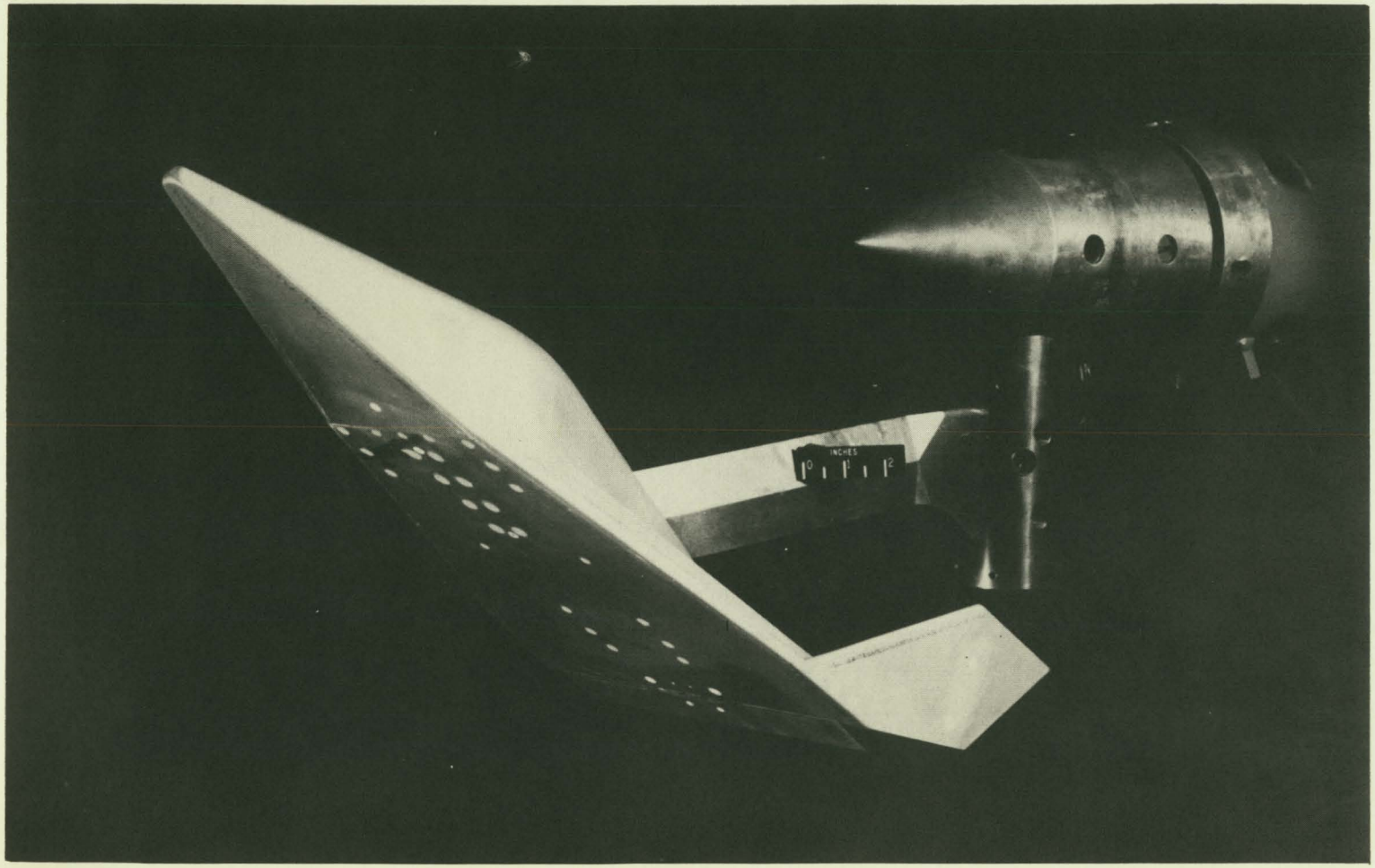

L-61-6319

(d) Three-quarter front view of basic BWE_4F configuration on high angle sting. $\delta_e = 0^\circ$.

Figure 3.- Concluded.

CONFIDENTIAL

CONFIDENTIAL

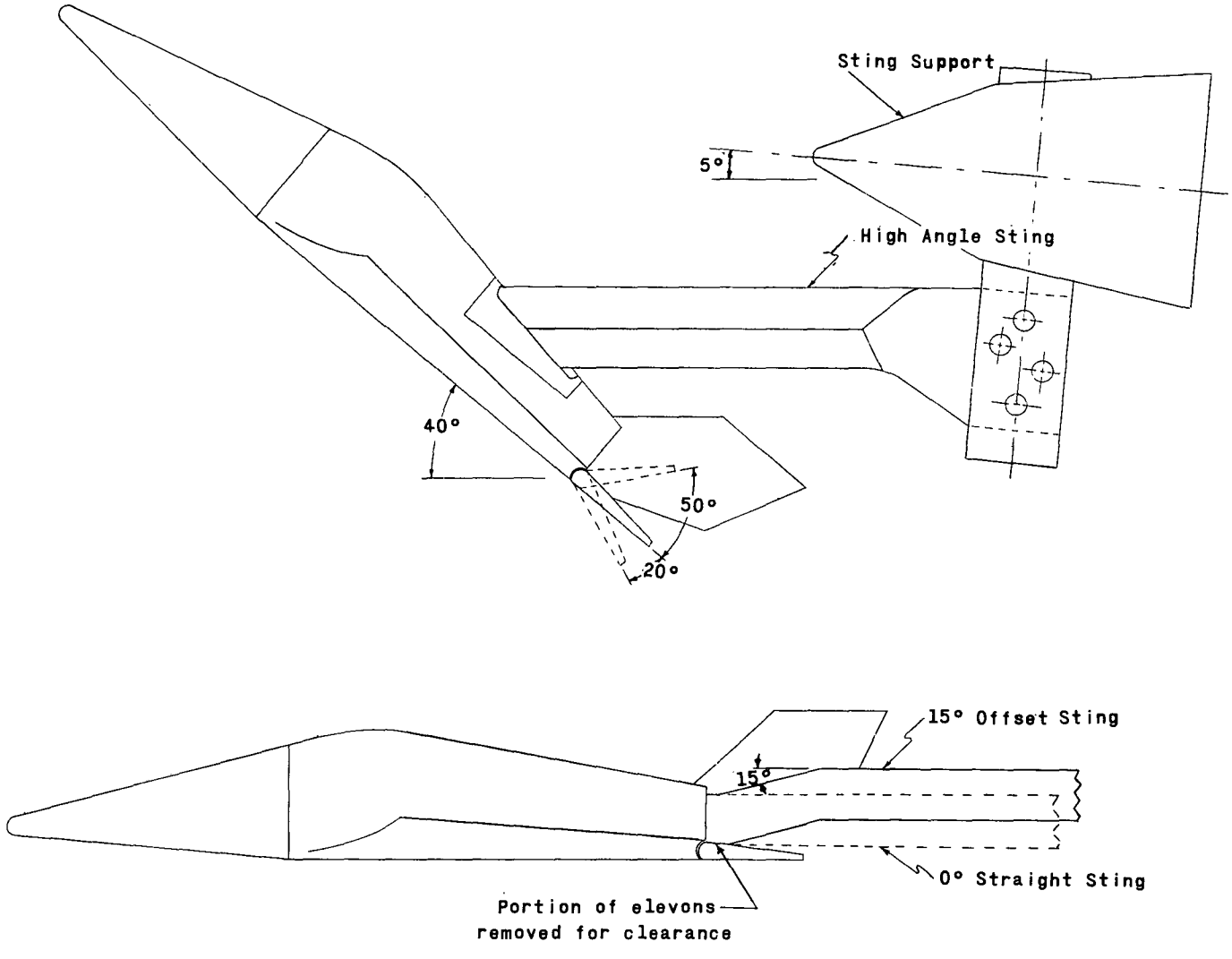

Figure 4.- Three sting arrangements used for tests (model left vertical fin omitted for clarity).

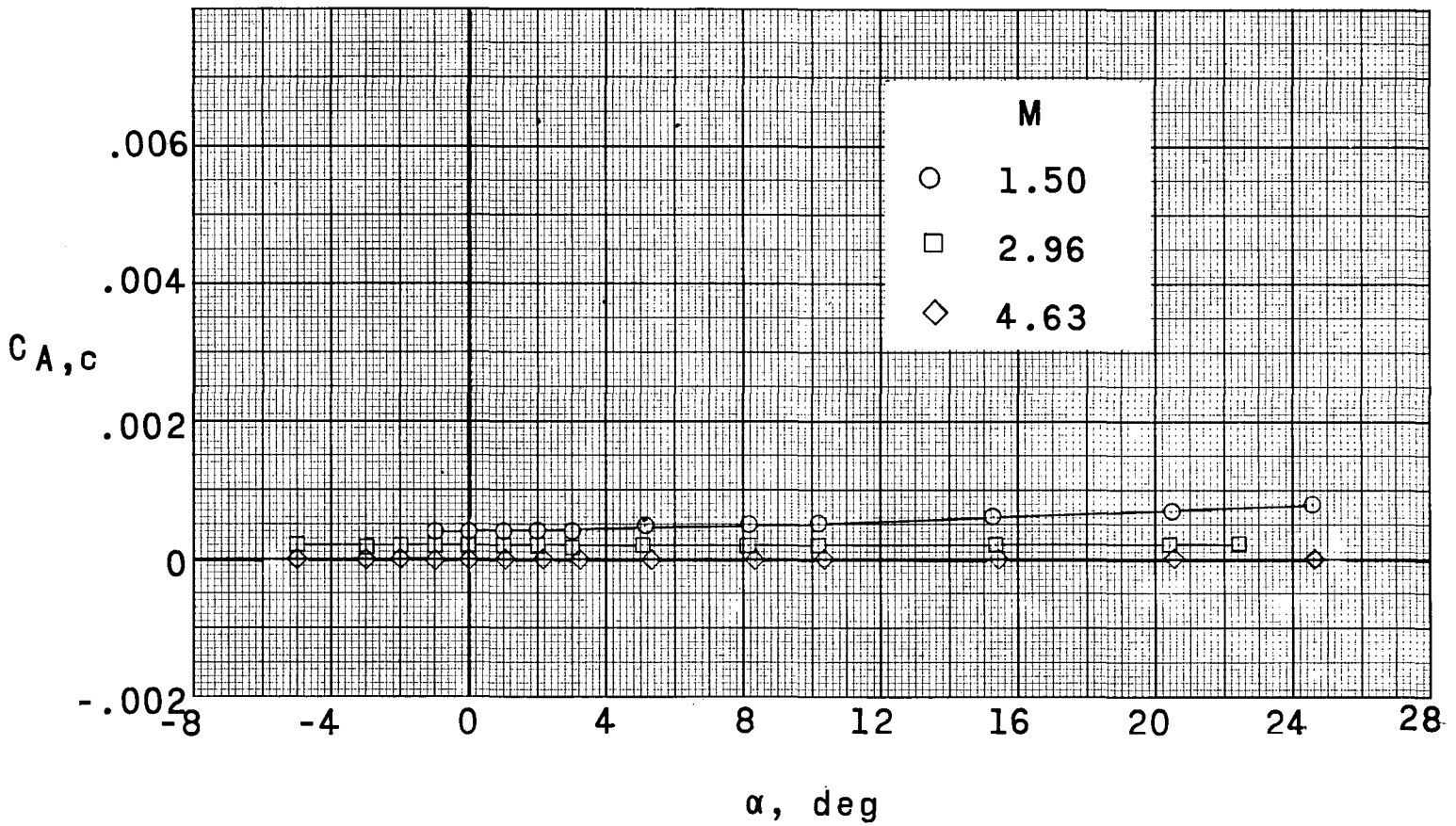

Figure 5.- Representative values of $C_{A,c}$ for the basic BWE_1F configuration. $\delta_e = 0^\circ$; $\delta_r = 0^\circ$.

CONFIDENTIAL

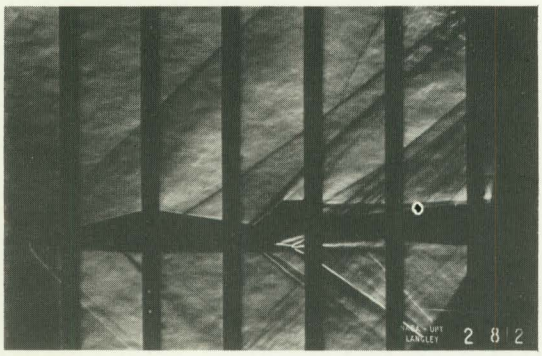

α = 0°

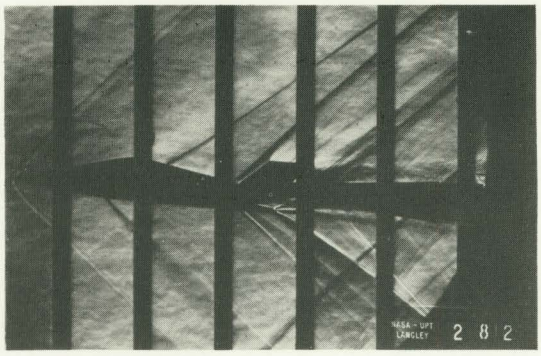

α = 5.1°

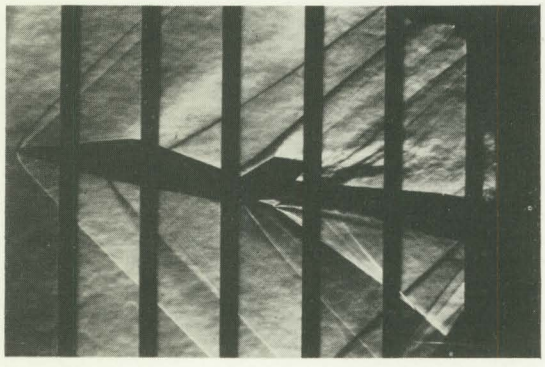

α = 10.2°

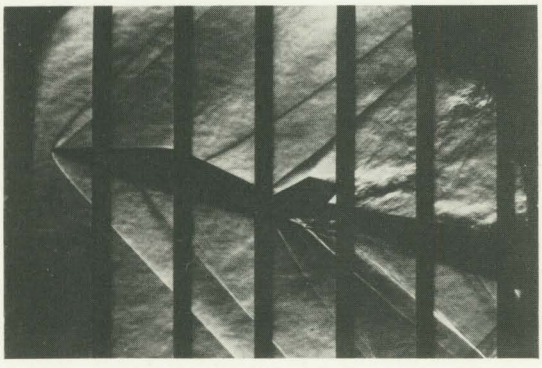

α = 15.3°

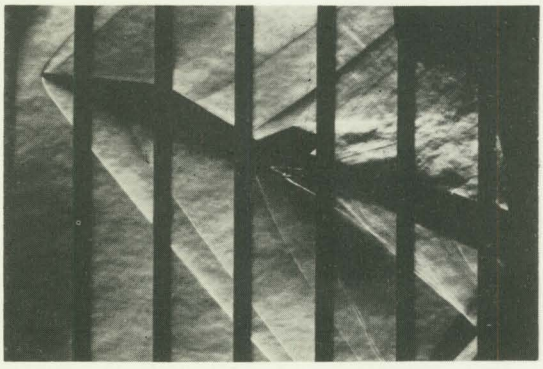

α = 20.4°

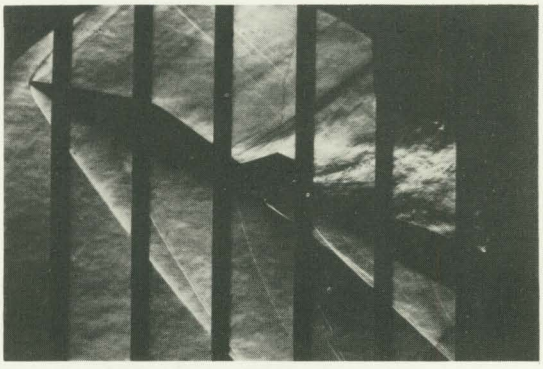

α = 24.5°

L-62-30

(a) Basic BWE_1F configuration with 15° offset sting at $M = 1.50$. $\delta_e = 0°$; $\delta_r = 0°$.

Figure 6.- Selected schlieren photographs.

CONFIDENTIAL

L-1905

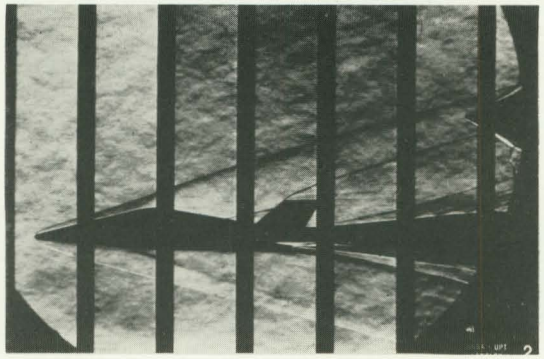

α = 0.2°

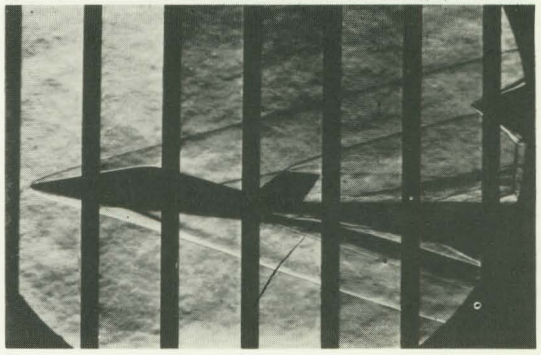

α = 5.2°

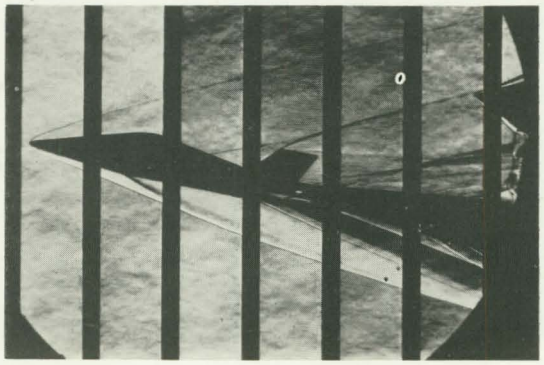

α = 10.3°

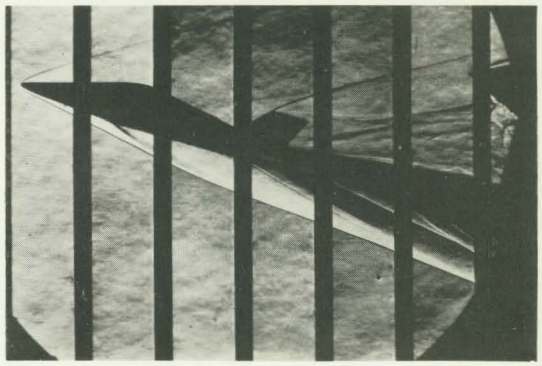

α = 15.4°

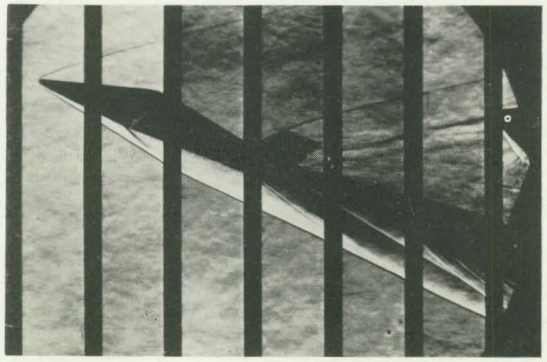

α = 20.5°

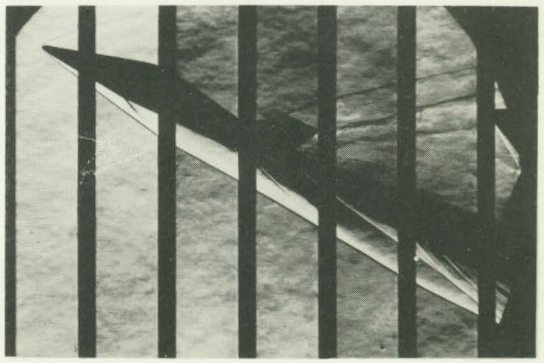

α = 24.5°

L-62-31

(b) Basic BWE_1F configuration with 0° straight sting at $M = 4.63$. $\delta_e = 0^\circ$; $\delta_r = 0^\circ$.

Figure 6.- Continued.

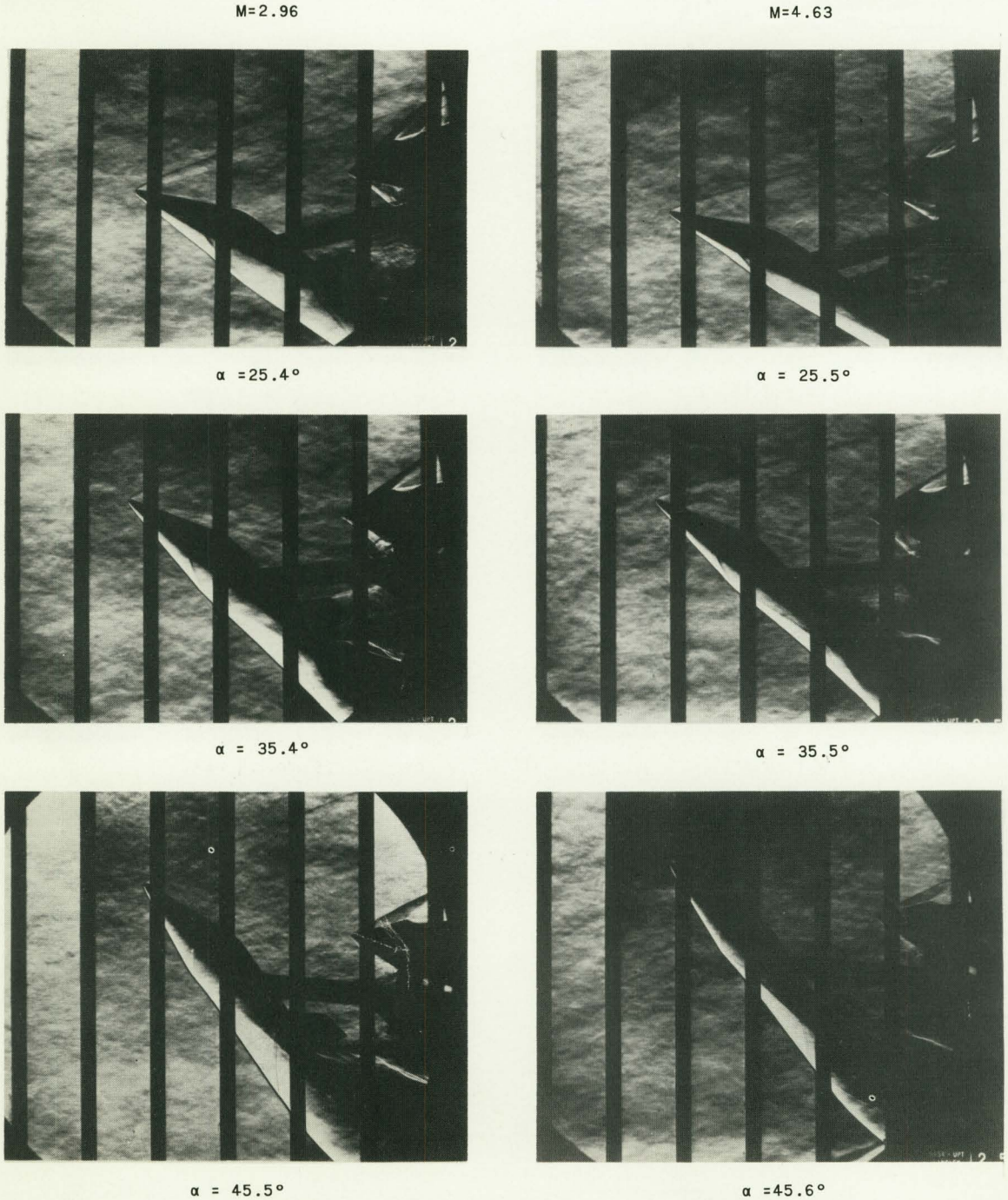

(c) Basic BWE_1F configuration with high angle sting L-62-32 at $M = 2.96$ and $M = 4.63$. $\delta_e = 0^\circ$; $\delta_r = 0^\circ$.

Figure 6.- Concluded.

L-1905

L-1905

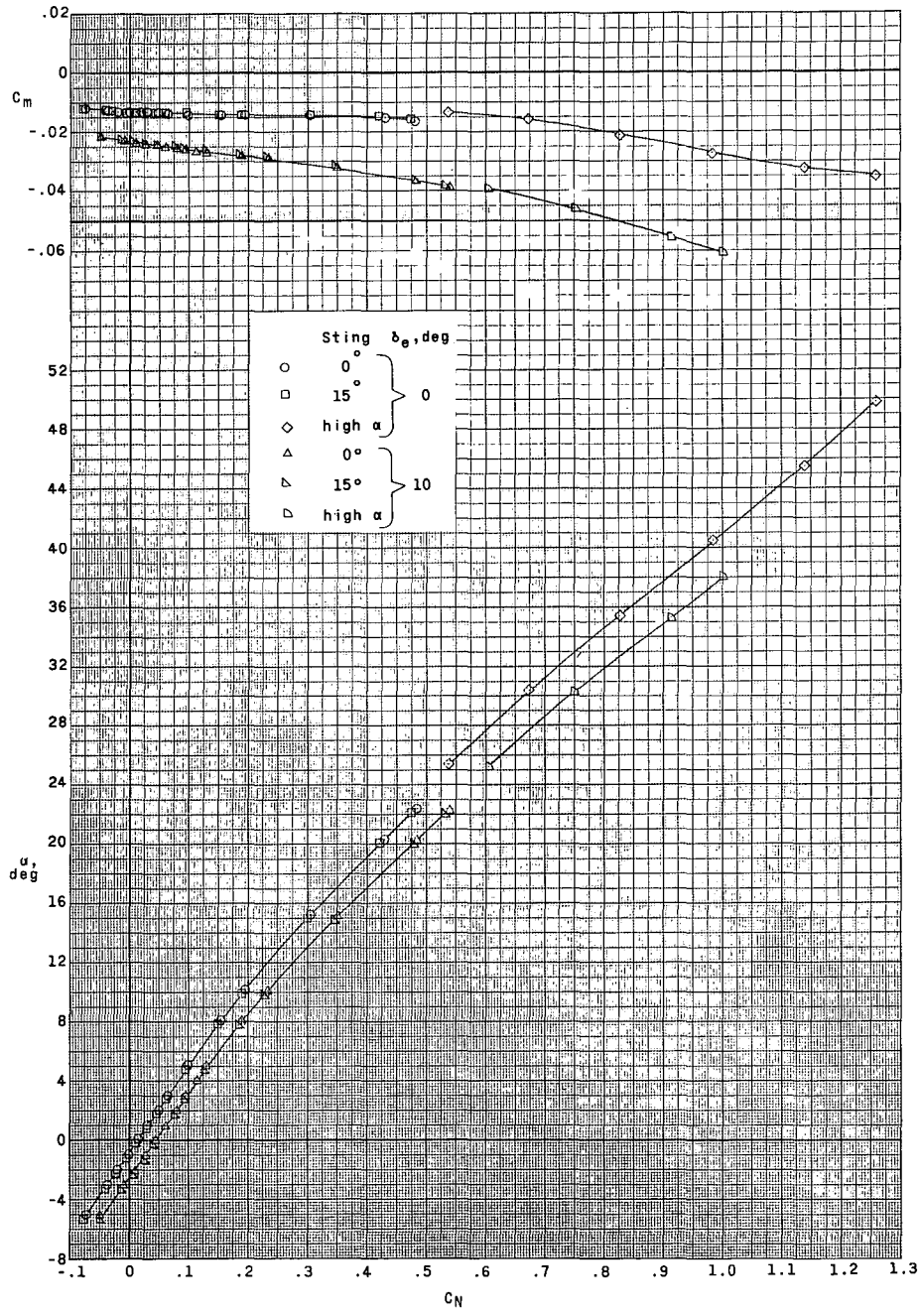

(a) C_m and α against C_N for basic BWE_1F configuration at $M = 2.96$. $\delta_r = 0^\circ$.

Figure 7.- Effect of sting arrangement on longitudinal data.

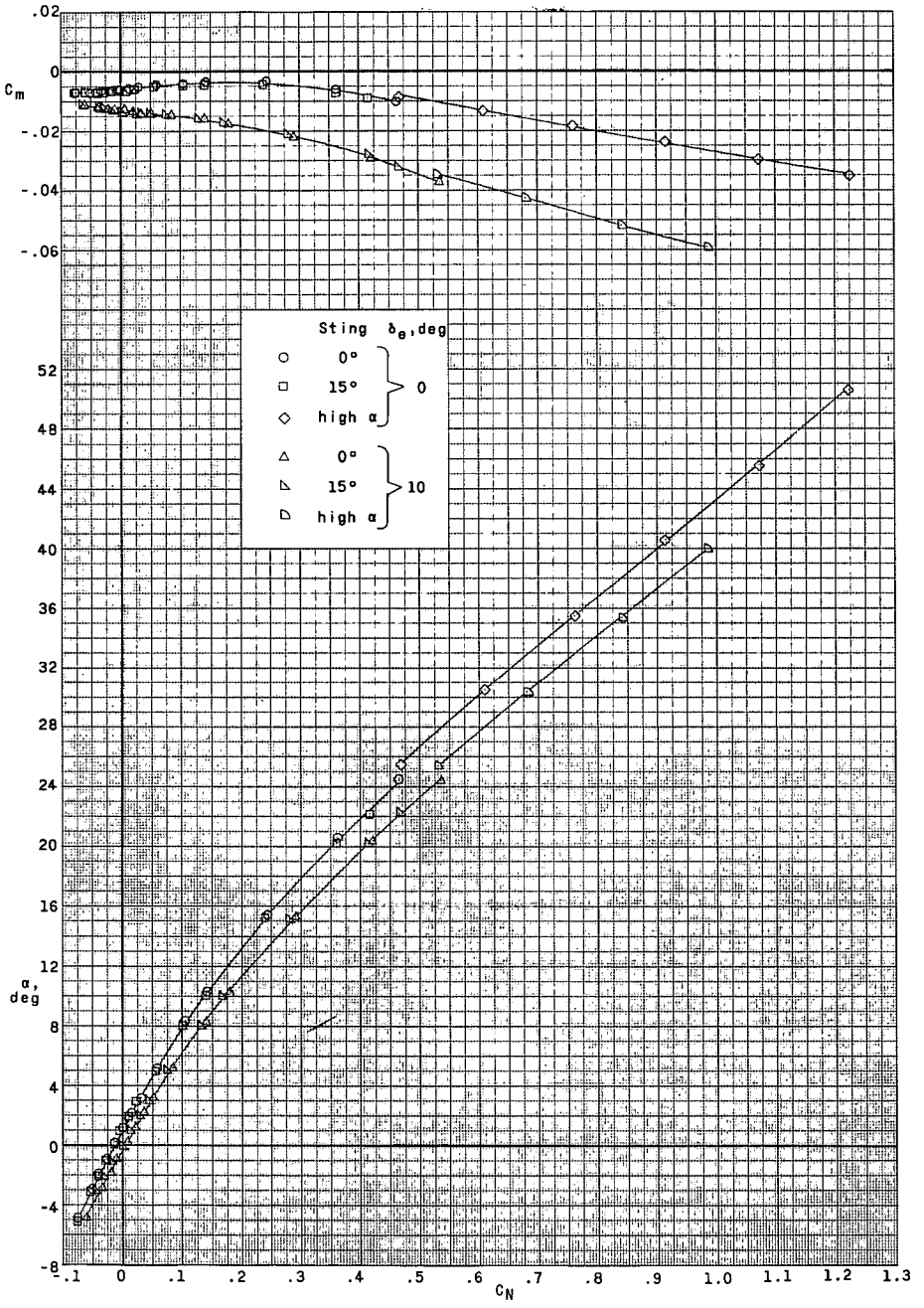

(b) C_m and α against C_N for the basic BWE_1F configuration at $M = 4.63$. $\delta_r = 0^o$.

Figure 7.- Continued.

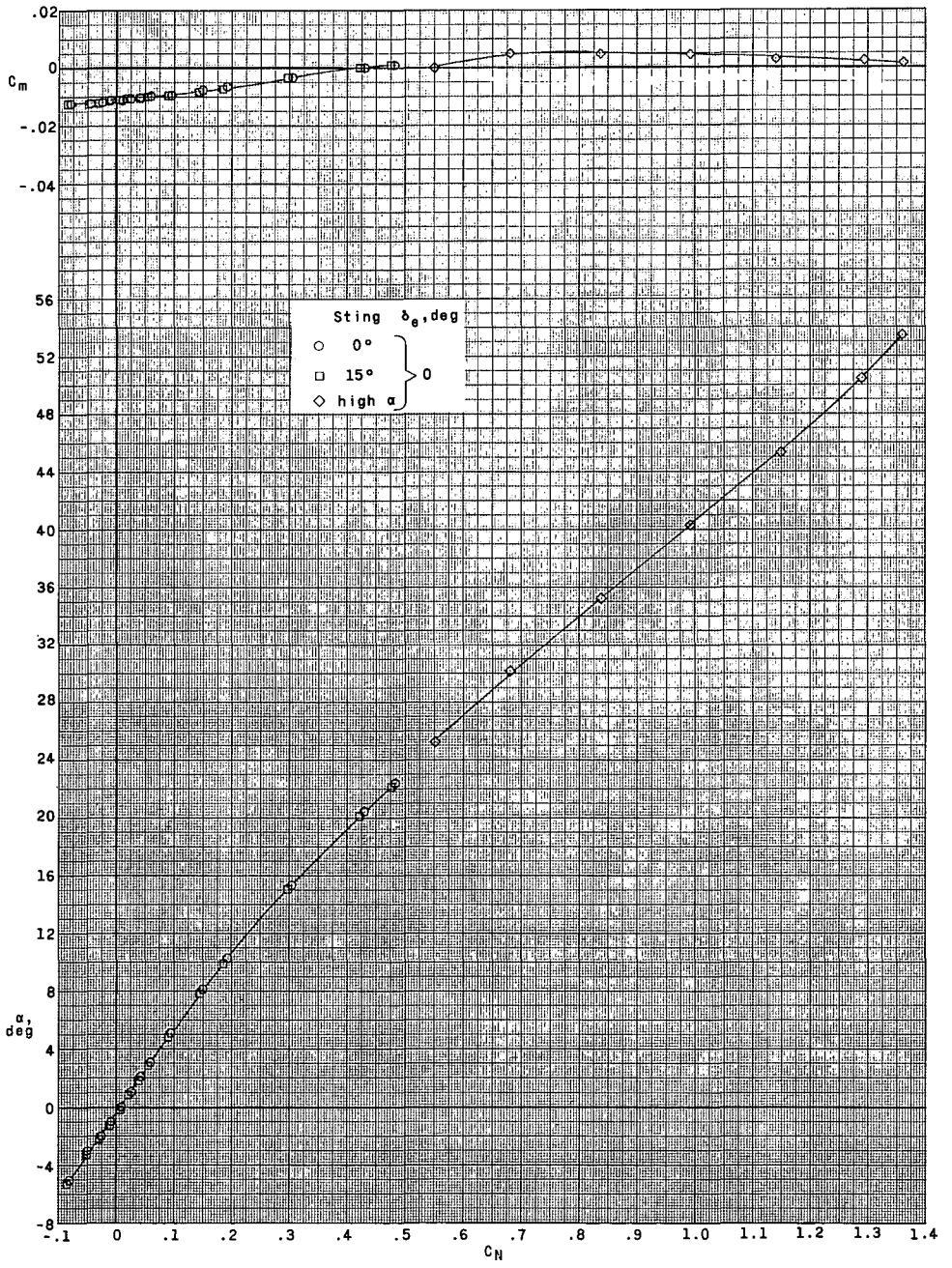

(c) C_m and α against C_N for the basic BWE_4F configuration at $M = 2.96$. $\delta_r = 0^o$.

Figure 7.- Continued.

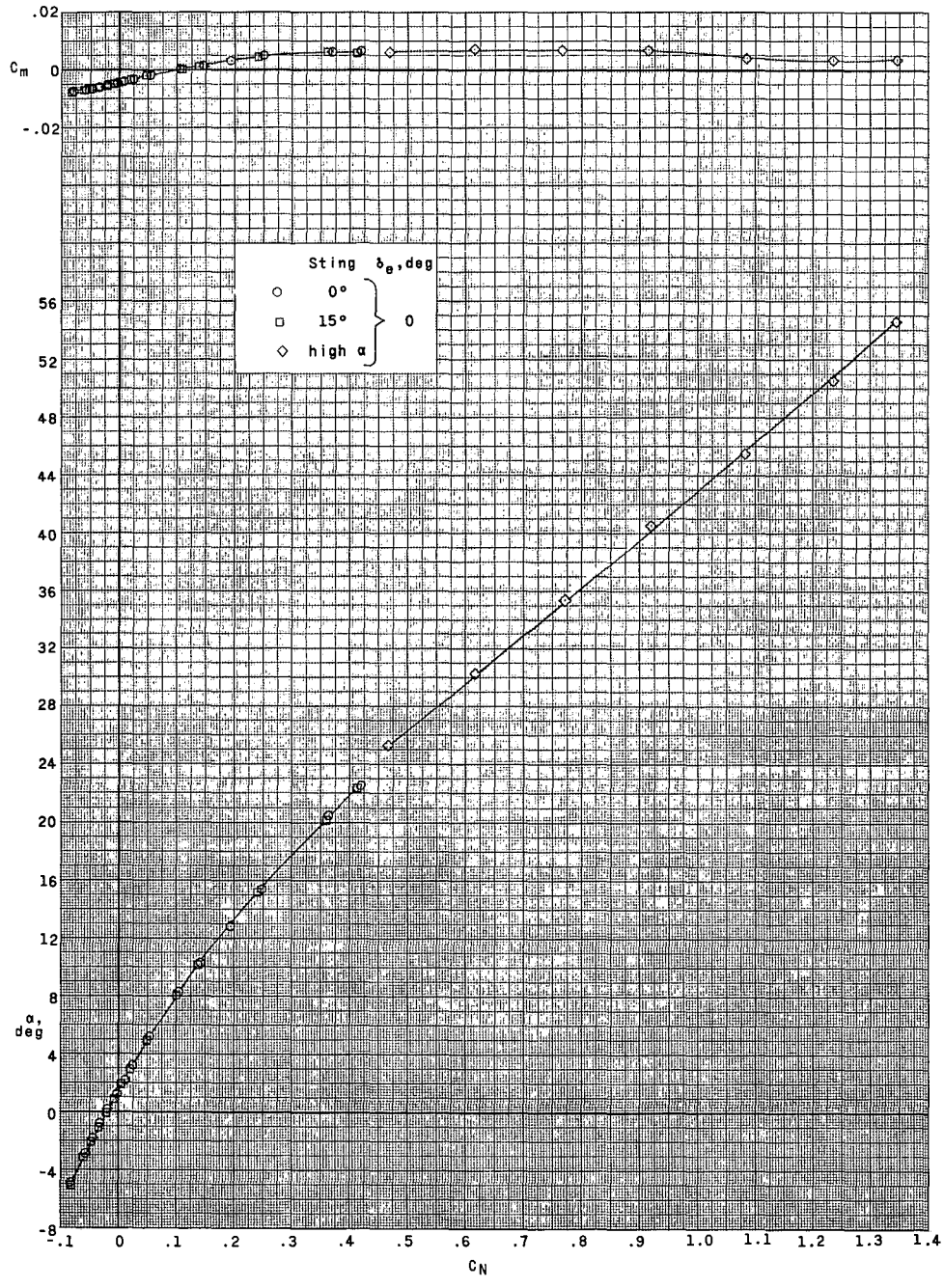

(d) C_m and α against C_N for the basic BWE_4F configuration at $M = 4.63$. $\delta_r = 0^\circ$.

Figure 7.- Continued.

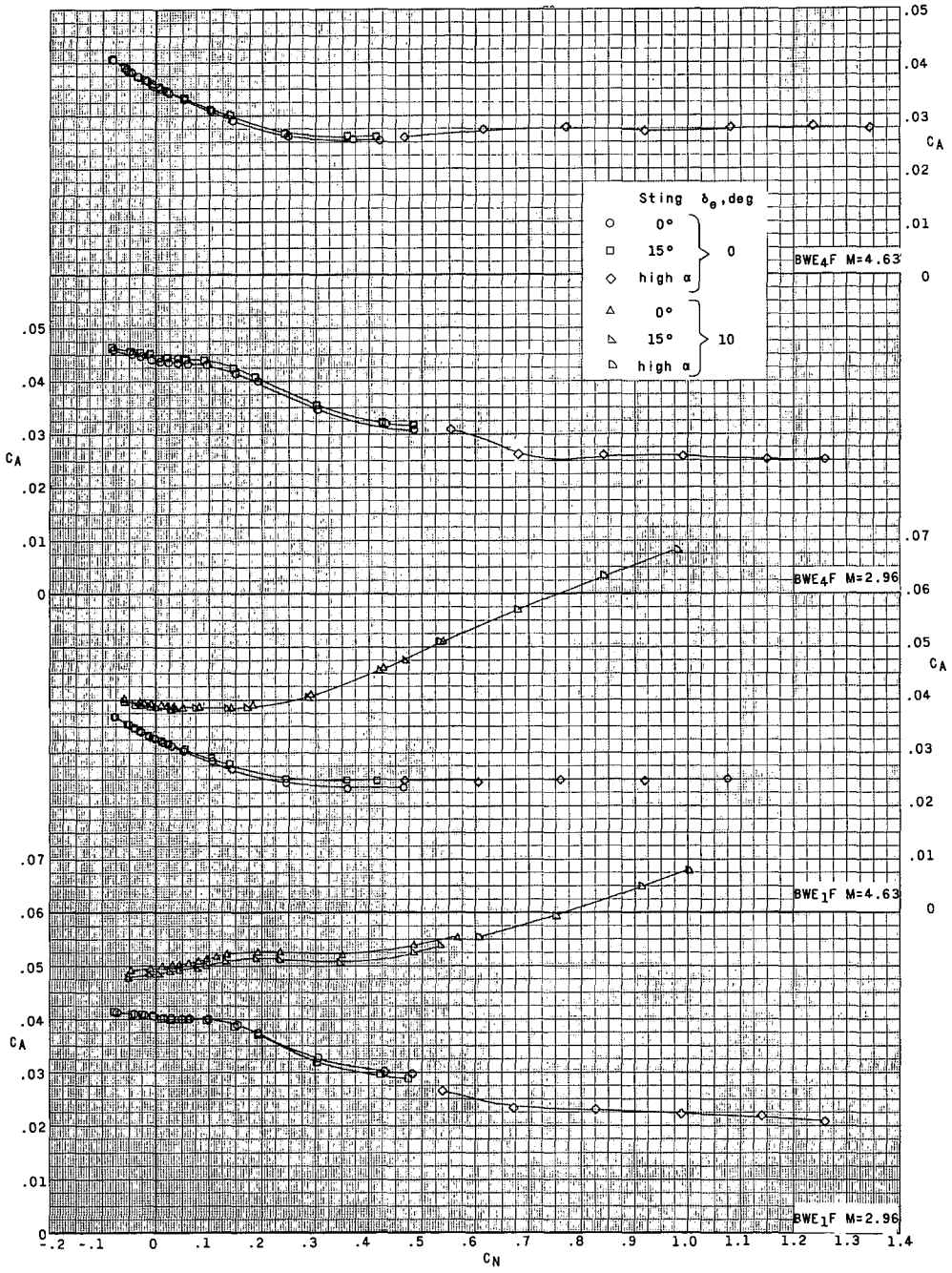

(e) Combined C_A against C_N for BWE_1F and BWE_4F at $M = 2.96$ and $M = 4.63$; $\delta_r = 0^o$.

Figure 7.- Concluded.

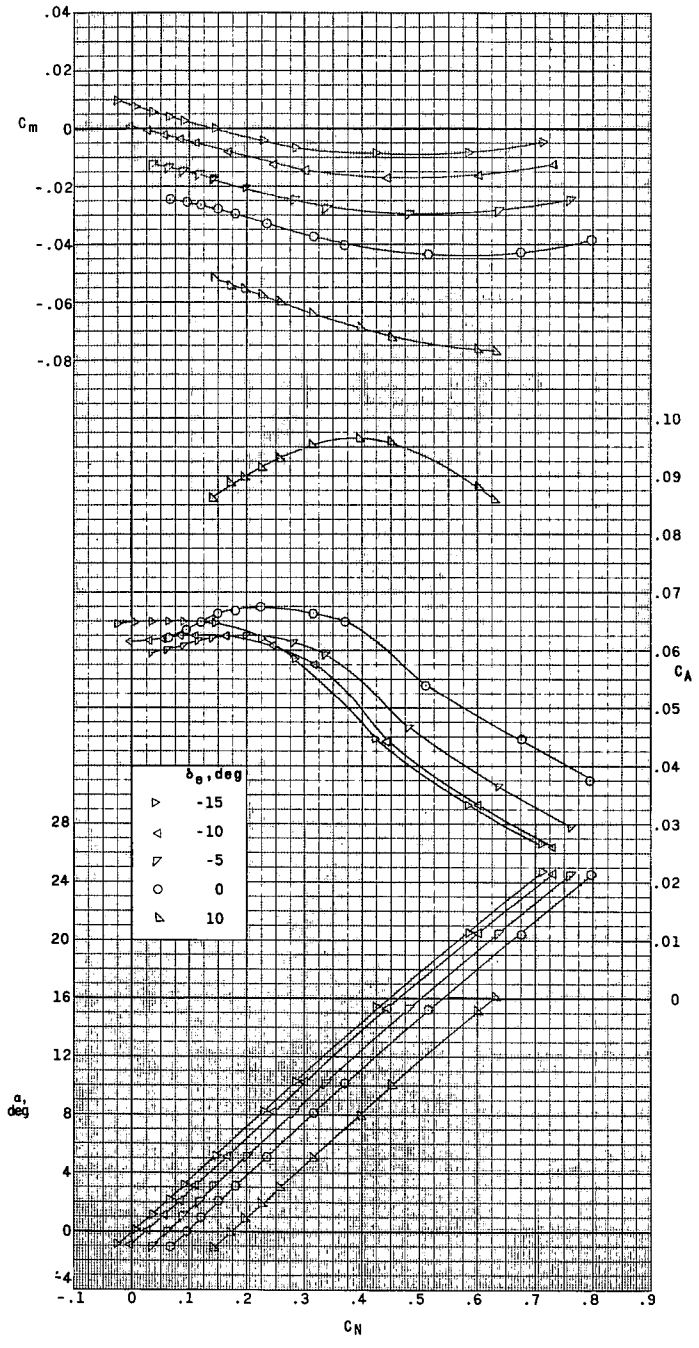

(a) M = 1.50.

Figure 8.- Longitudinal aerodynamic characteristics of basic BWE_1F configuration. $\delta_r = 0^o$.

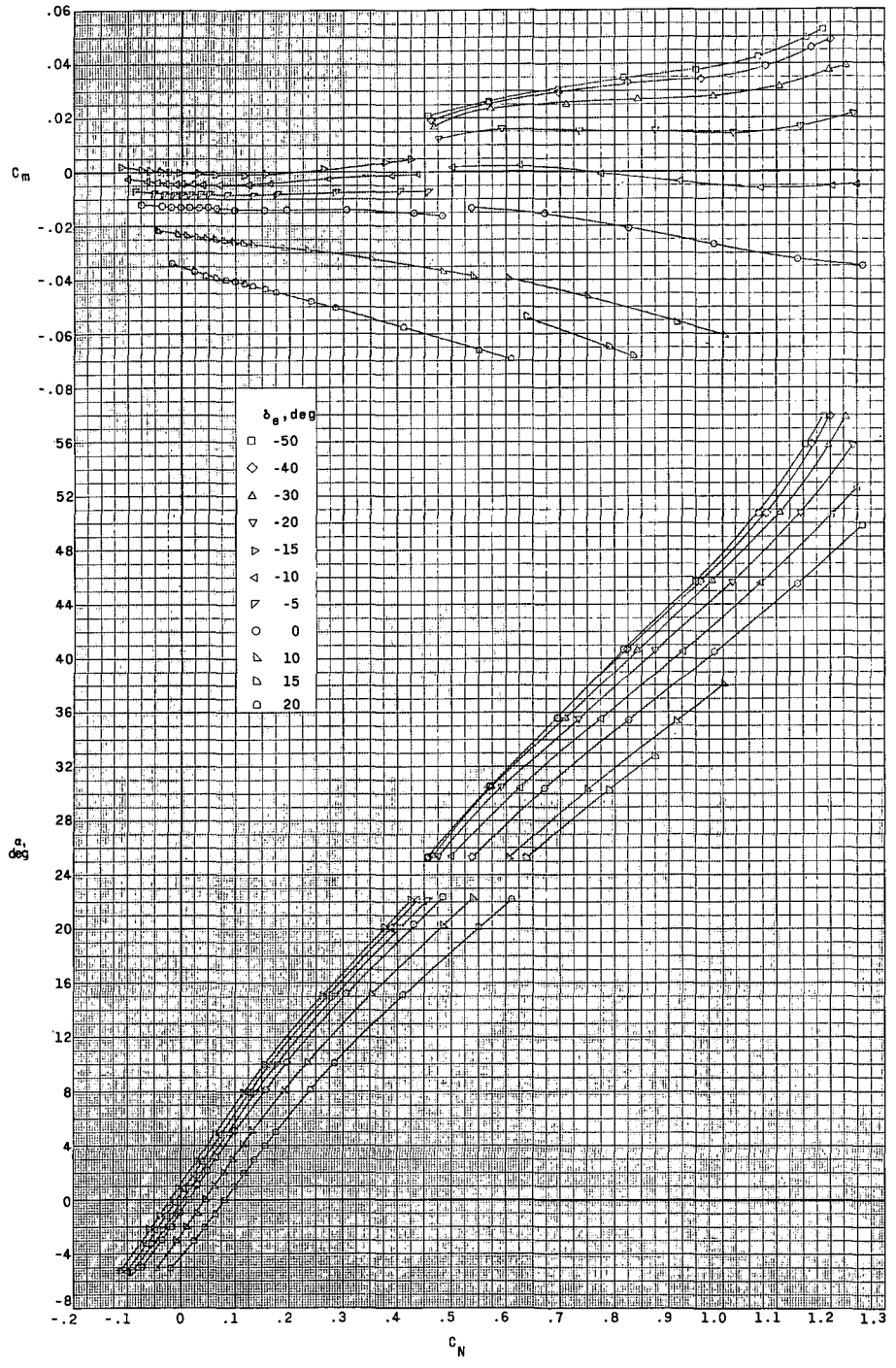

(b) M = 2.96.

Figure 8.- Continued.

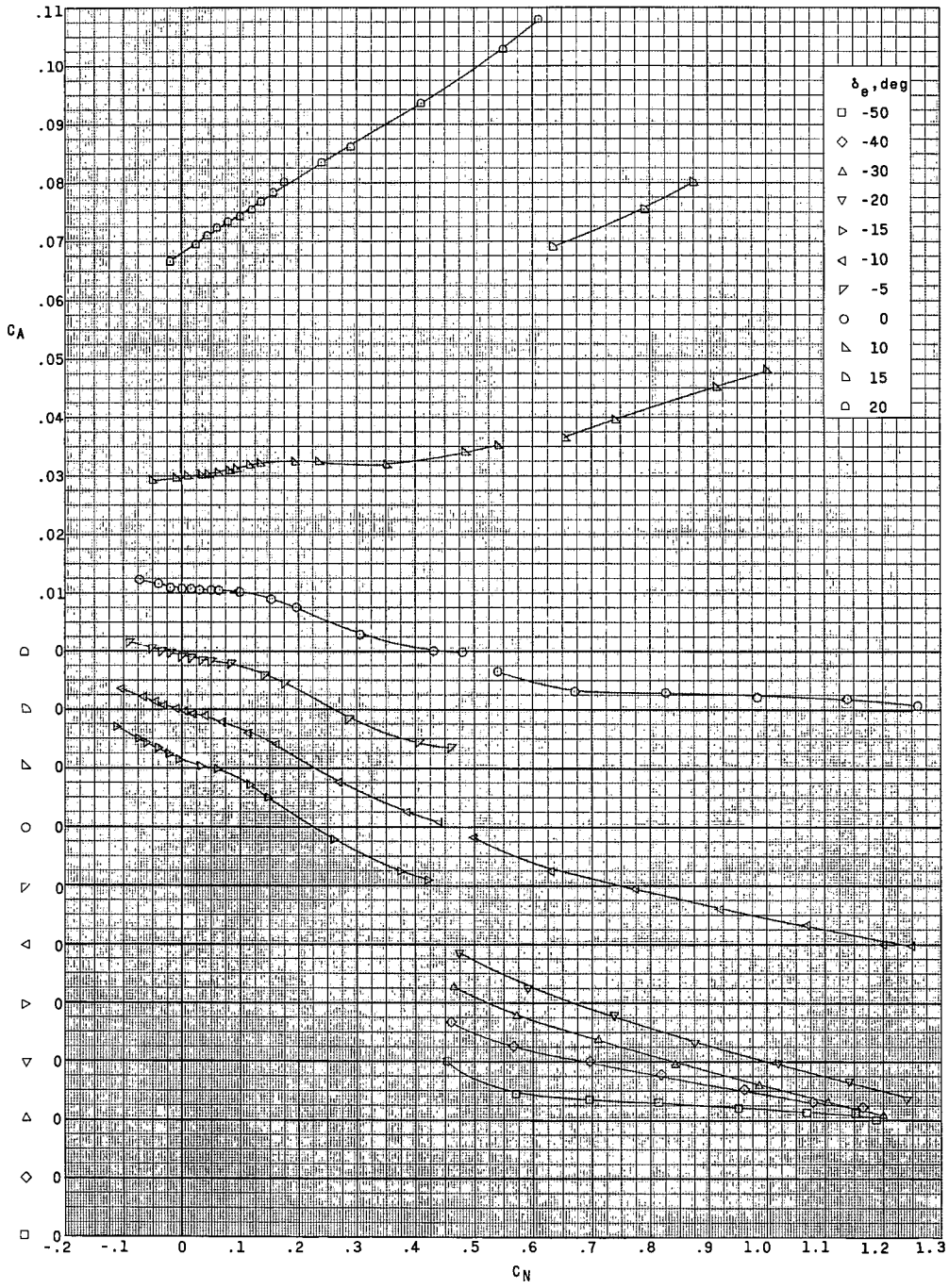

(b) Concluded.

Figure 8.- Continued.

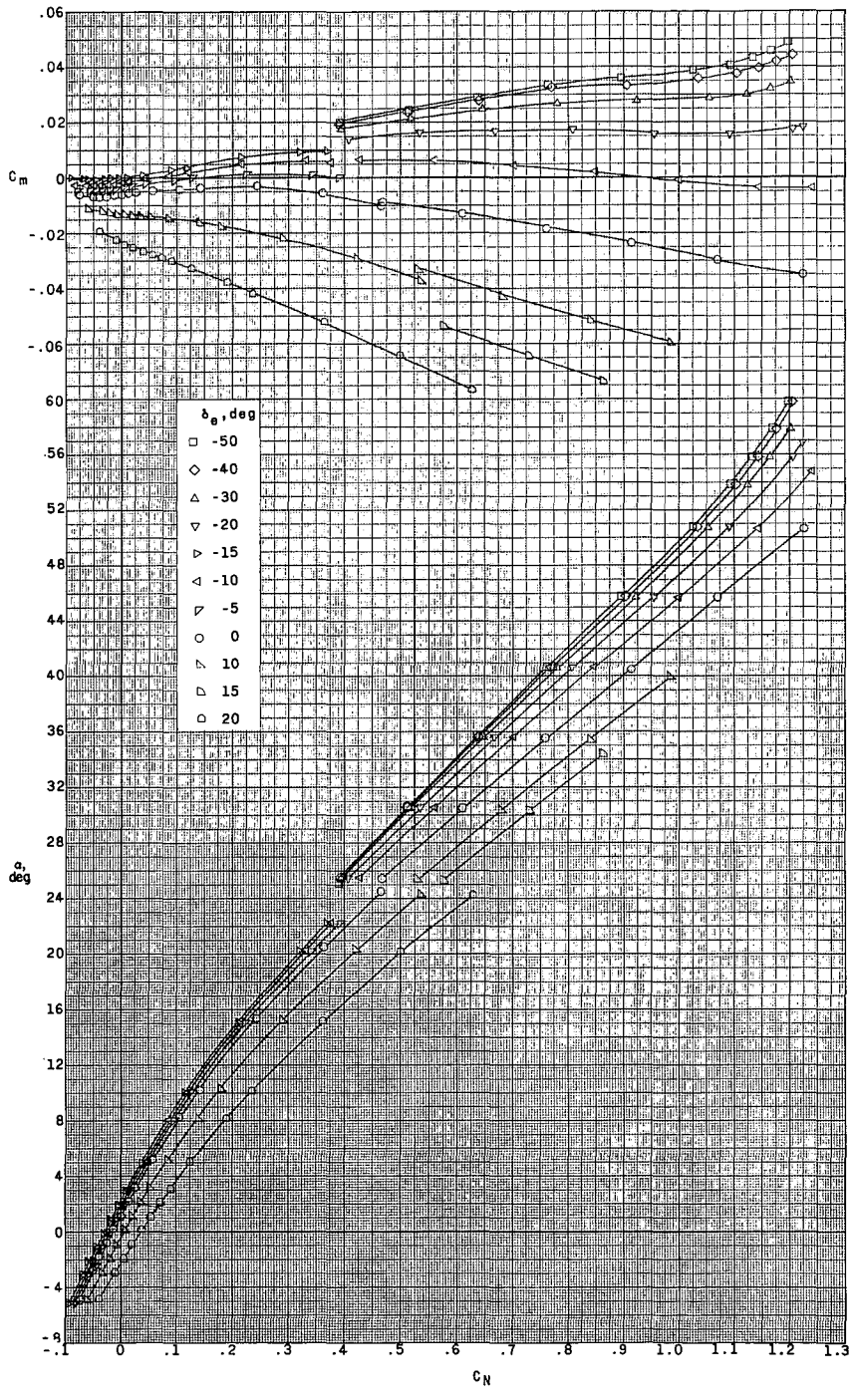

(c) M = 4.63.

Figure 8.- Continued.

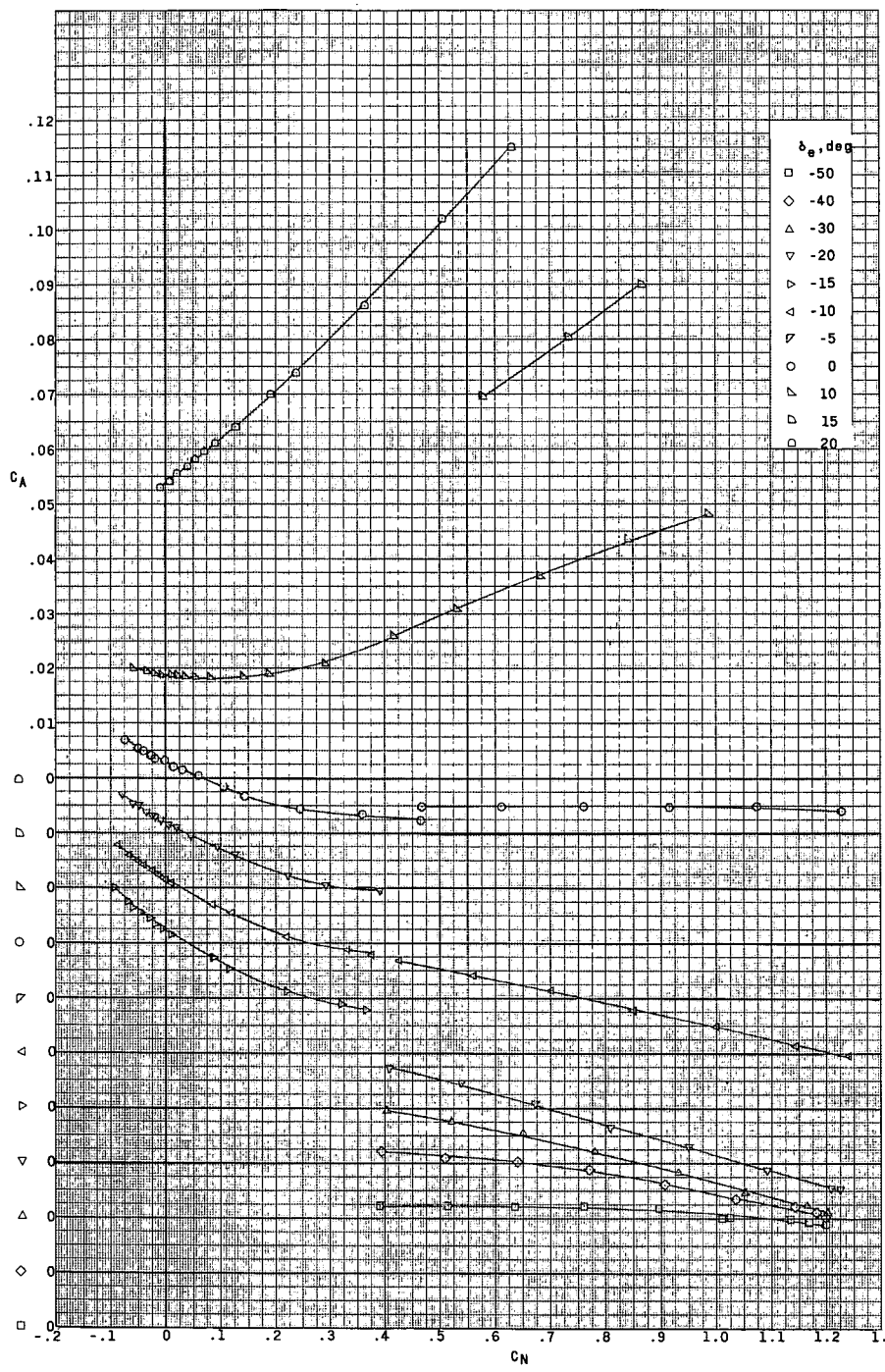

(c) Concluded.

Figure 8.- Concluded.

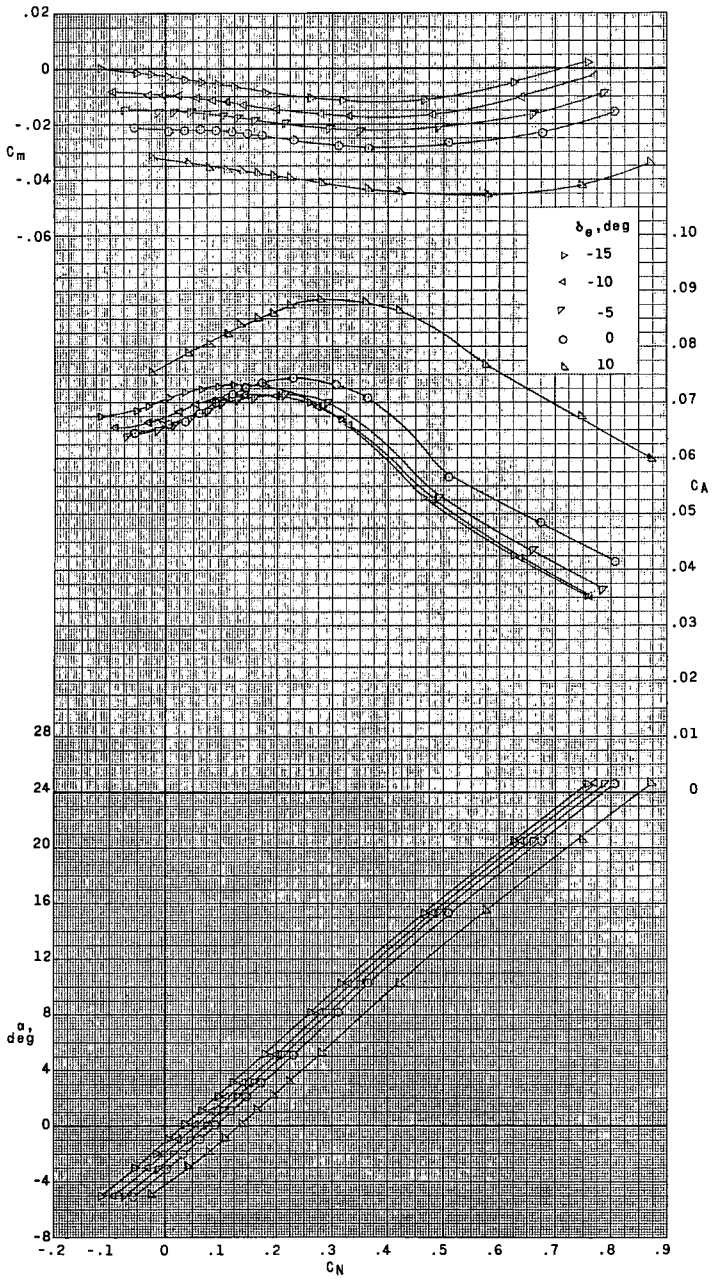

(a) M = 1.50.

Figure 9.- Longitudinal aerodynamic characteristics of basic BWE_4F configuration. $\delta_r = 0^\circ$.

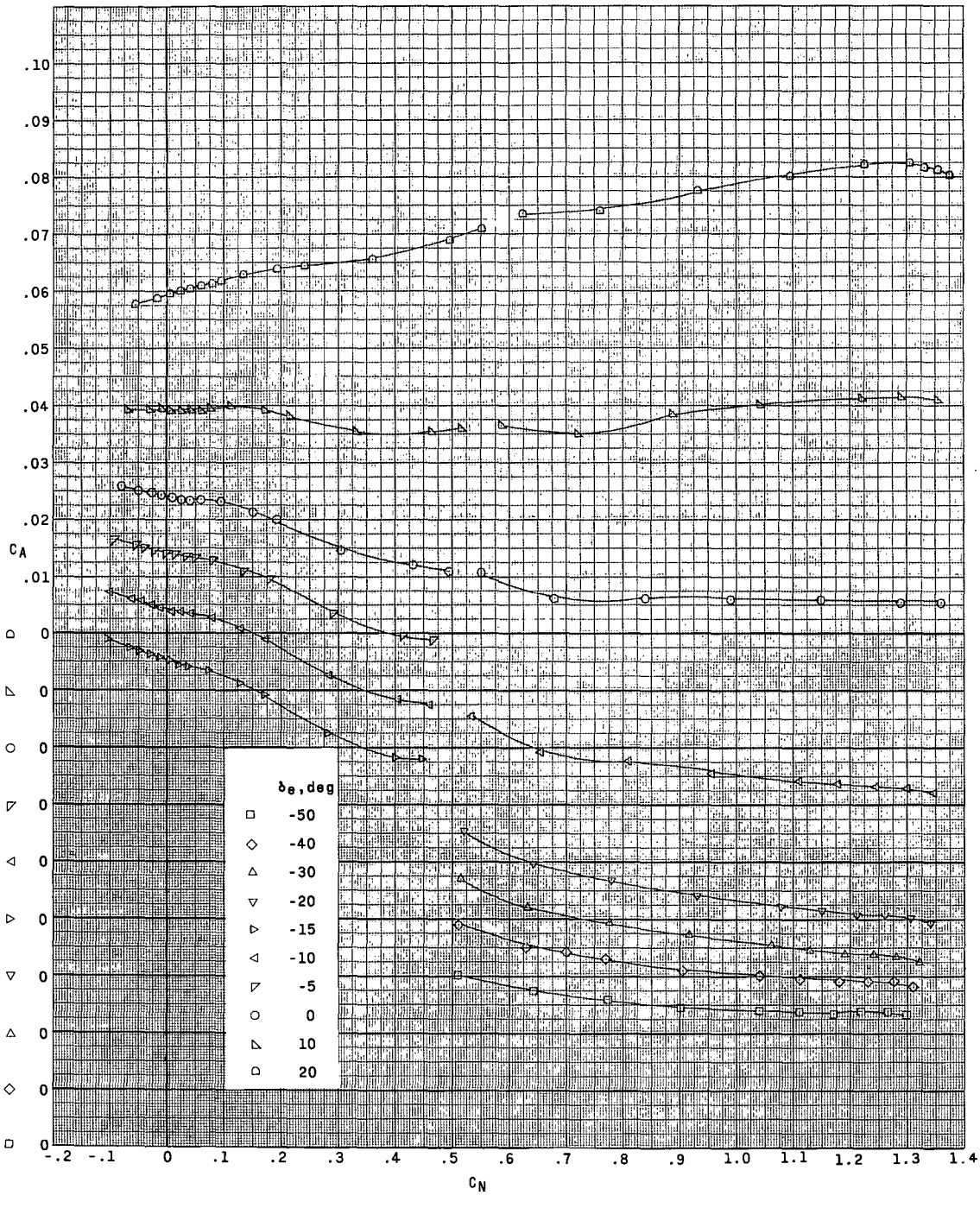

(b) M = 2.96.

Figure 9.- Continued.

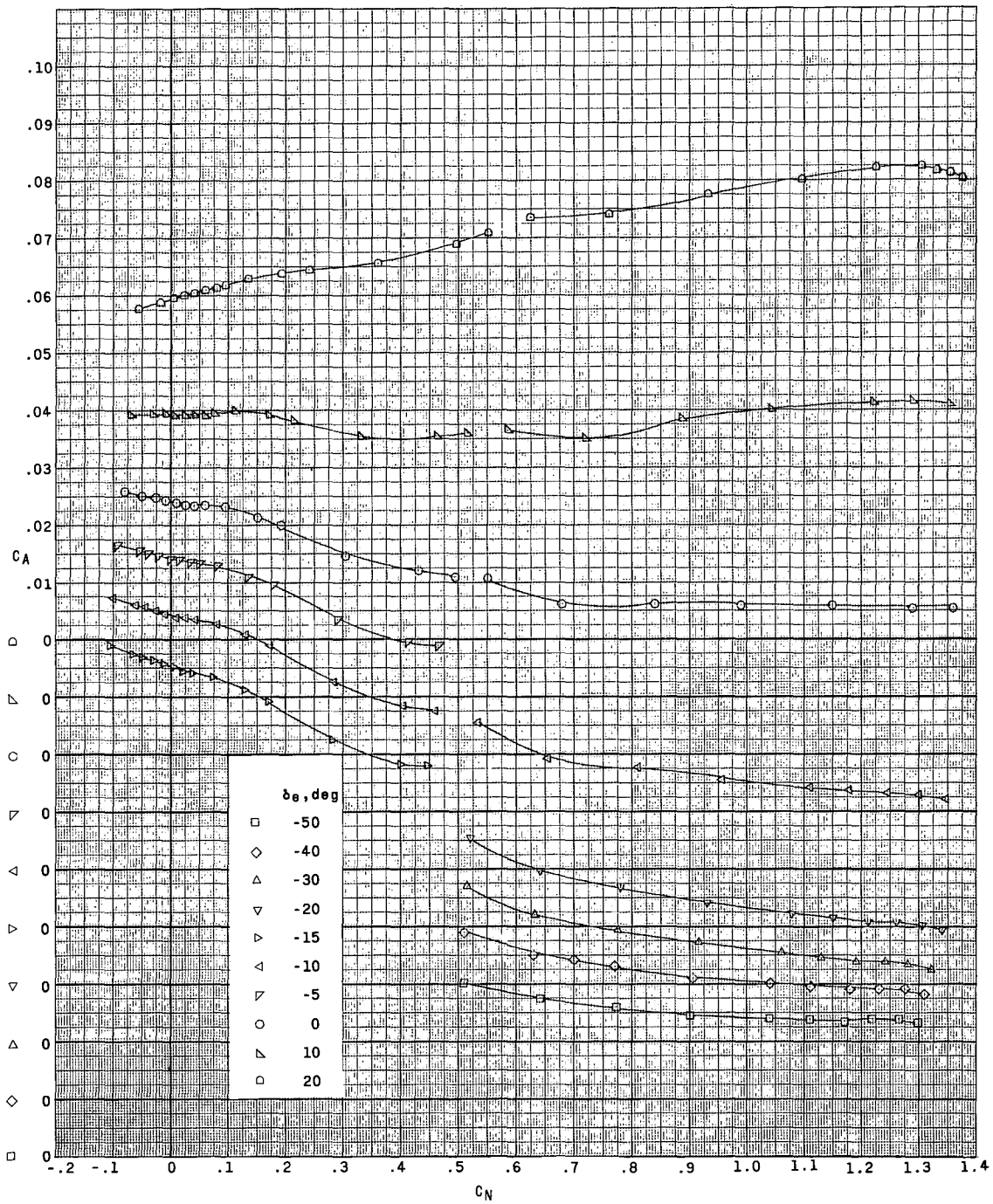

(b) Concluded.

Figure 9.- Continued.

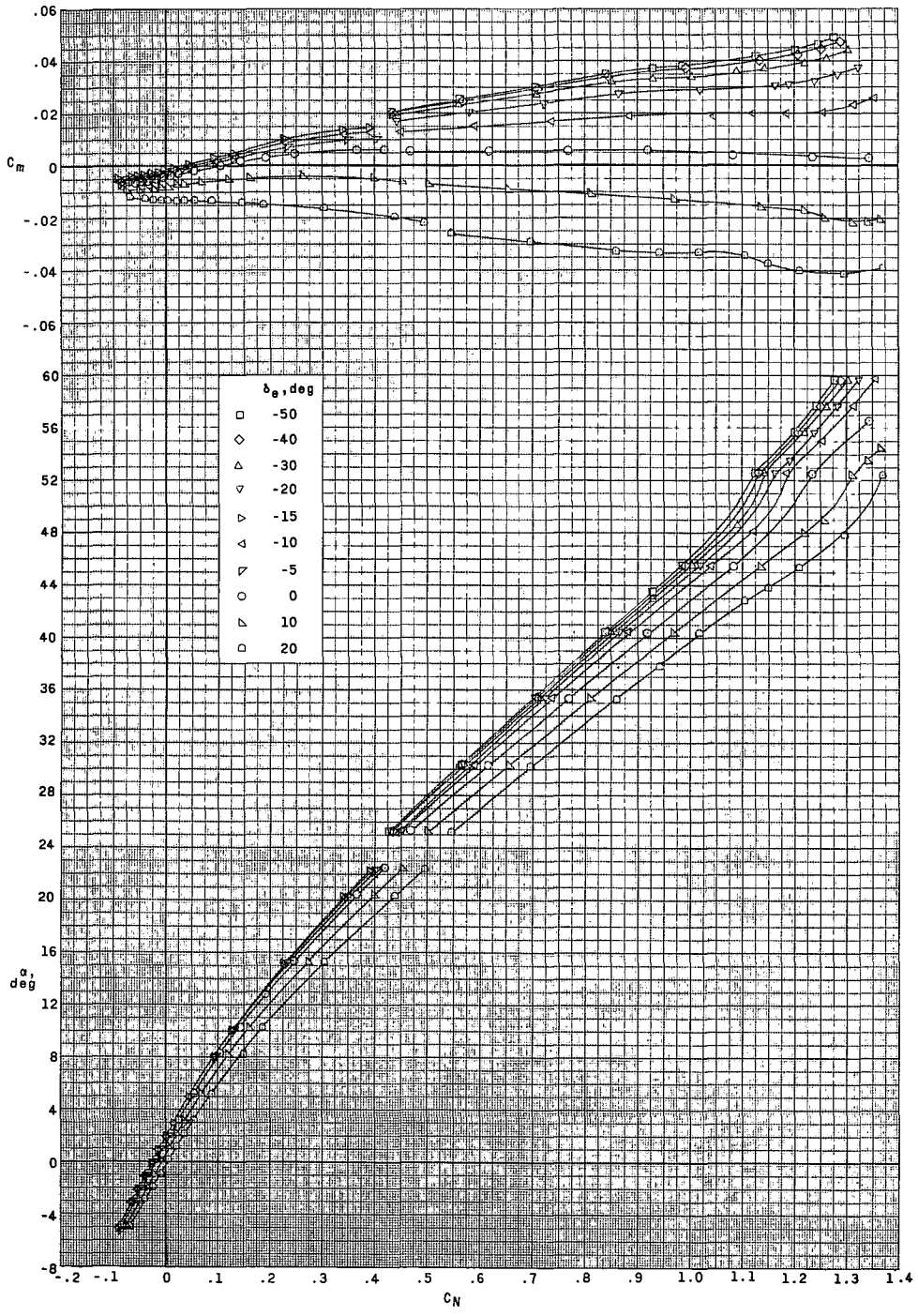

(c) M = 4.63.

Figure 9.- Continued.

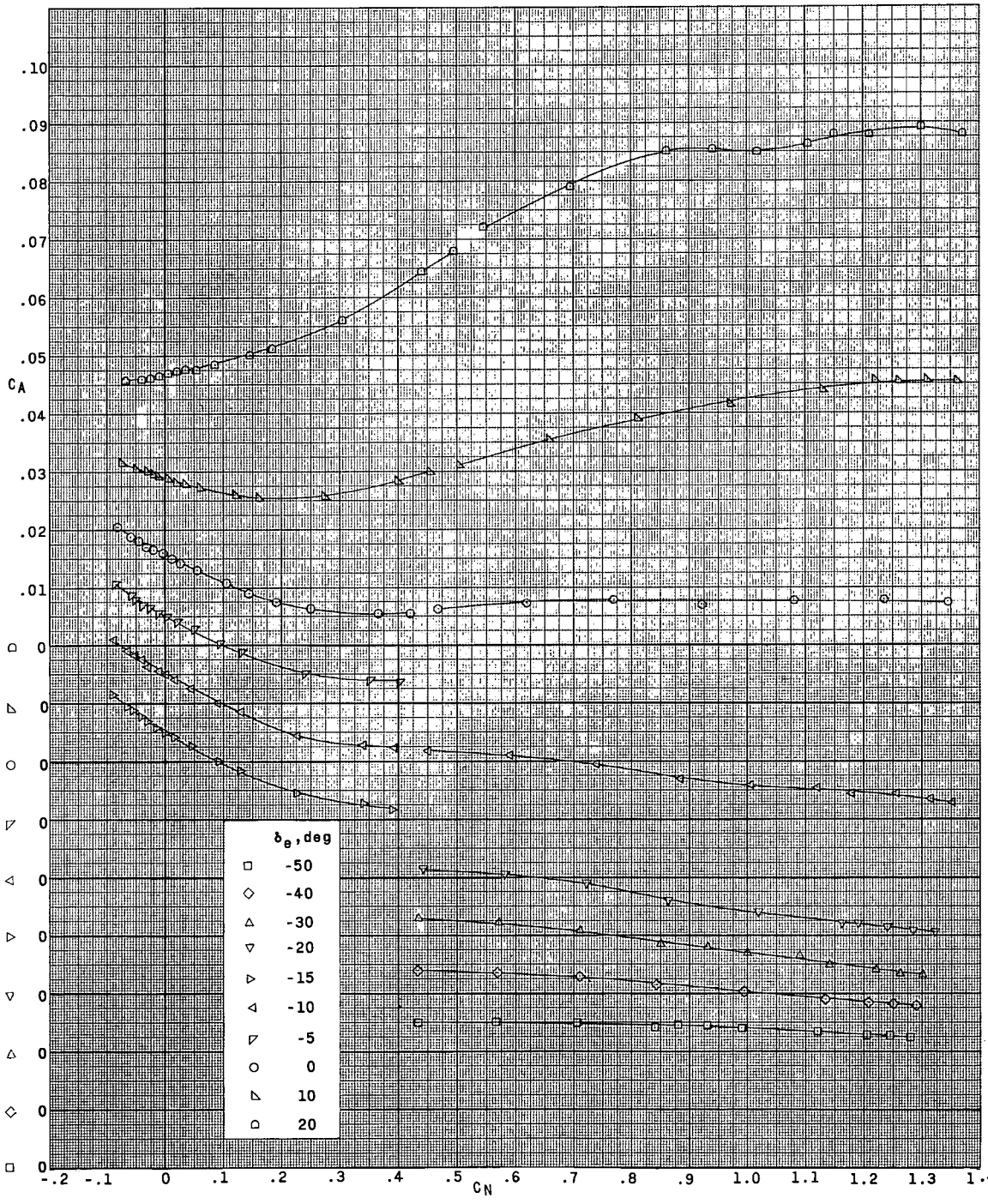

(c) Concluded.

Figure 9.- Concluded.

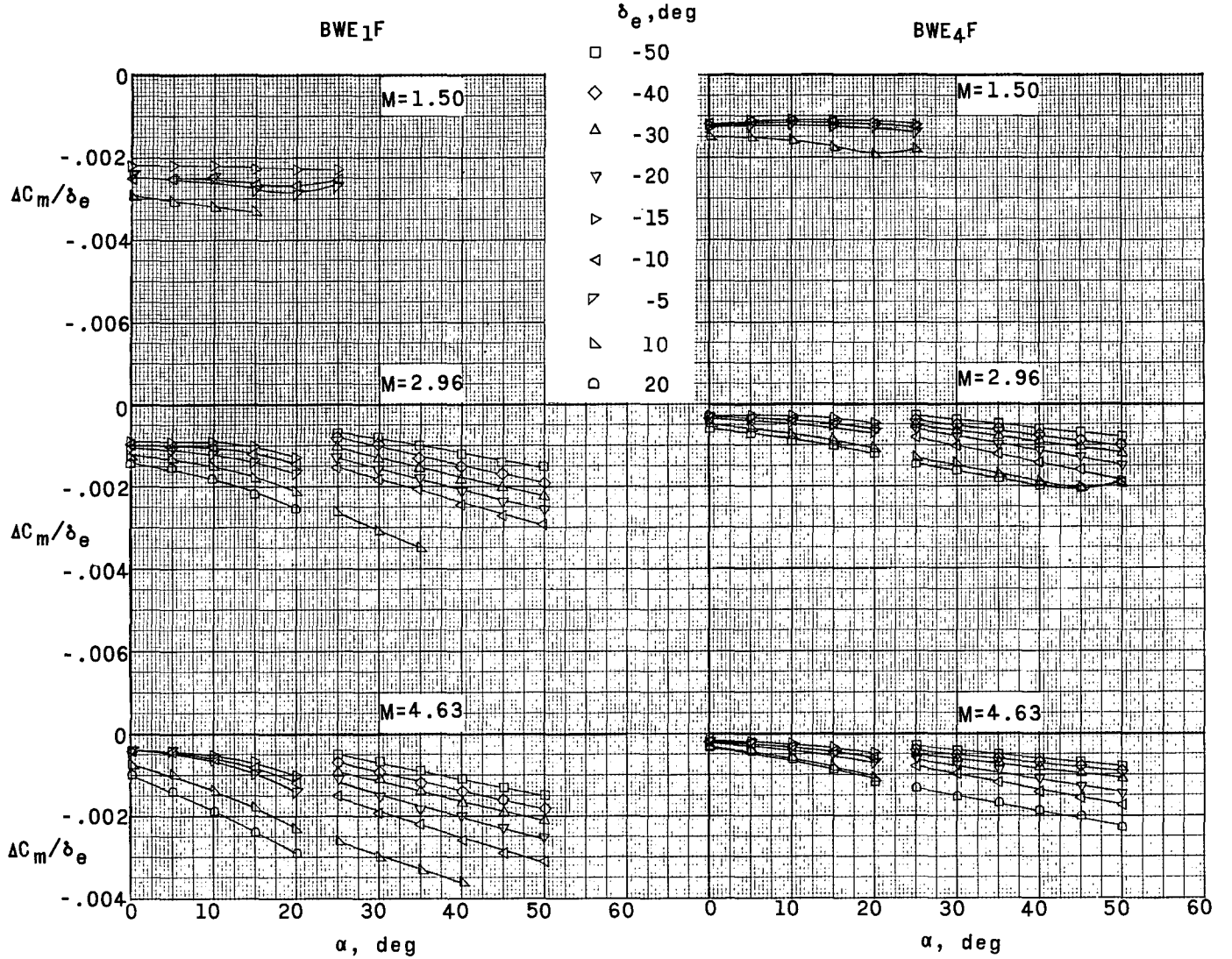

Figure 10.- Elevon effectiveness of basic configurations BWE_1F and BWE_4F. $\delta_r = 0^\circ$.

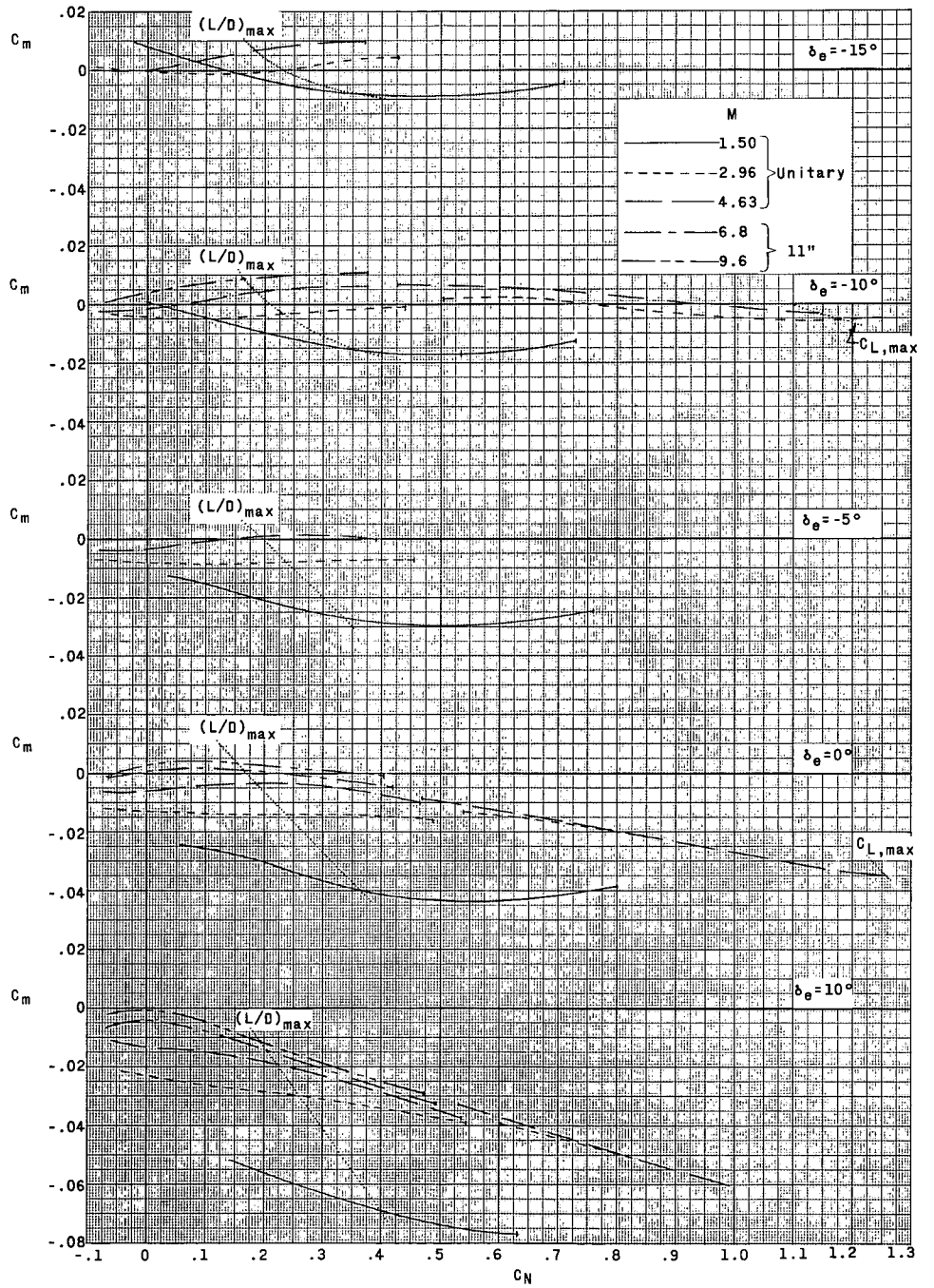

Figure 11.- Pitching-moment characteristics of basic BWE_1F configuration at supersonic and hypersonic speeds. $\delta_r = 0^o$.

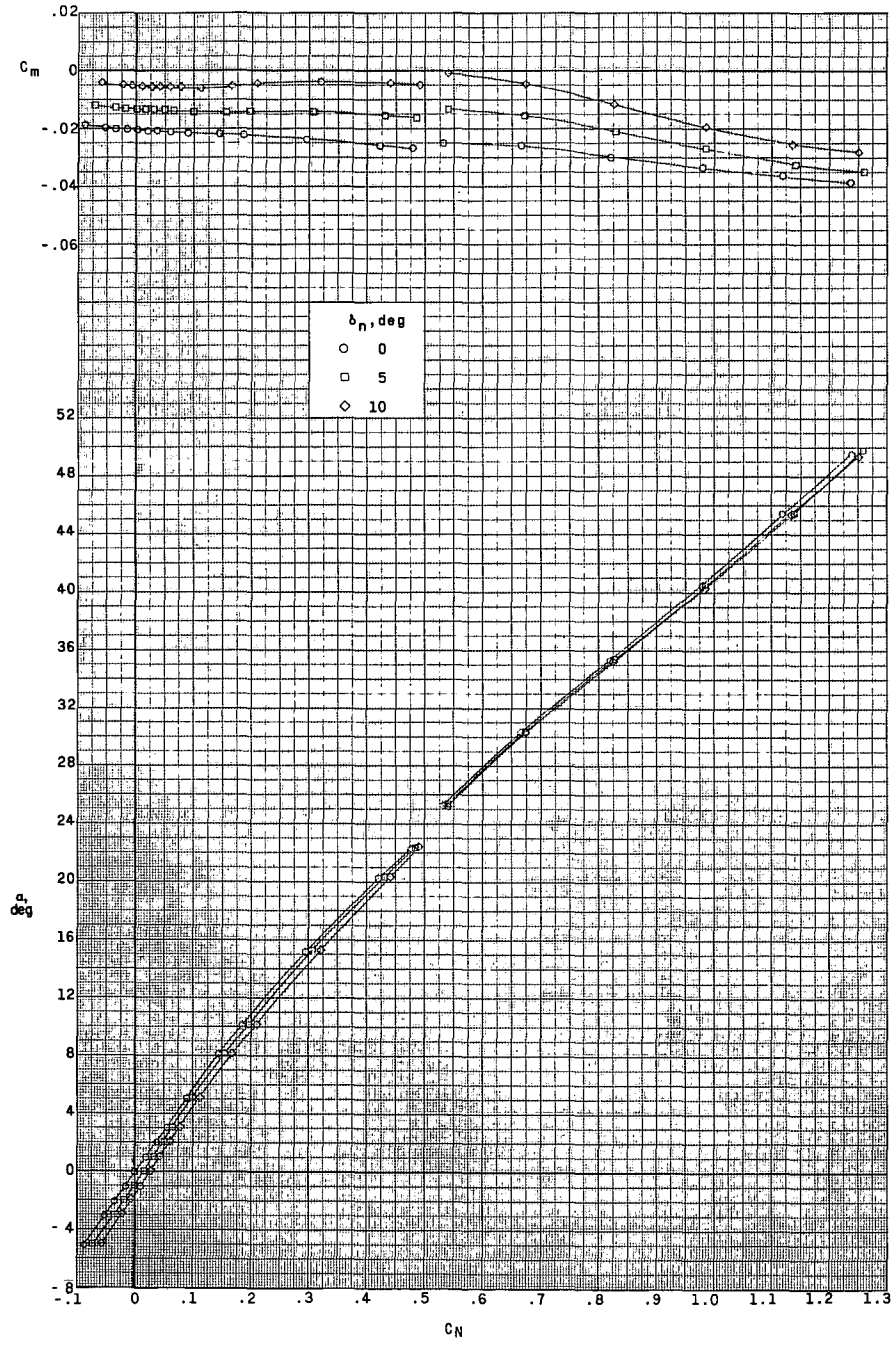

(a) C_m and α against C_N for M = 2.96.

Figure 12.- Effect of nose cant on the longitudinal aerodynamic characteristics of BWE_1F configuration. $\delta_e = 0^\circ$; $\delta_r = 0^\circ$.

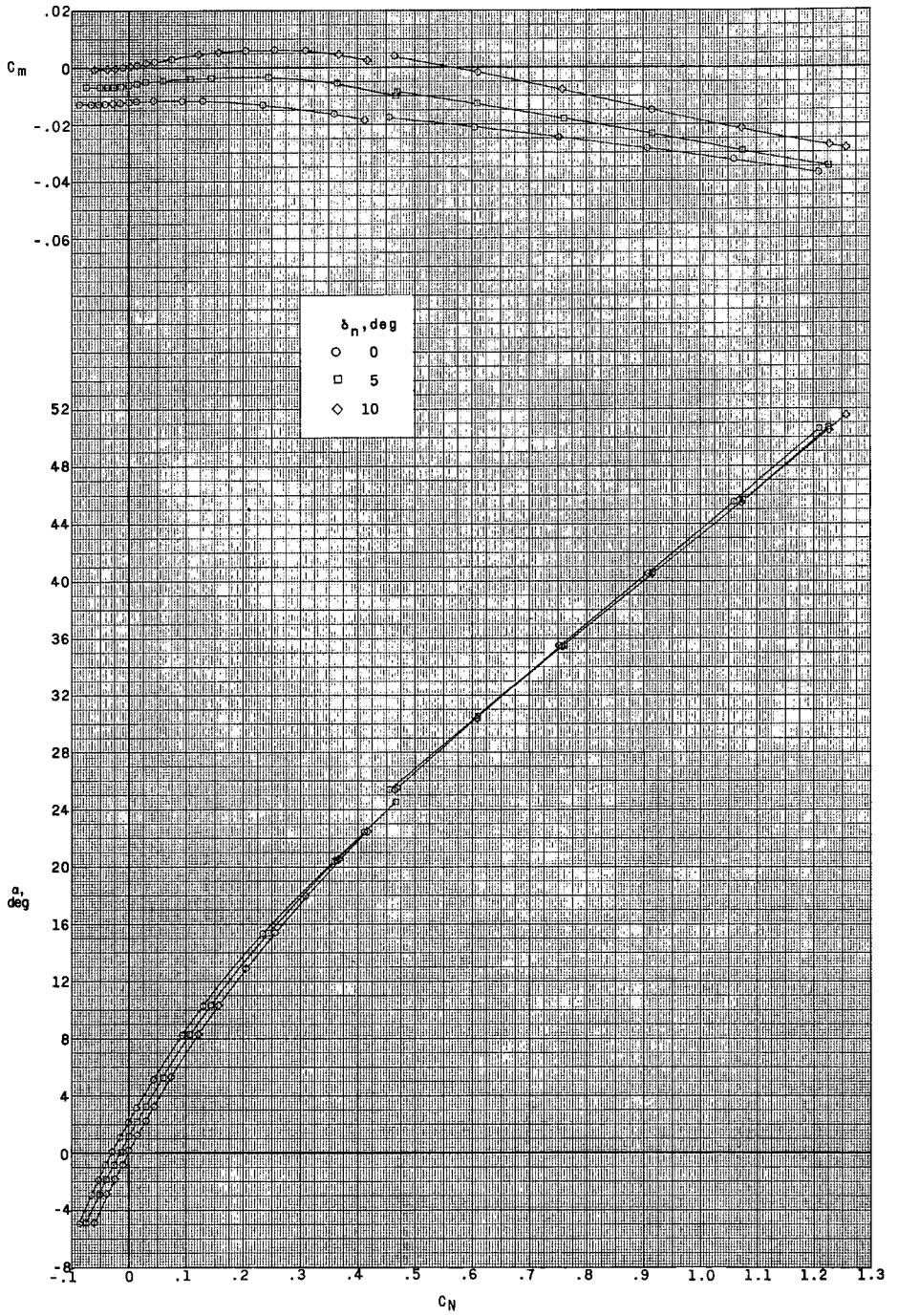

(b) C_m and α against C_N for $M = 4.63$.

Figure 12.- Continued.

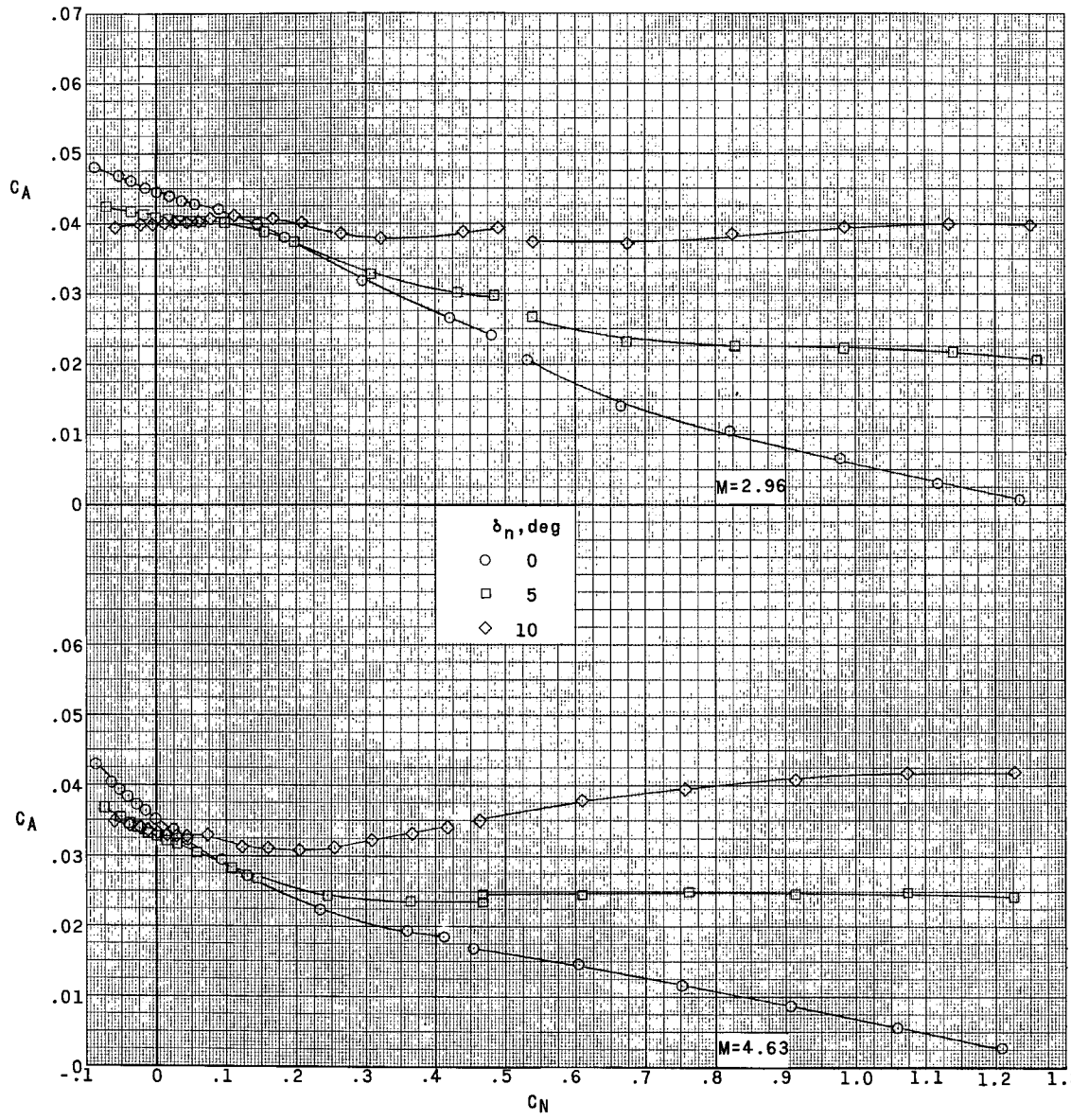

(c) C_A against C_N for M = 2.96 and M = 4.63.

Figure 12.- Concluded.

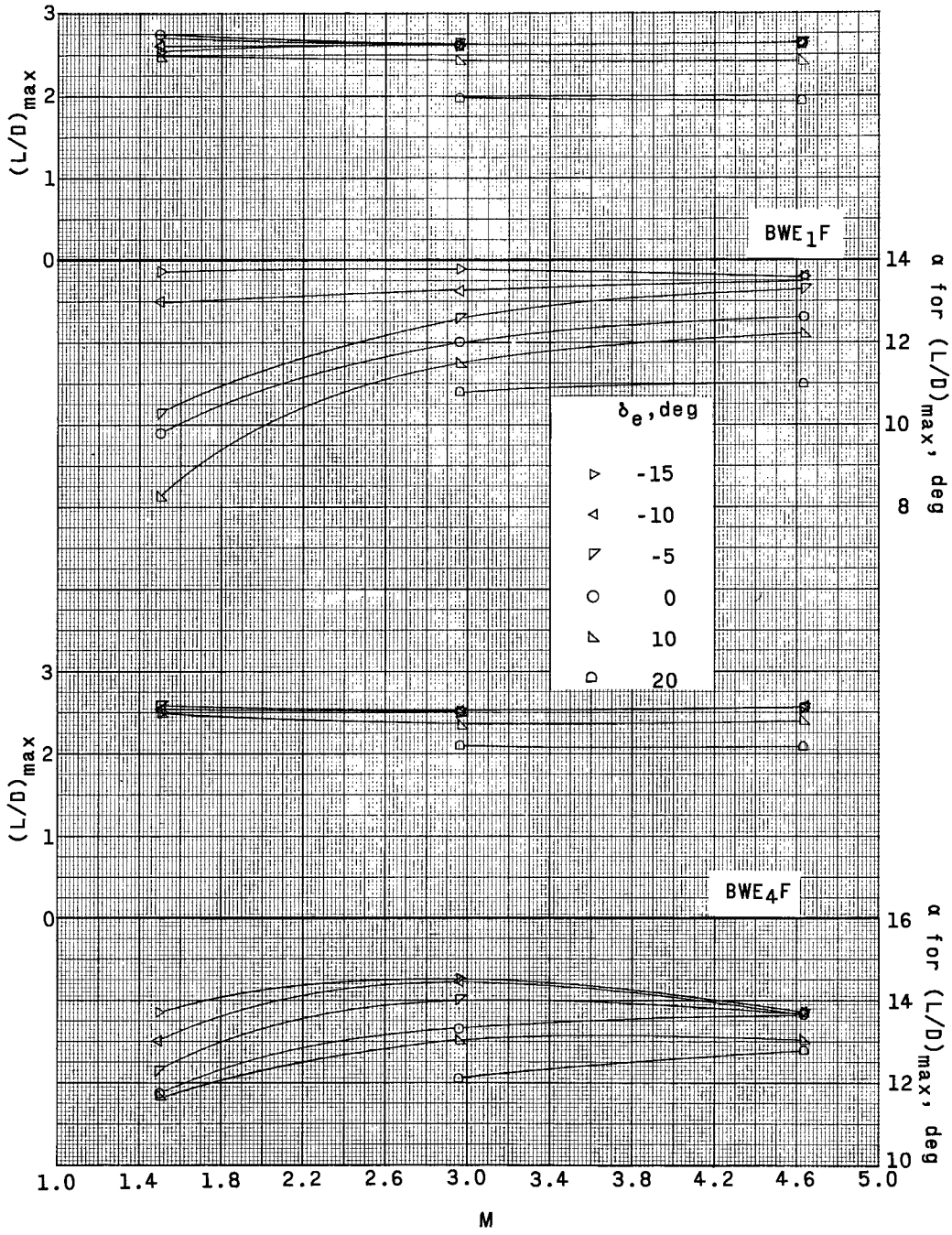

Figure 13.- Maximum lift-drag ratio and angle of attack for maximum lift-drag ratio, against Mach number for the BWE_1F and BWE_4F configurations. $\delta_r = 0^\circ$; $\delta_n = 5^\circ$.

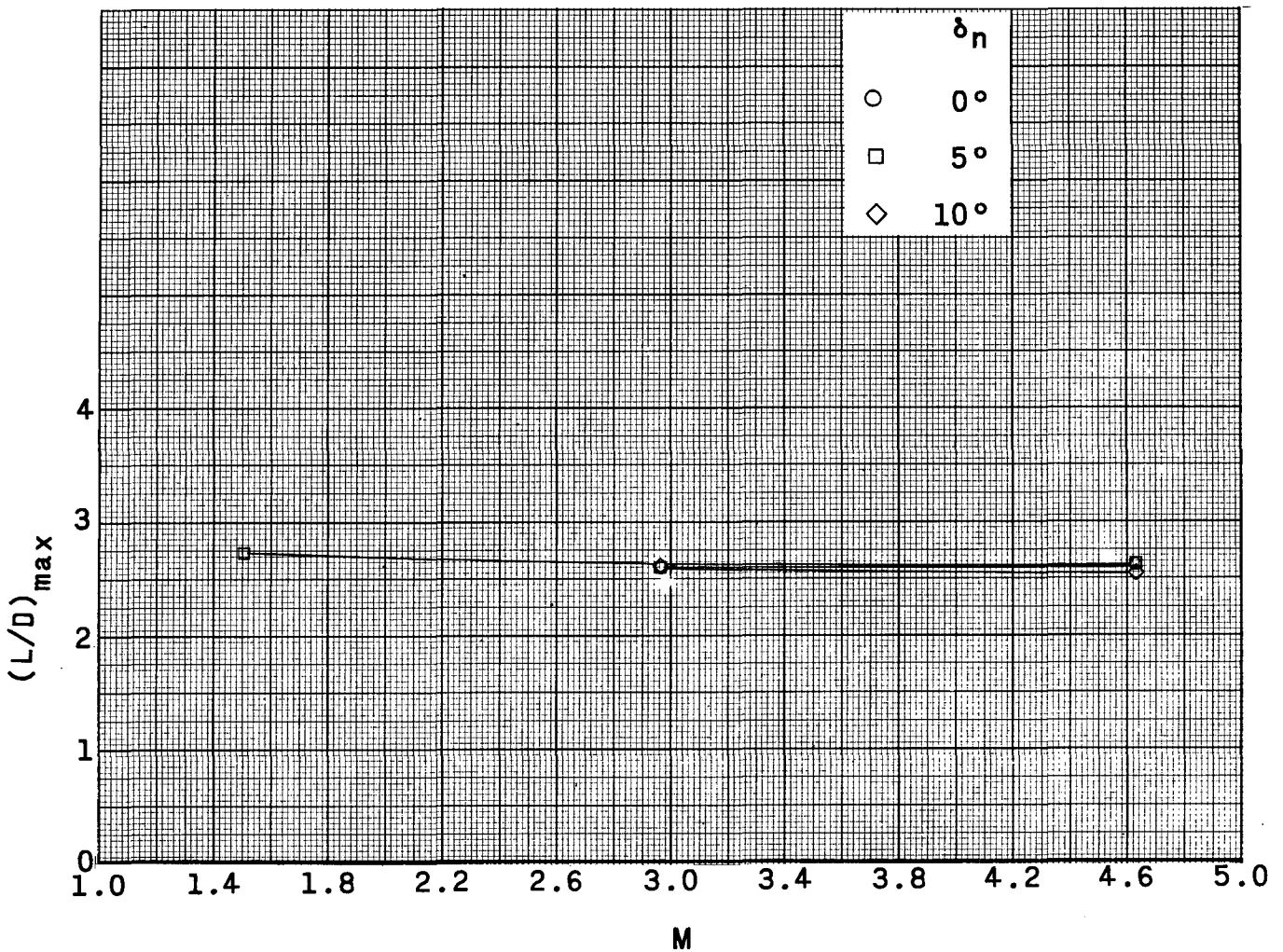

Figure 14.- Effect of nose cant on $(L/D)_{max}$ over test Mach number range.

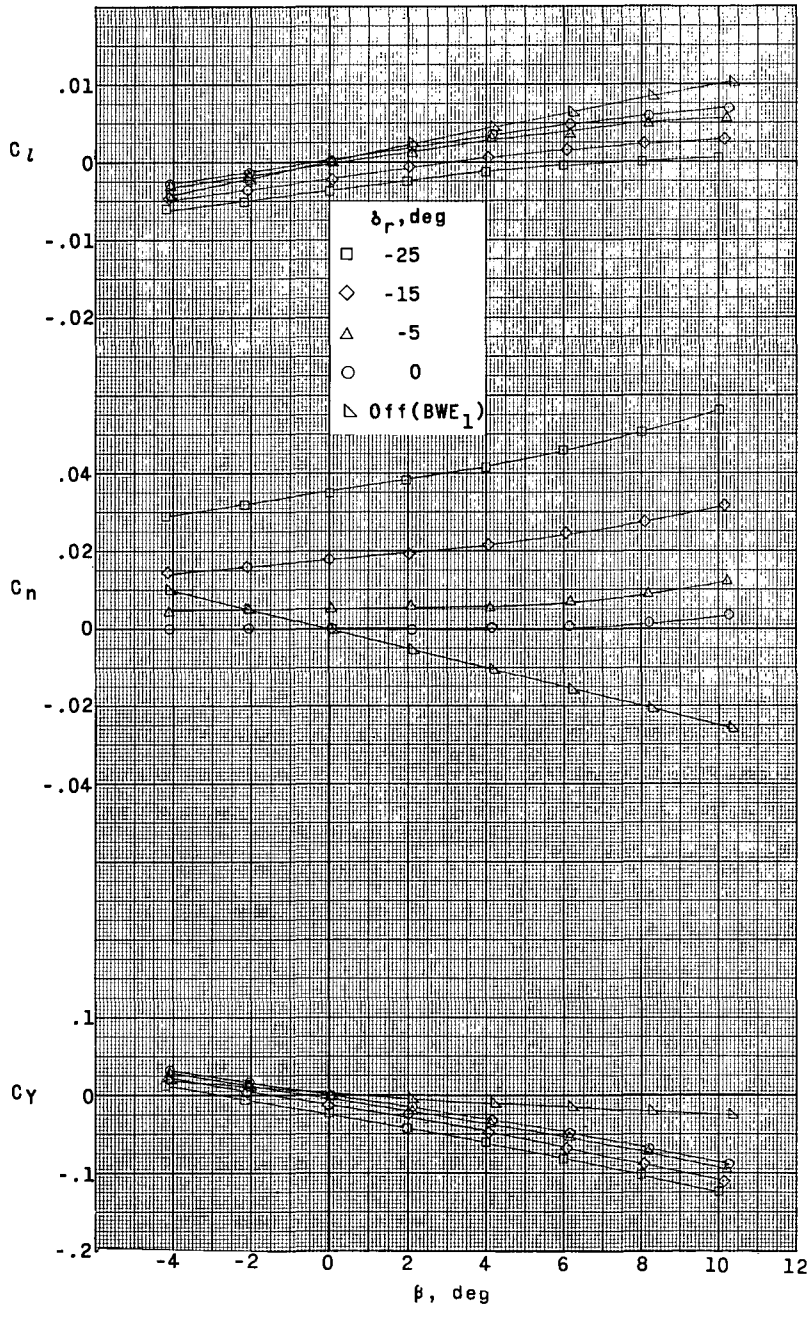

(a) $\alpha = 0^\circ$.

Figure 15.- Lateral stability and control characteristics of BWE_1F configuration at $M = 2.96$, including rudders-off case (BWE_1). $\delta_n = 5^\circ$; $\delta_e = 0^\circ$.

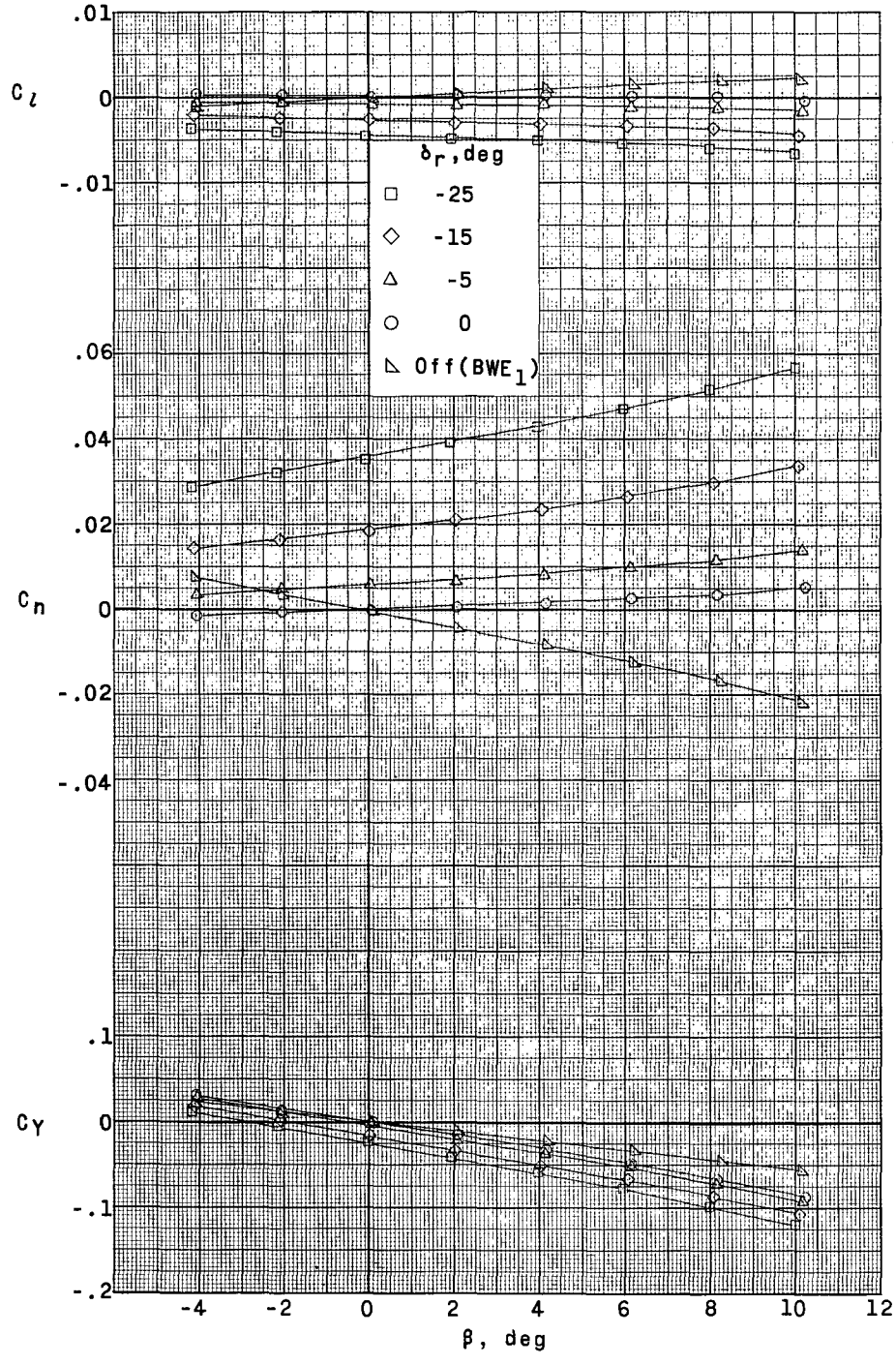

(b) $\alpha = 10^{\circ}$.

Figure 15.- Continued.

L-1903

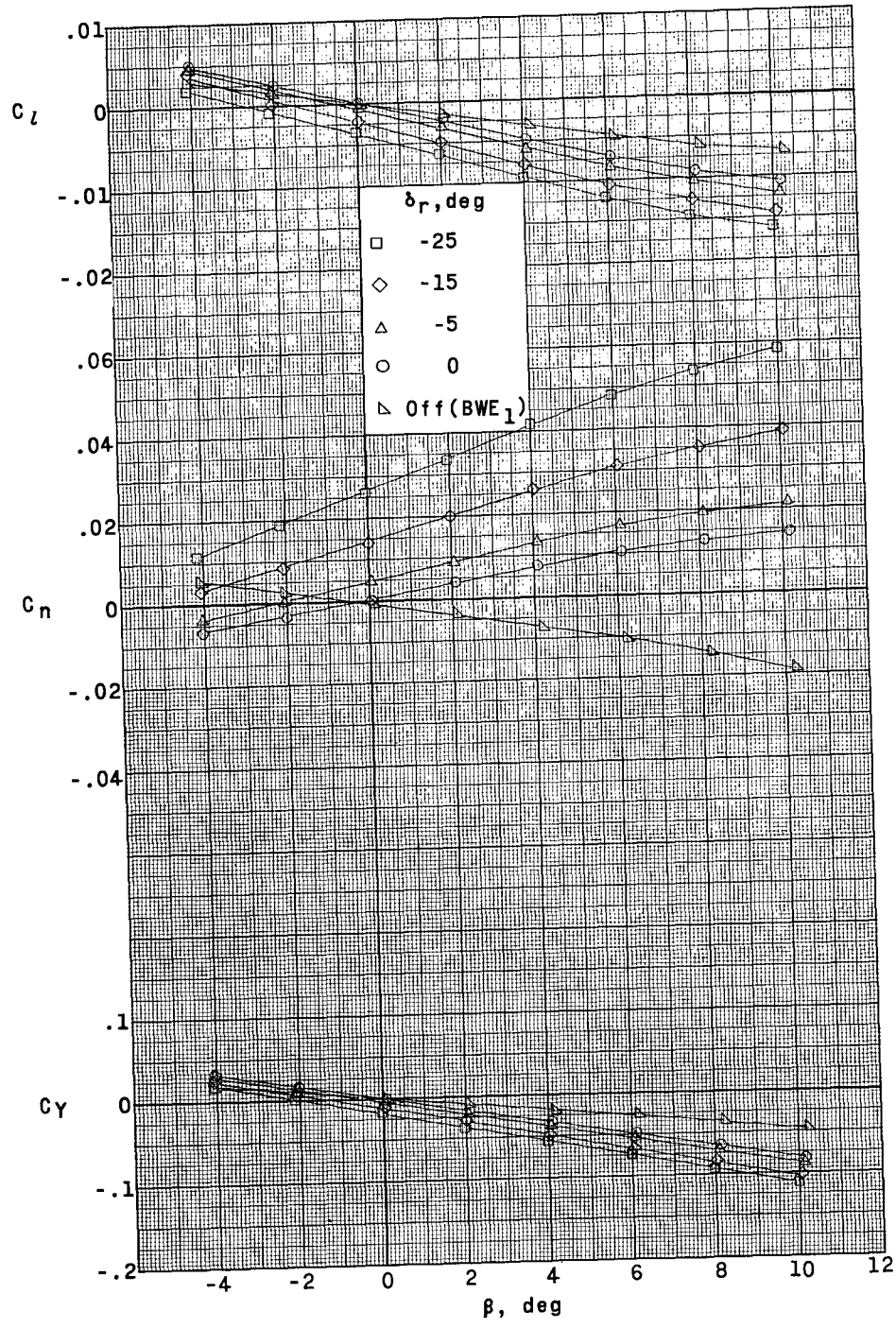

(c) $\alpha = 20^{\circ}$.

Figure 15.- Continued.

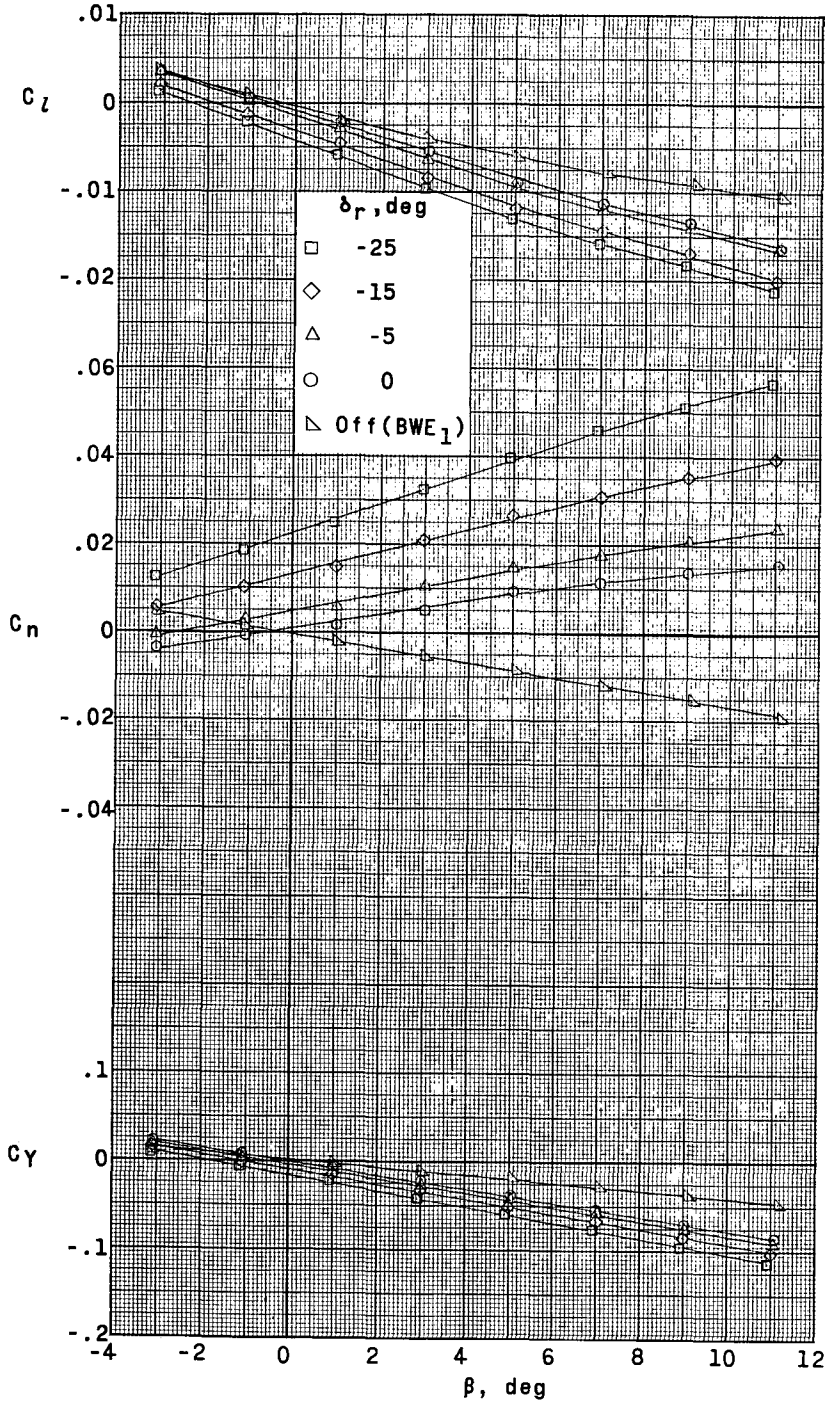

(d) $\alpha = 25^\circ$.

Figure 15.- Continued.

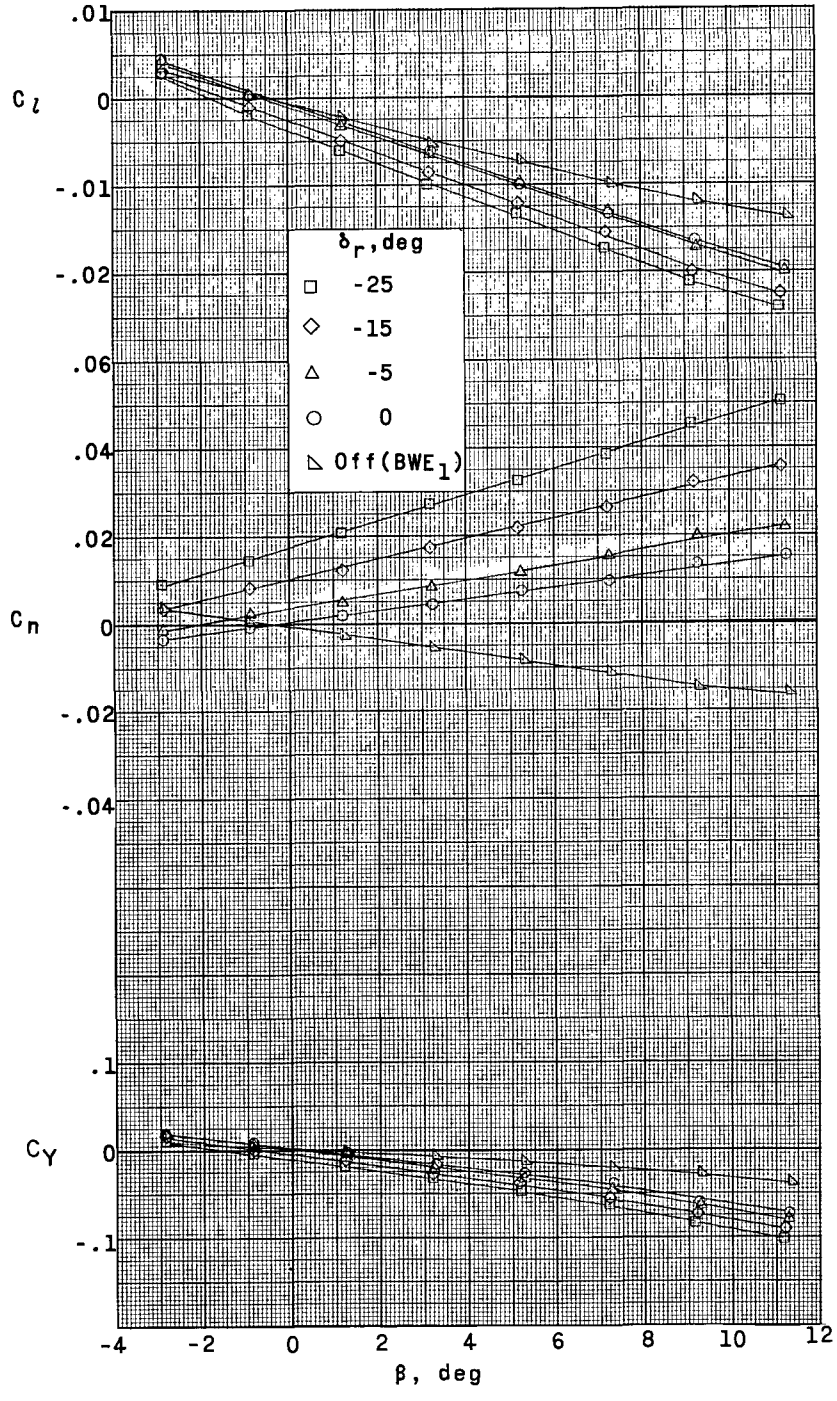

(e) $\alpha = 30^{\circ}$.

Figure 15.- Continued.

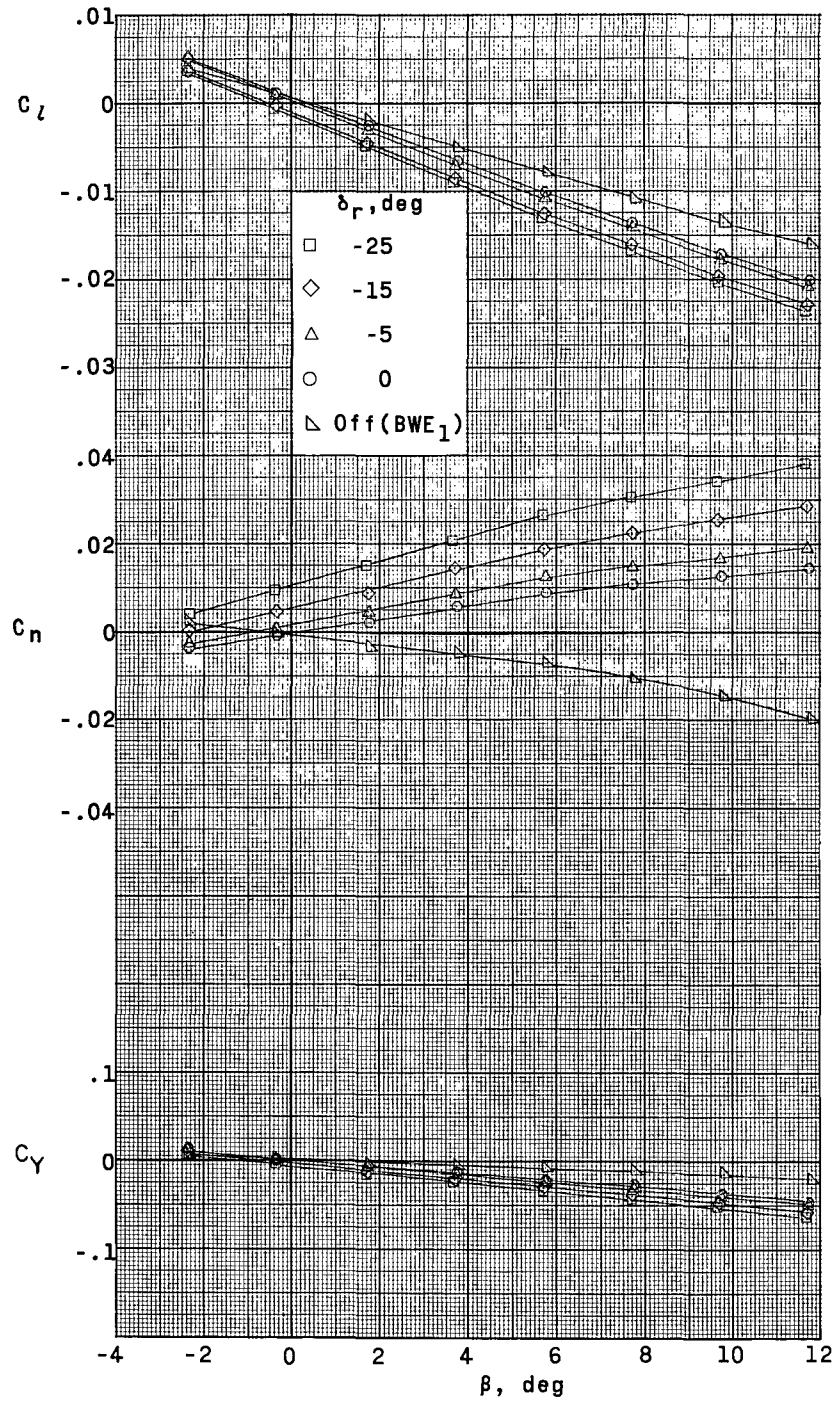

(f) $\alpha = 40^\circ$.

Figure 15.- Continued.

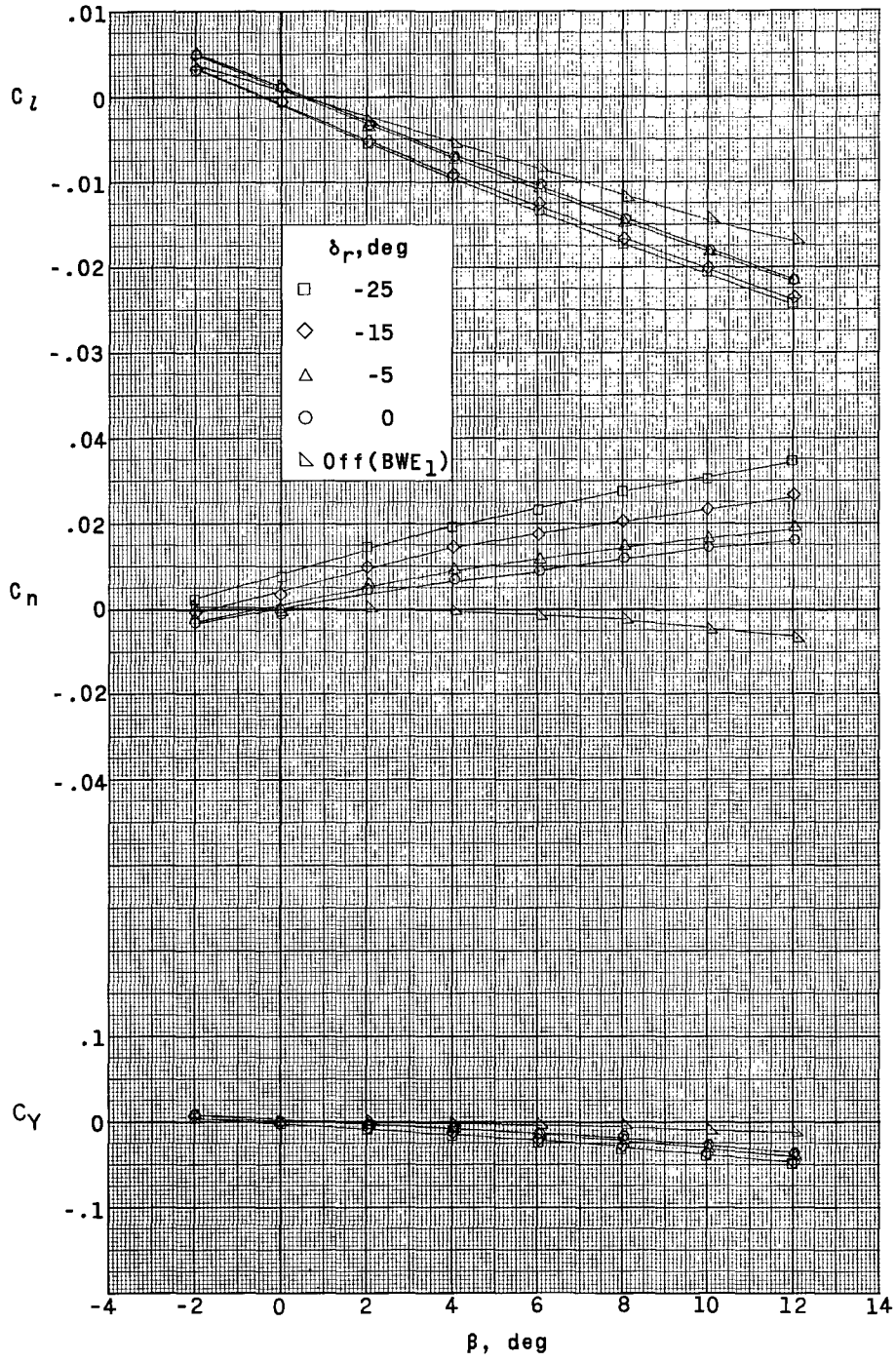

(g) $\alpha = 45^\circ$.

Figure 15.- Concluded.

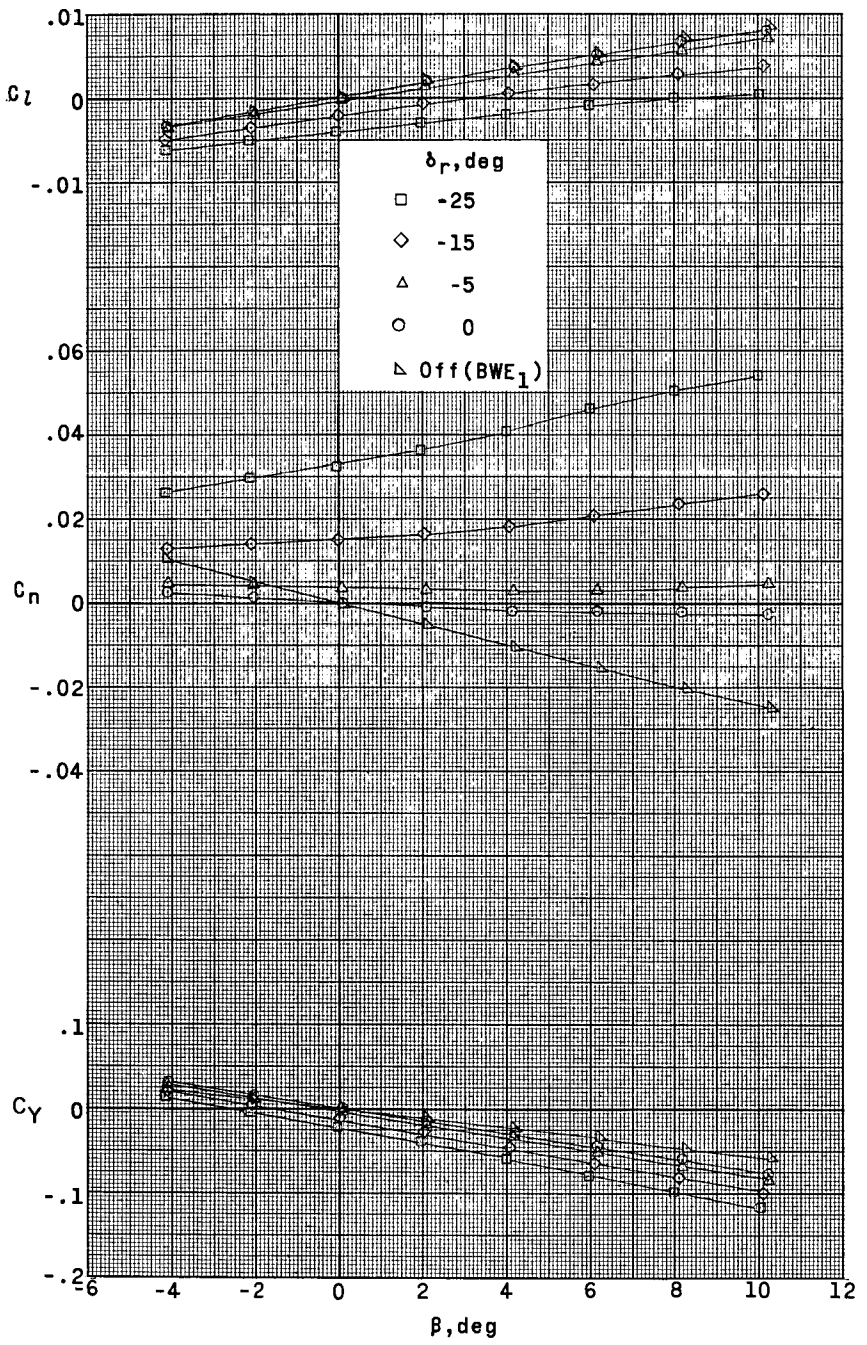

(a) $\alpha = 0^\circ$.

Figure 16.- Lateral stability and control characteristics of BWE_1F configuration at $M = 4.63$, including rudders-off case (BWE_1). $\delta_n = 5^\circ$; $\delta_e = 0^\circ$.

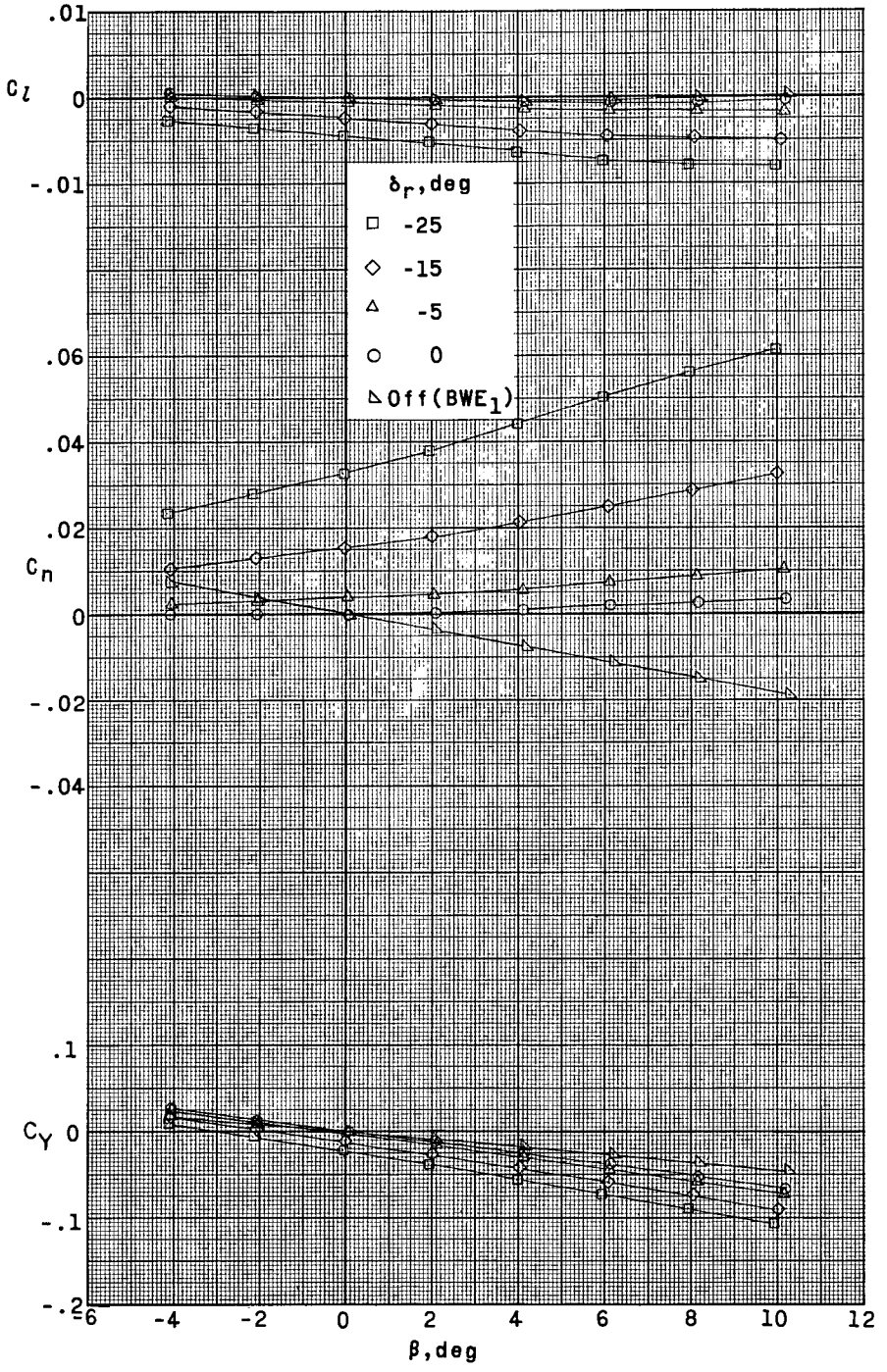

(b) $\alpha = 10^{\circ}$.

Figure 16.- Continued.

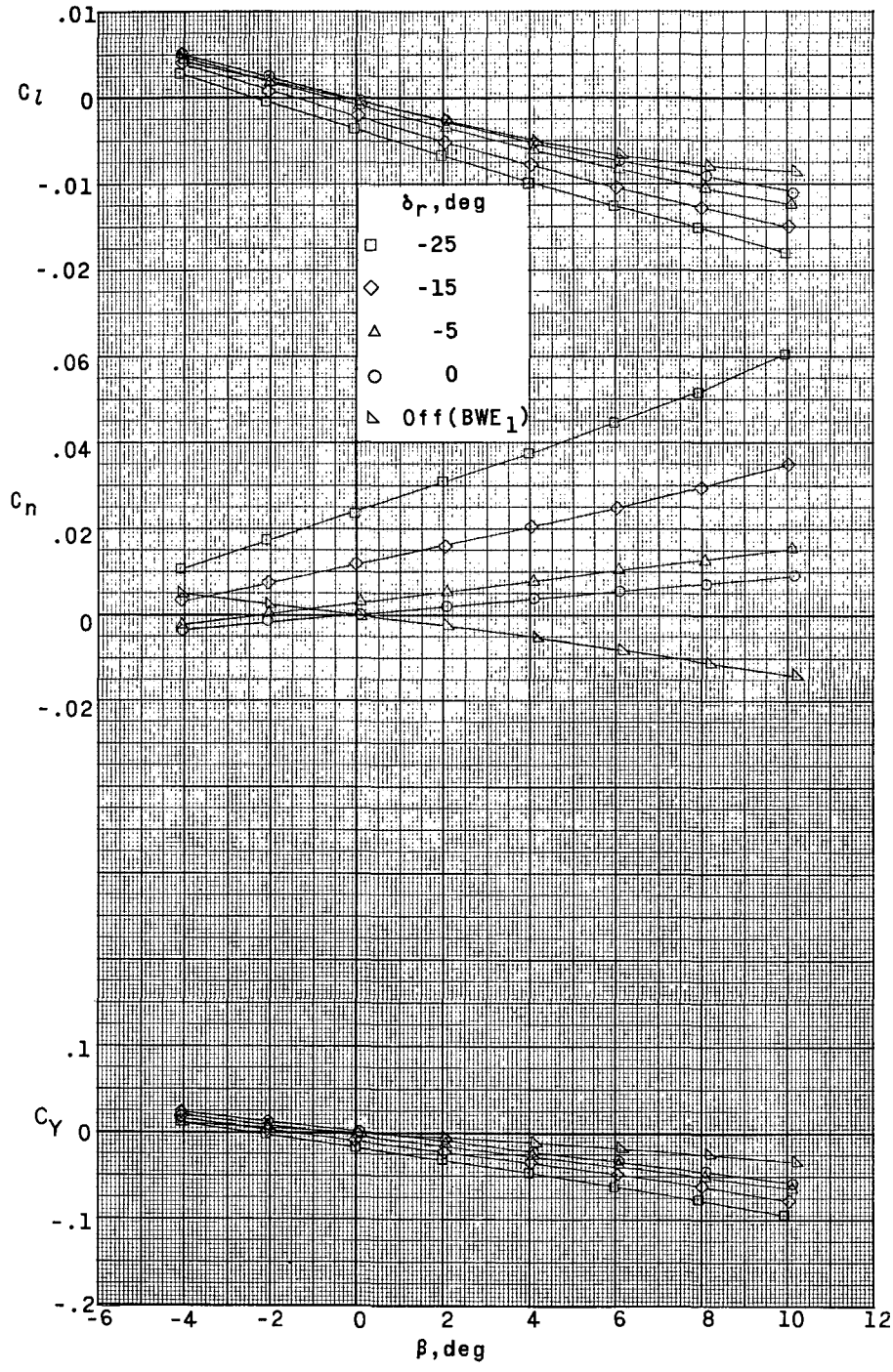

(c) $\alpha = 20^{\circ}$.

Figure 16.- Continued.

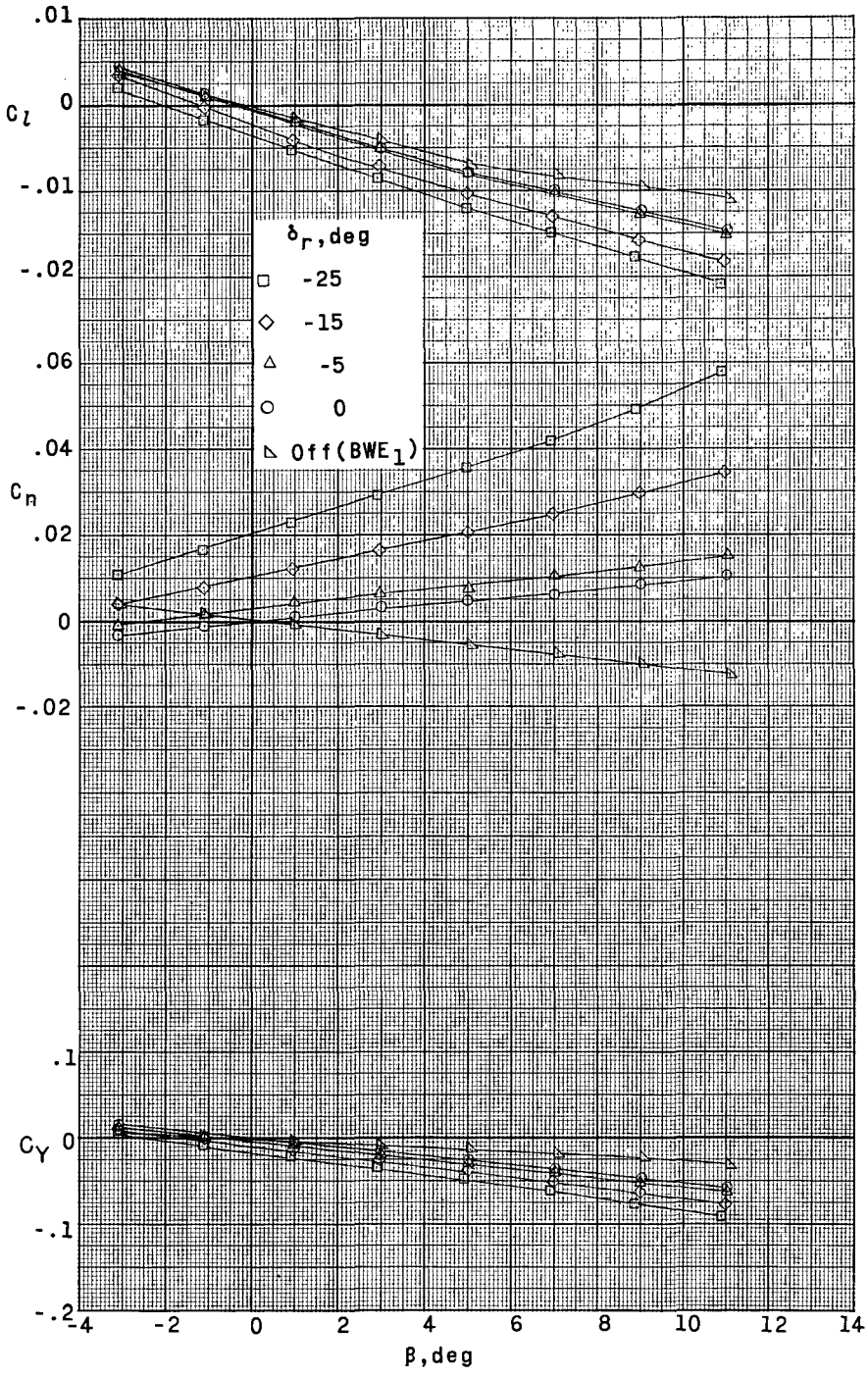

(d) $\alpha = 25^\circ$.

Figure 16.- Continued.

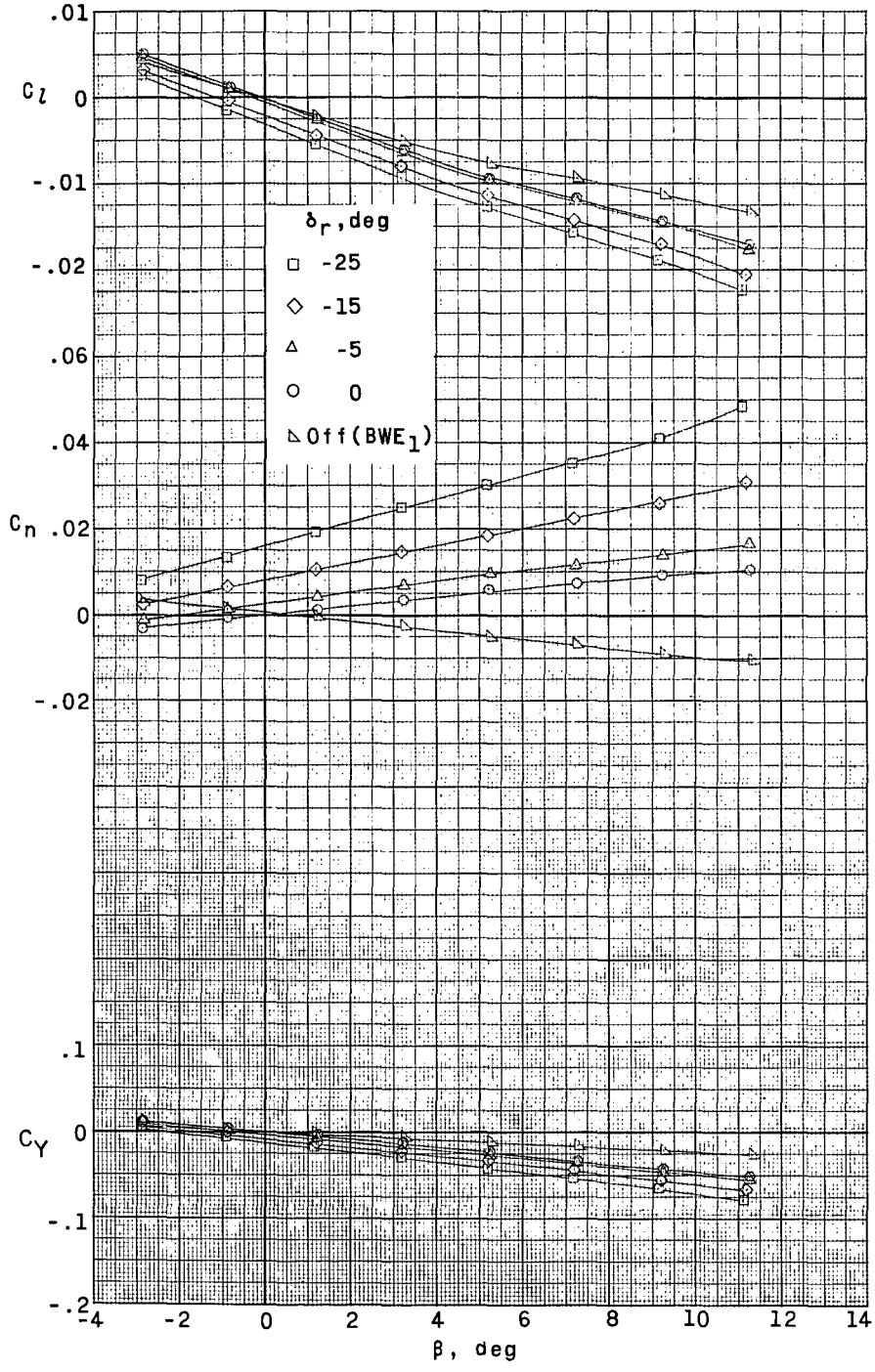

(e) $\alpha = 30^{\circ}$.

Figure 16.- Continued.

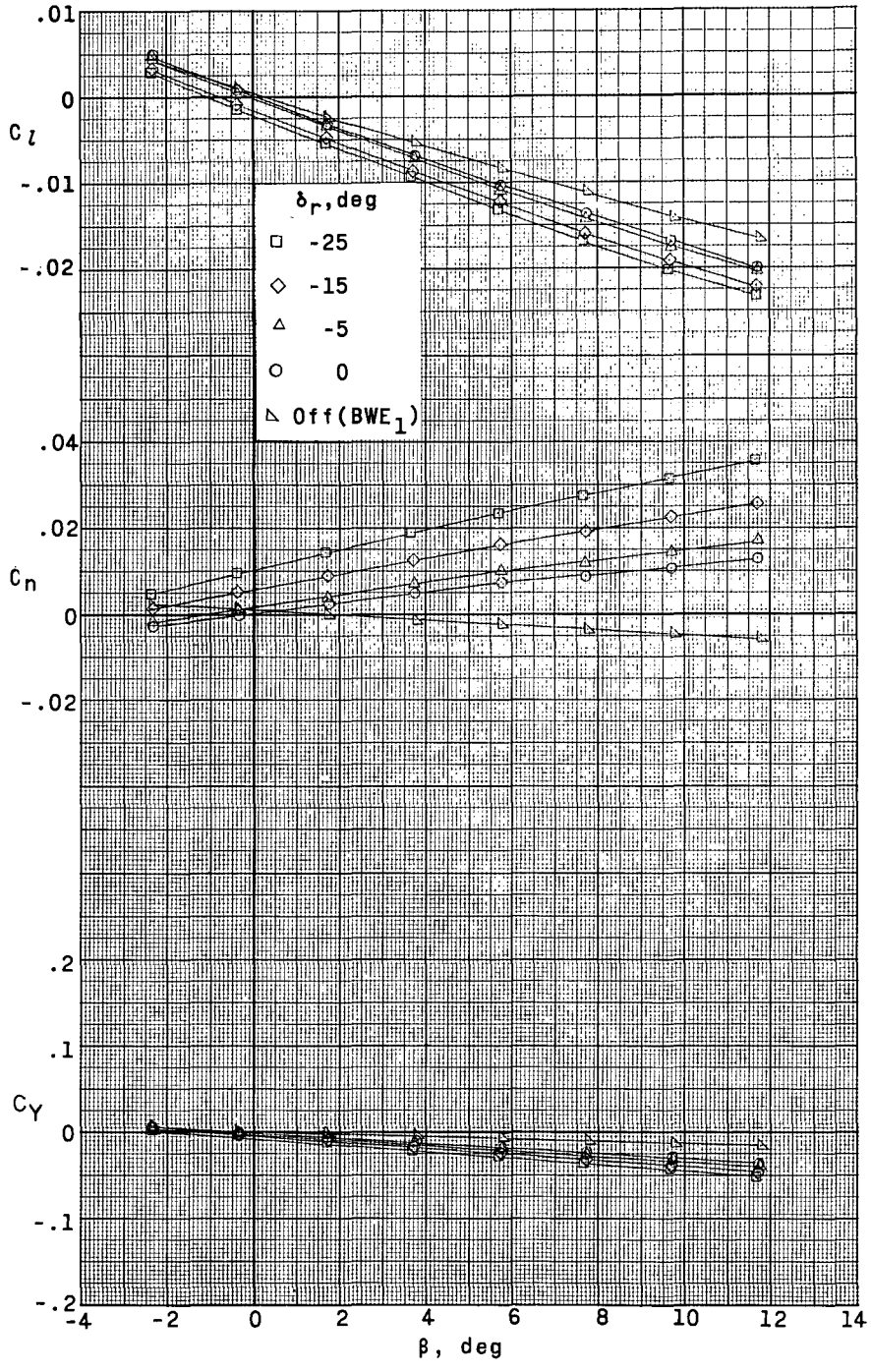

(f) $\alpha = 40^{\circ}$.

Figure 16.- Continued.

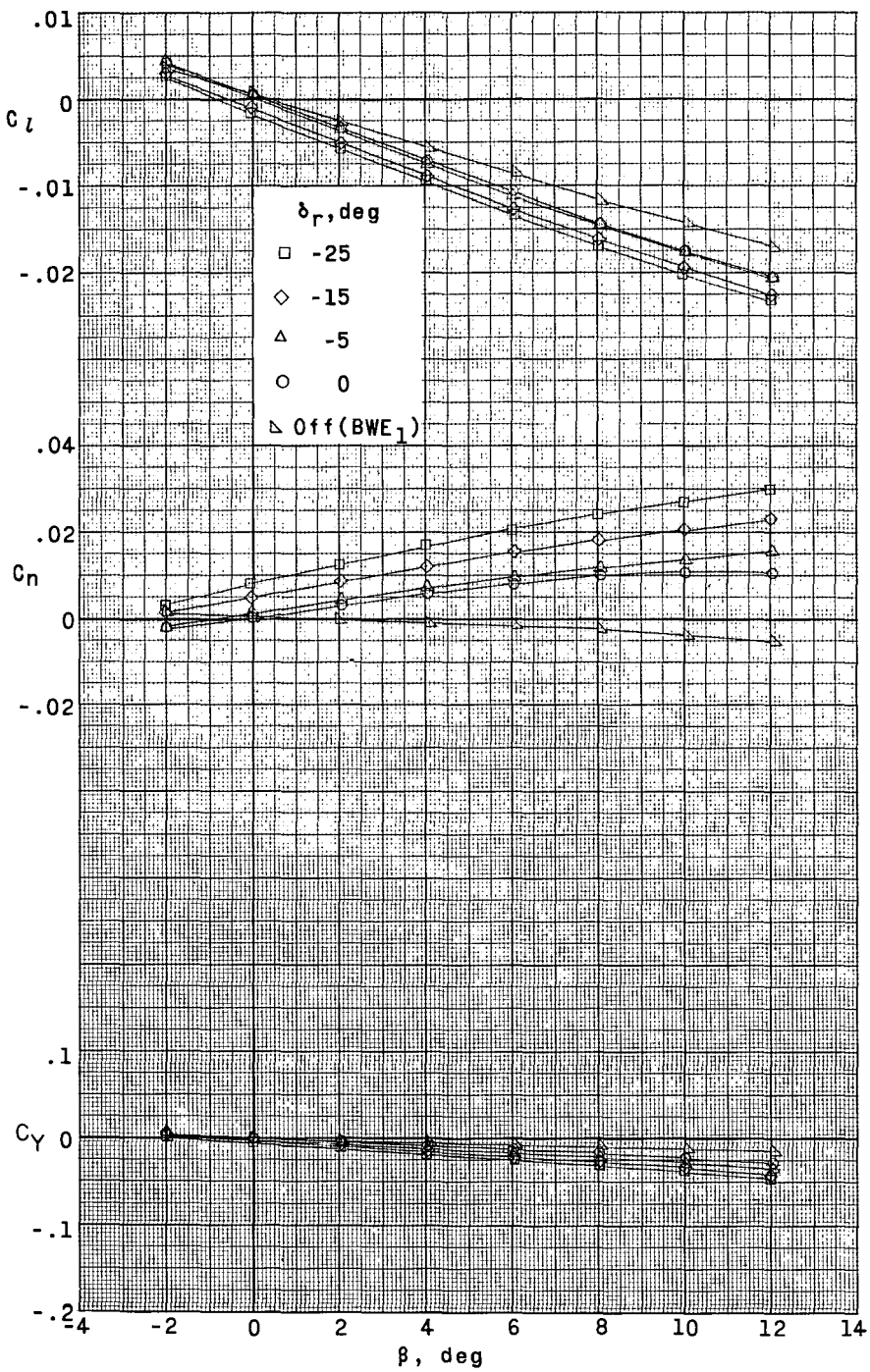

(g) $\alpha = 45^\circ$.

Figure 16.- Concluded.

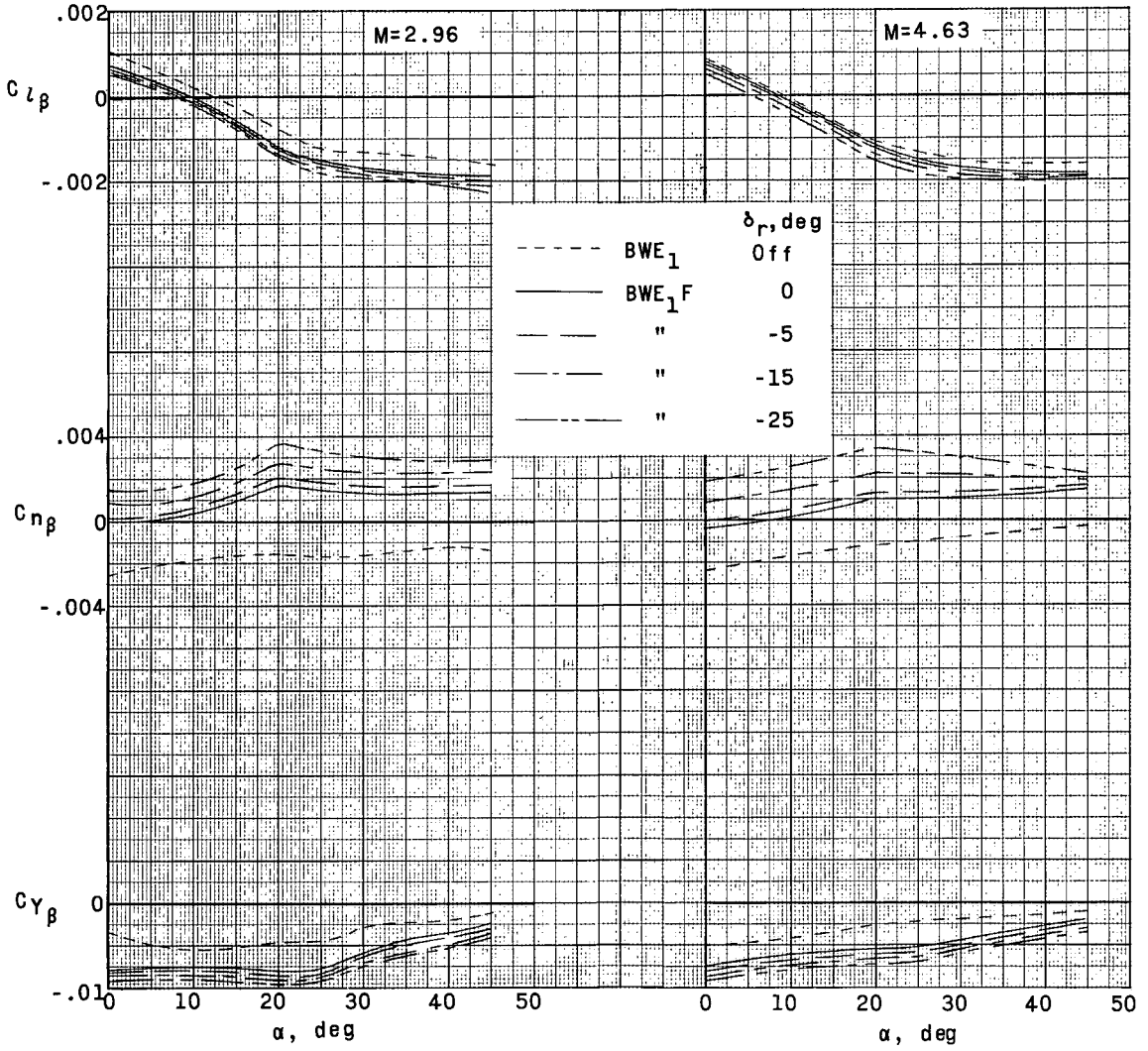

Figure 17.- Summary of lateral stability characteristics of BWE_1F configuration, at M = 2.96 and M = 4.63, including right rudder deflections and vertical fins removed (BWE_1). $\delta_n = 5^\circ$; $\delta_e = 0^\circ$.

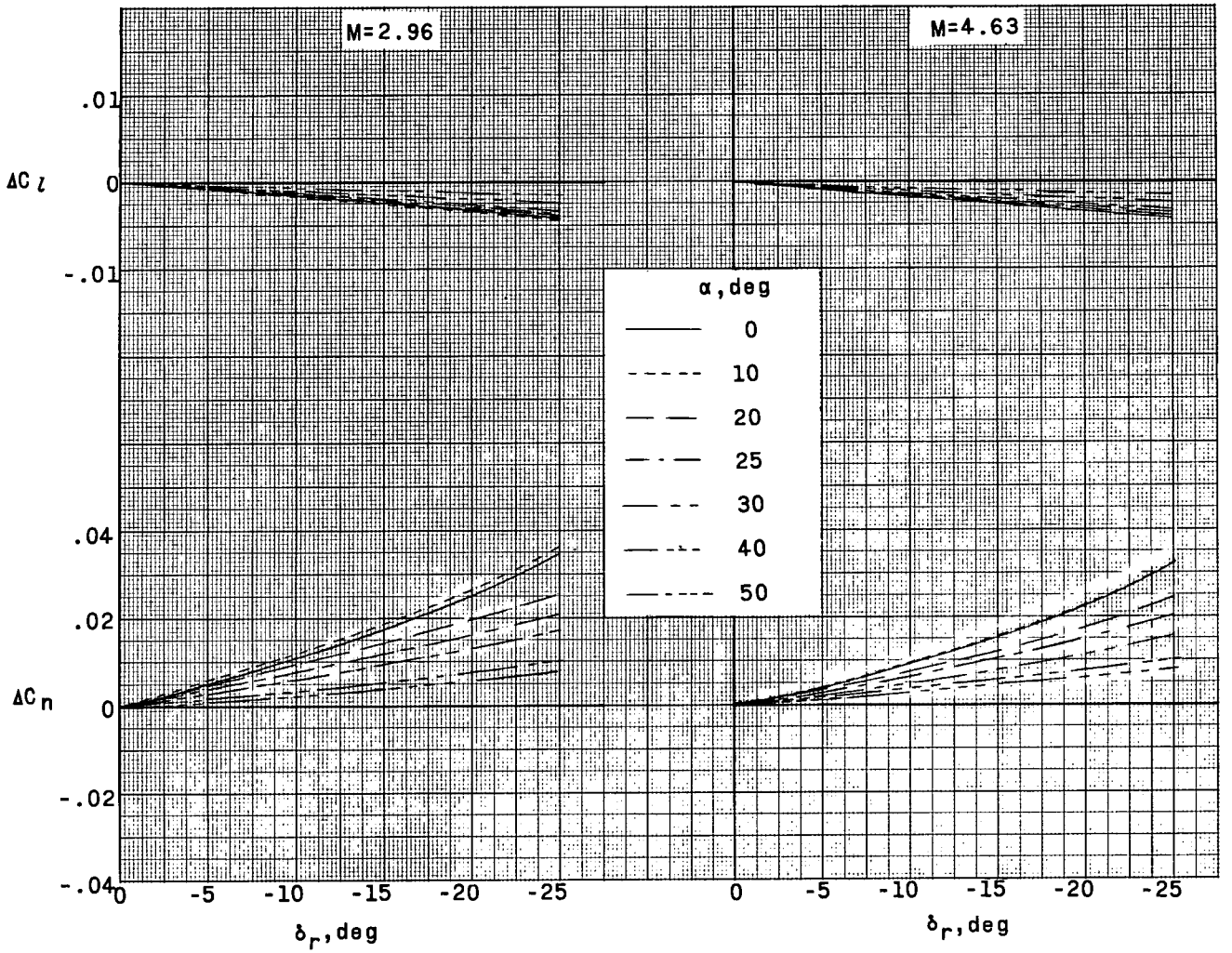

Figure 18.- Summary of rudder lateral control characteristics of BWE_1F configuration. $\delta_n = 5^\circ$; $\delta_e = 0^\circ$.

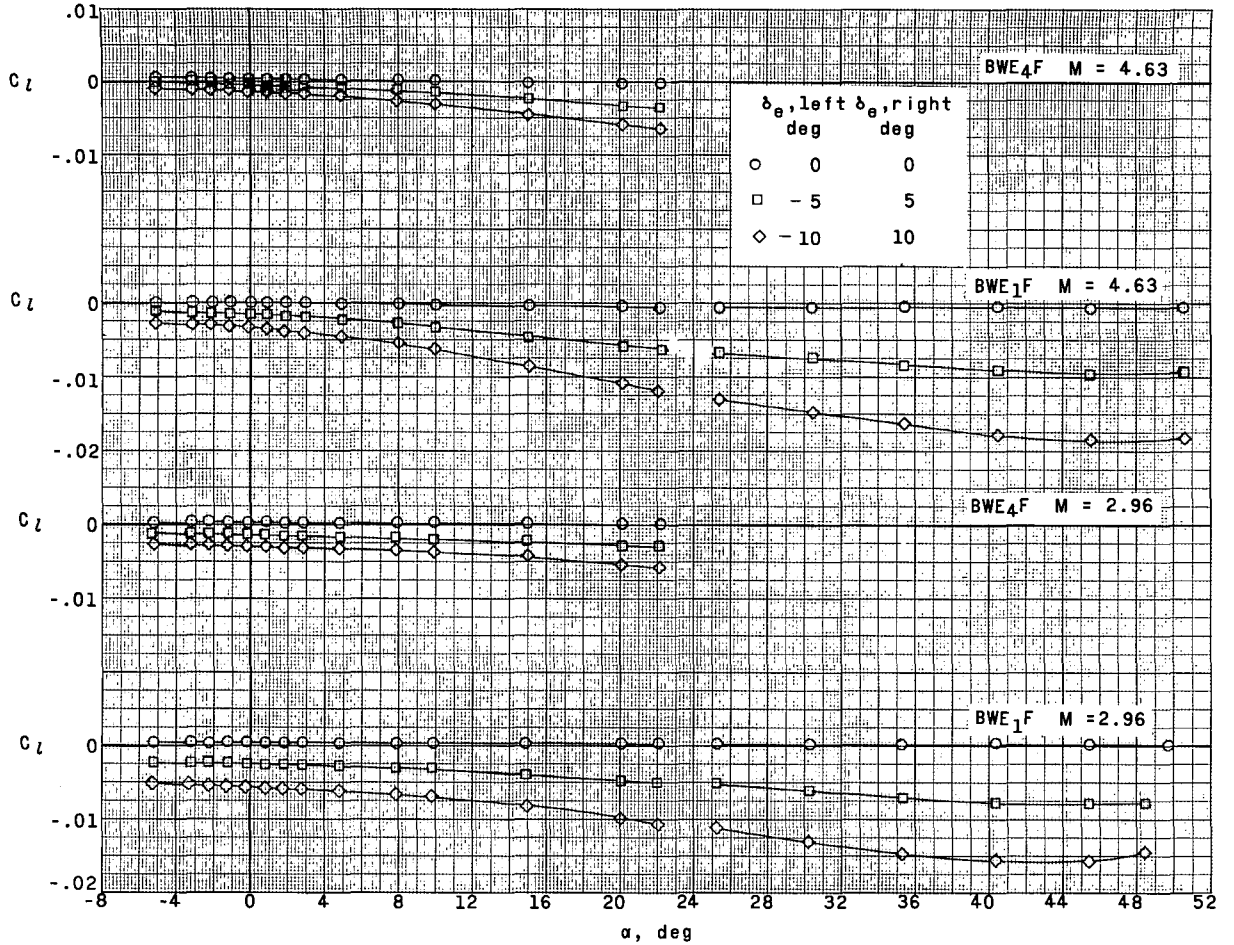

(a) Rolling moment.

Figure 19.- Effect of differential elevon deflections for both BWE_1F and BWE_4F configurations at $M = 2.96$ and $M = 4.63$. $\delta_r = 0^\circ$.

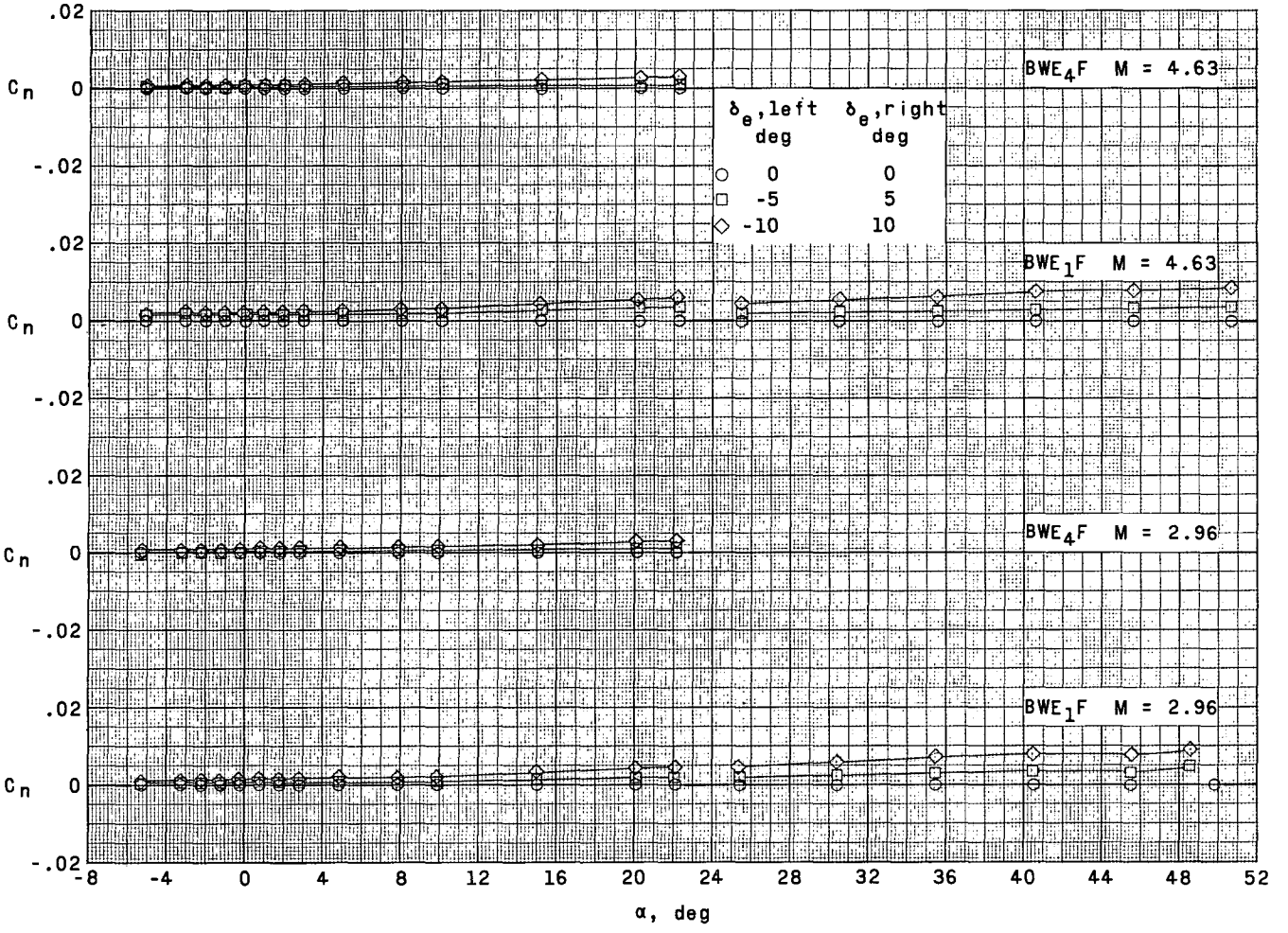

(b) Yawing moment.

Figure 19.- Concluded.

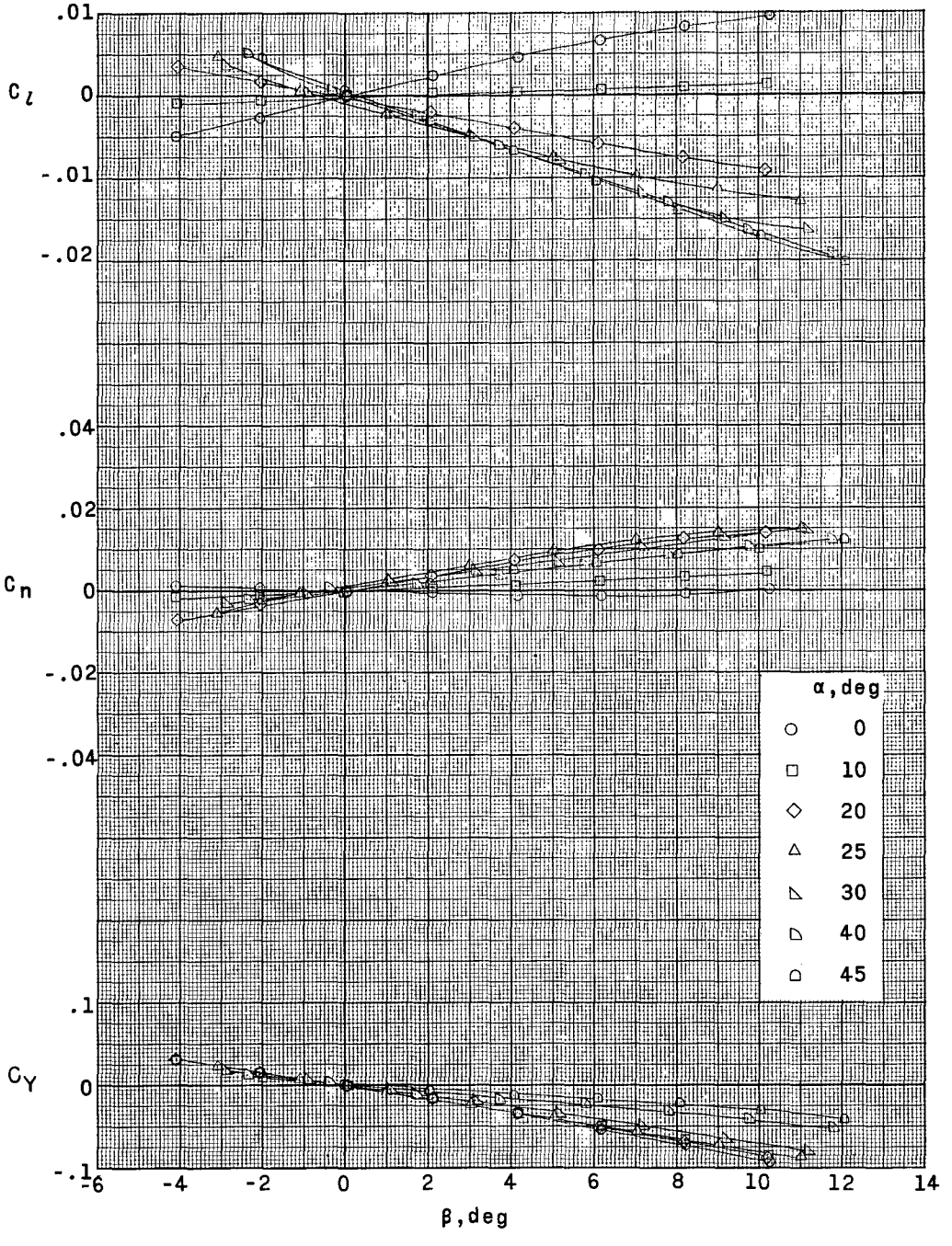

(a) $\delta_n = 0^\circ$.

Figure 20.- Effect of nose cant on the lateral stability characteristics of the BWE_1F configuration at $M = 2.96$. $\delta_e = 0^\circ$; $\delta_r = 0^\circ$.

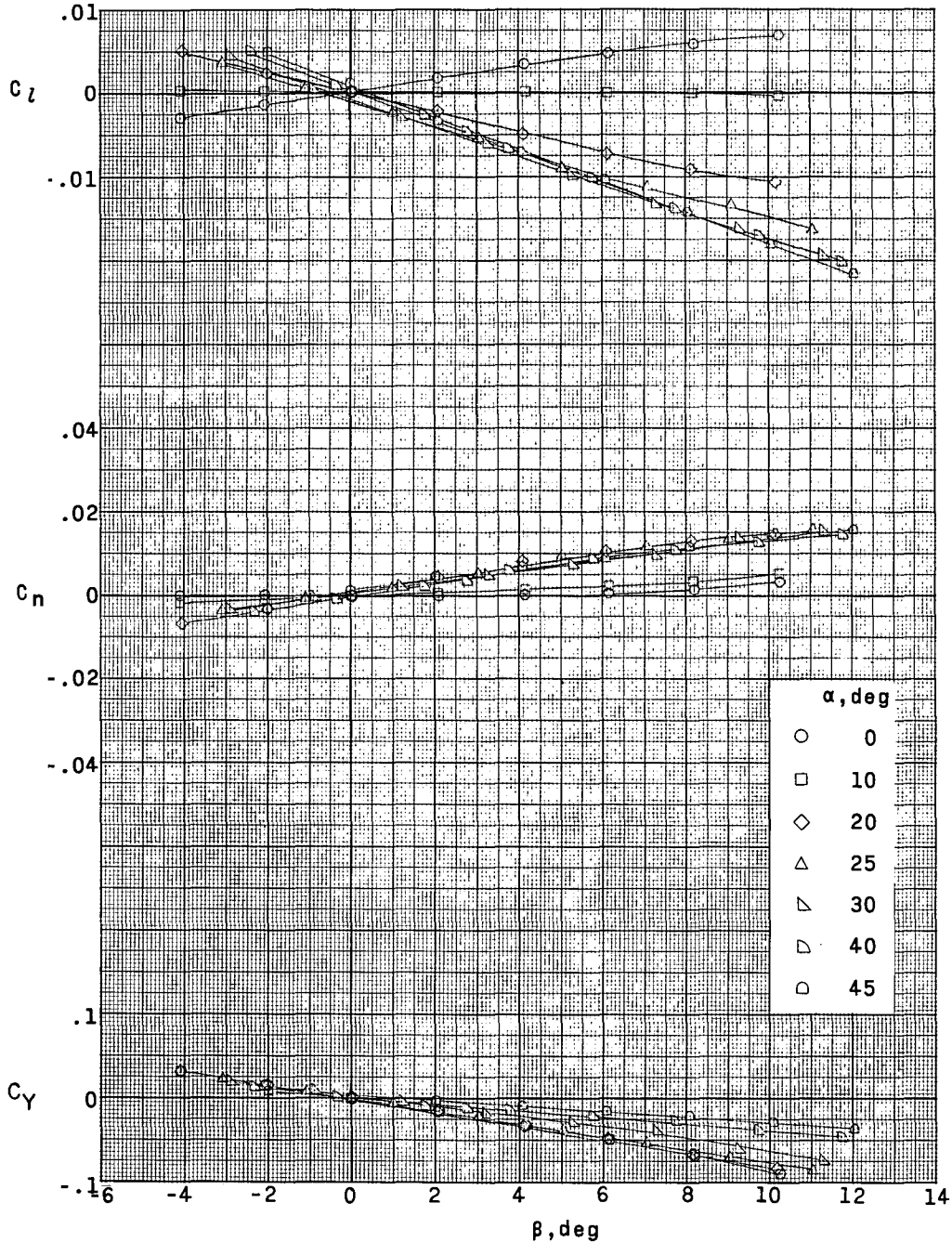

(b) $\delta_n = 5^\circ$.

Figure 20.- Continued.

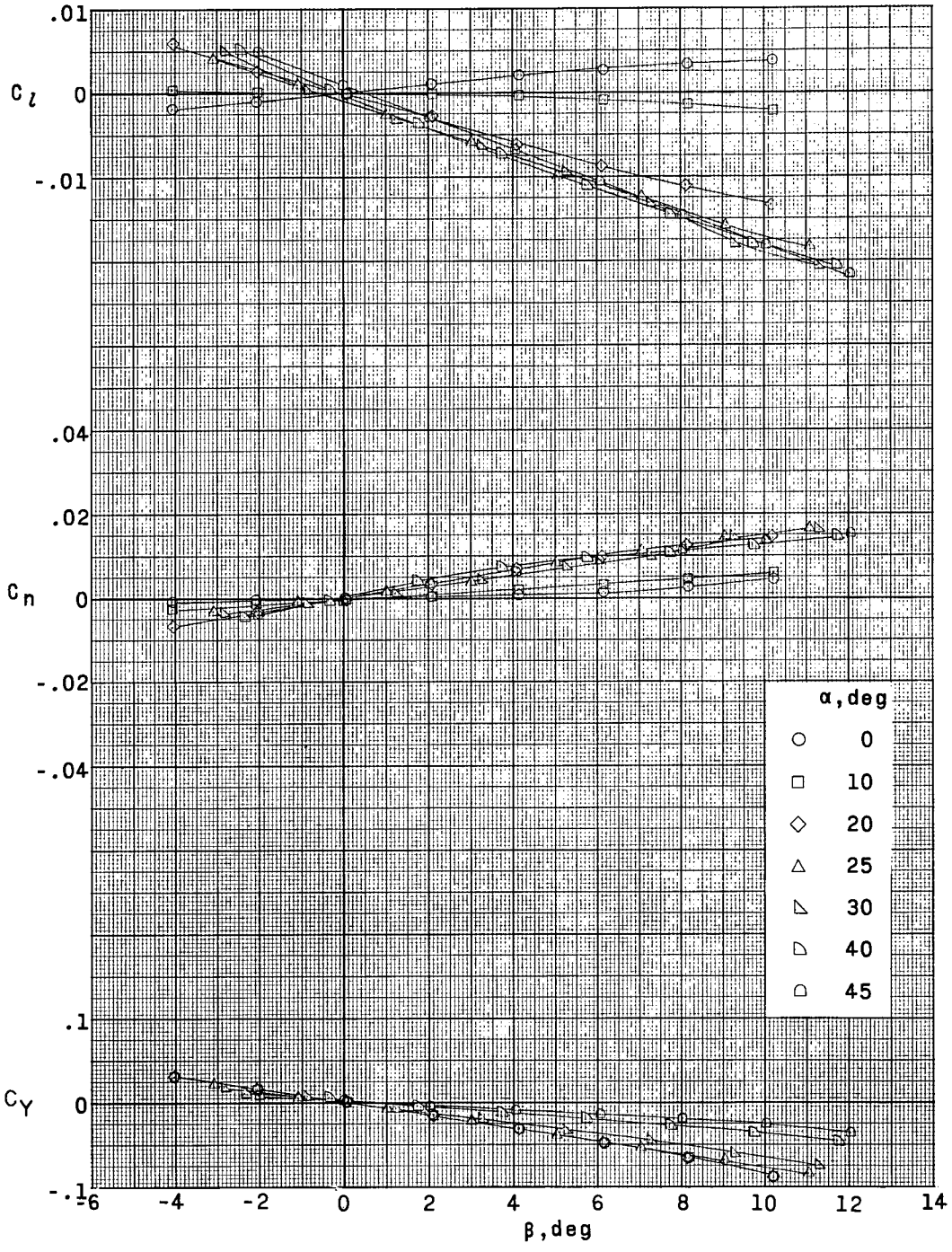

(c) $\delta_n = 10^o$.

Figure 20.- Concluded.

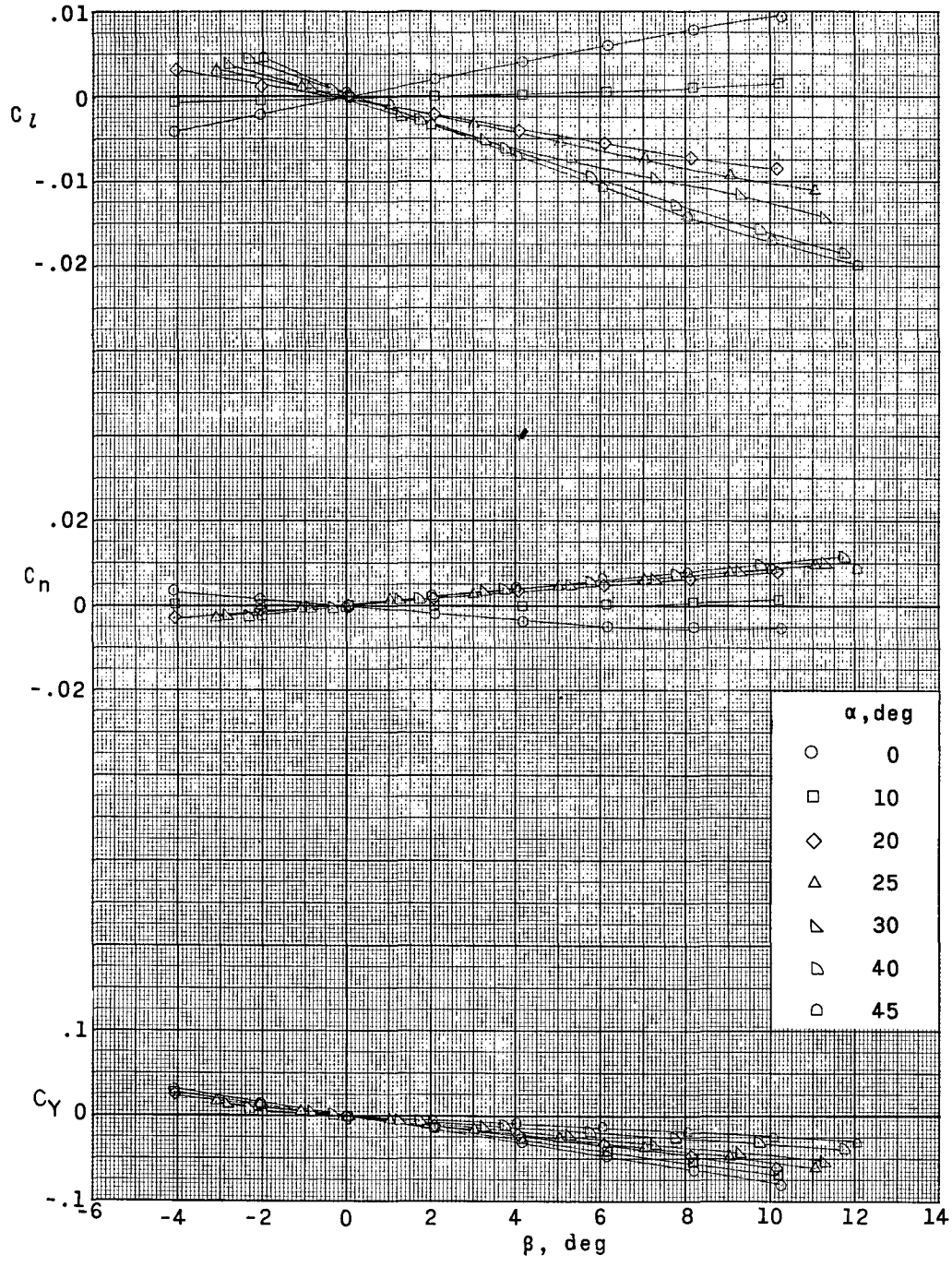

(a) $\delta_n = 0^\circ$.

Figure 21.- Effect of nose cant on the lateral stability characteristics of the BWE_1F configuration at $M = 4.63$. $\delta_e = 0^\circ$; $\delta_r = 0^\circ$.

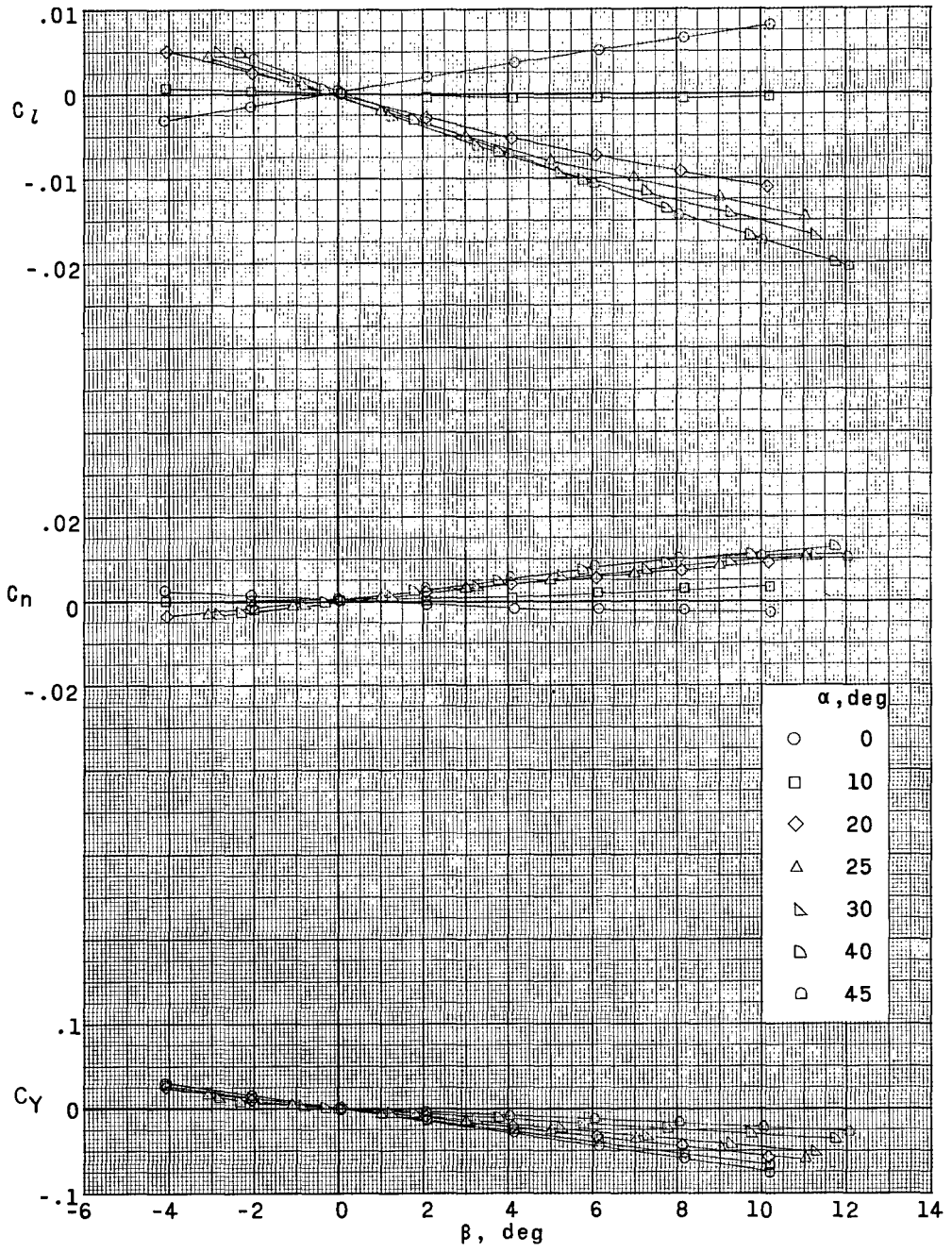

(b) $\delta_n = 5^\circ$.

Figure 21.- Continued.

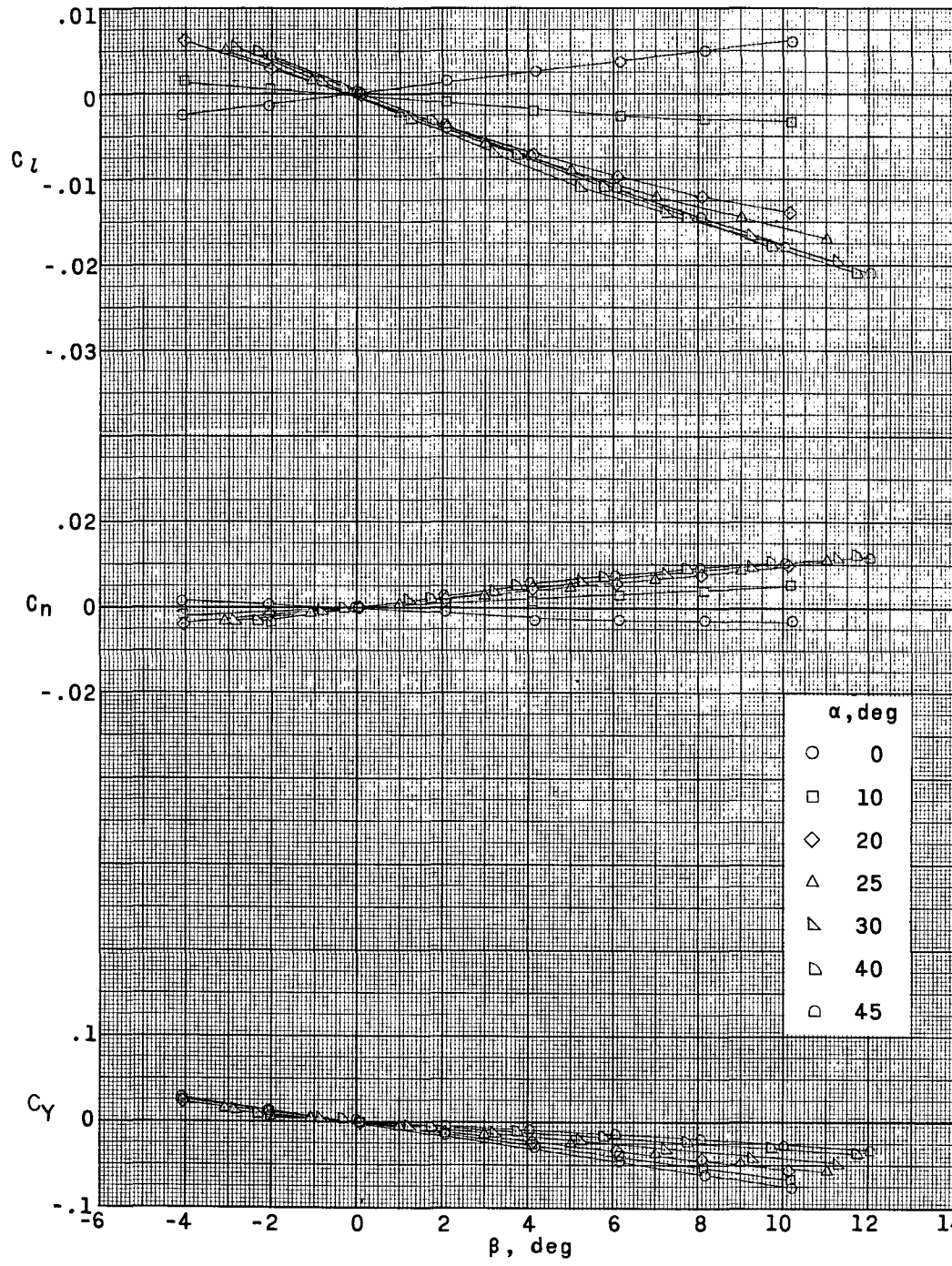

(c) $\delta_n = 10^\circ$.

Figure 21.- Concluded.

NASA-Langley, 1962 L-1905

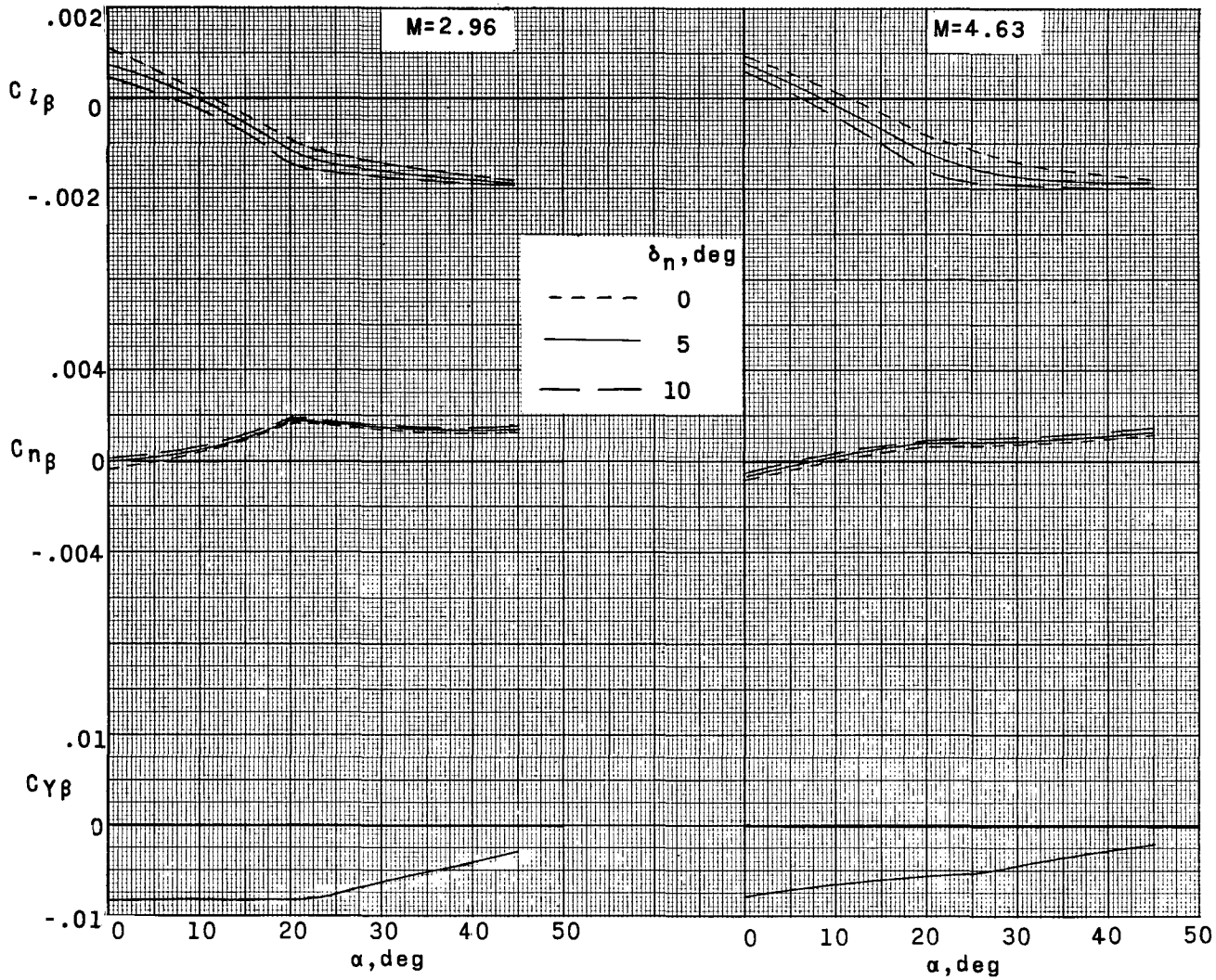

Figure 22.- Summary of the effect of nose cant on the lateral stability characteristics of the BWE_1F configuration. $\delta_e = 0^\circ$; $\delta_r = 0^\circ$.